A METHODOLOGY FOR DETERMINATION OF PERFORMANCE BASED DESIGN PARAMETERS

A THESIS SUBMITTED TO
THE GRADUATE SCHOOL OF NATURAL AND APPLIED SCIENCES
OF
THE MIDDLE EAST TECHNICAL UNIVERSITY

BY

UFUK YAZGAN

IN PARTIAL FULFILLMENT OF THE REQUIREMENTS FOR THE DEGREE OF

MASTER OF SCIENCE

IN

THE DEPARTMENT OF CIVIL ENGINEERING

SEPTEMBER 2003

Approval of the Graduate School of Natural and Applied Sciences

_____

Prof. Dr. Canan ÖZGEN

Director

I certify that this thesis satisfies all the requirements as a thesis for the degree of Master of Science.

_____

Prof. Dr. Mustafa TOKYAY

Head of the Department

This is to certify that we have read this thesis and that in our opinion it is fully adequate, in scope and quality, as a thesis for the degree of Master of Science.

_____

Prof. Dr. Polat GÜLKAN

Supervisor

_____

Assist. Prof. Dr. Ahmet YAKUT

Co-Supervisor

Examining Committee Members

Assist. Prof. Dr. Dede Sinan AKKAR (Chairman) _____

Prof. Dr. Polat GÜLKAN _____

Assist. Prof. Dr. Cem TOPKAYA _____

Assist. Prof. Dr. Ahmet YAKUT _____

Dr. Altuğ ERBERİK _____

ABSTRACT

A METHODOLOGY FOR DETERMINATION OF PERFORMANCE BASED DESIGN PARAMETERS

Yazgan, Ufuk

M.S., Department of Civil Engineering

Supervisor: Prof. Dr. Polat Gülkan

Co-supervisor: Assist. Prof. Dr. Ahmet Yakut

September 2003, 119 pages

Establishment of relationships for predicting the lateral drift demands of near-fault ground motions is one of the major challenges in earthquake engineering. Excessive lateral drifts caused by earthquake ground motions are the major causes of structural damage observed in structures. In this study, some of the fundamental characteristics of near-fault ground motions are examined. Response characteristics of elastic frame structures to near-fault ground motions are investigated. An approximate method for estimating the elastic ground story and interstory drifts for regular frame type structures is presented. Inelastic displacement demands imposed on elasto-plastic single degree of freedom (SDOF) systems subjected to near-fault ground are examined. Three equations for estimating the maximum lateral inelastic displacement demand from the maximum elastic displacement demand are established. Two of these equations relate the inelastic and elastic displacement demands through natural period and strength reduction factor. The third equation

relates the inelastic and elastic displacement demands through the ratio of natural period to pulse period and the strength reduction factor. Efficiency of the natural period to pulse period ratio for estimating the inelastic displacement ratio is shown. Error statistics of the proposed equations are presented and compared with similar studies in the literature. According to the results, these equations can be used for quick and rough estimates of displacement demands imposed on regular elastic moment resisting frames and elasto-plastic single degree of systems.

Keywords: drift demand, near-fault ground motion, inelastic displacement ratio, beam to column stiffness ratio, strength-based displacement amplification, pulse period

ÖZ

PERFORMANSA DAYALI HESAP PARAMETRELERİNİN TESBİTİ İÇİN BİR YÖNTEM

Yazgan, Ufuk
Yüksek Lisans, İnşaat Mühendisliği Bölümü
Tez Yöneticisi: Prof. Dr. Polat Gülkan
Yardımcı Tez Yöneticisi: Doç. Dr. Ahmet Yakut

Eylül 2003, 119 sayfa

Yakın mesafe depremlerinin içerdiği mahalli yerdeğiştirme taleplerinin belirlenmesi deprem mühendisliğinin üzerinde en yoğun çalışılan alanlarından biridir. Deprem sonucu yapılarda oluşan yapısal ve yapısal olmayan hasarın en önemli nedenlerinden biri yapıların deprem sırasında maruz kaldığı büyük yer değiştirme talepleridir. Bu çalışma yakın mesafe depremlerinin temel özelliklerini ve bu depremlere maruz kalan çerçeve tipi yapıların davranımını incelemektedir. Çerçeve tipi yapıların birinci kat ve maksimum kat arası ötelemesini bulmak için bir yaklaşık yöntem sunulmaktadır. Çalışma sırasında elastik olmayan tek serbestlik dereceli sistemlerin yakın mesafe depremleri sırasında maruz kaldığı elastik ötesi yerdeğiştirme talepleri incelenmiştir. Bu yapıların maruz kaldığı elastik ötesi yerdeğistirme talebinin maksimum elastik yerdeğiştirme talebine olan oranını tahmin etmek için üç ifade geliştirilmiştir. Bu ifadelerin ikisi elastik ve elastik ötesi yerdeğiştirme taleplerini doğal periyoda ve taban kesme kuvveti azaltma katsayısına

göre ilişkilendirmektedir. Üçüncü ifade ise elastik ve elastik ötesi davranımı, sistemin doğal periyodunun depremin impulsif periyoduna oranı ve taban kesme kuvveti azaltma katsayısına göre ilişkilendirmektedir. Sistemin doğal perioyudunun impulsif periyoda oranının, sistemin elastik ötesi davranımı üzerinde çok belirgin bir etkisi olduğu gösterilmektedir. Bu çalışmada geliştirilmiş olan yaklaşık yöntemlerin hata istatistikleri, başka araştırmacılar tarafından ileri sürülmüş yaklaşık yöntemlerle karşılaştırılmaktadır. Sonuçlar, bu ifadelerin yakın mesafe depremleriyle sarsılan elastik düzenli çerceve tipi binaların ve elastik olmayan tek serbestlik dereceli sistemlerin maruz kaldığı yerdeğiştirme talebinin kolay ve yaklaşık bir tahmini için kullanılabileceğini göstermektedir.

Anahtar sözcükler: öteleme talebi, yakın mesafe yer hareketleri, elastik ötesi yer değiştirme oranı, kiriş-kolon rijidite oranı, kuvvete dayalı elastik ötesi yerdeğiştirme faktörü, impulsif periyot

ACKNOWLEDGEMENTS

The research presented in this dissertation has been made possible with contributions from many individuals to whom I am indebted. This study was performed under the supervision of Prof. Dr. Polat Gülkan, Dr. Sinan Akkar and Dr. Ahmet Yakut. I would like to express my sincere appreciation for their invaluable support, guidance and insights throughout the study. Not only have I benefited from their wealth knowledge, insight and experience in earthquake engineering, they have also been a great source of inspiration and encouragement throughout my study. It has been a privilege to work under their guidance.

I would like to express my appreciation to Dr. Altuğ Erberik and Dr. Cem Topkaya, for taking the time to review my thesis study and attending my thesis presentation.

I would like to extend my deepest gratitude to my teacher Dr. Erhan Karaesmen for being such an invaluable source of knowledge, inspiration and encouragement. I would like to thank Prof.Dr. Yalçın Mengi, Prof.Dr. Haluk Sucuoğlu and Prof.Dr. Semih Yücemen for all they had taught me on earthquake engineering, structural dynamics and reliability of systems.

I would like to thank my friends; Emre Özdemir, Selim Günay, Sinan Akarsu, Tolga Yılmaz, Serdar Soyöz, İlker Kazaz, Bora Acun, Volkan Aydoğan, Hüsnü Dal and Yalçın Kaymak, for their support and help during my studies.

I would like to thank my beloved friend Feray Dağlı, for being such an invaluable person and all the things she had done for me.

My dear family deserves the greatest thanks for their endless love, support, friendship, understanding and endurance. Without their support, I could never perform this study. I am greatly indebted to them for everything that they have done for me.

TABLE OF CONTENTS

LIST OF TABLES

LIST OF FIGURES

CHAPTER 1

INTRODUCTION

1.1 Statement of the Problem

Establishment of relationships for predicting the lateral drift demands of near-fault ground motions is one of the major challenges in earthquake engineering. Excessive lateral drifts caused by earthquake ground motions are the major causes of structural damage observed in structures. A large amount of research has been performed on the estimation of global displacement demands, such as roof drift. In the last decade there has been a growing interest in the estimation of local displacement demands. The unexpected level of damage observed in well-engineered structures after the 1994 Northridge and 1995 Kobe earthquakes forced the engineering community to focus on the effects of near-fault ground motions. Studies on the effects of near-fault ground motions on structures showed that the strong ground motion pulses observed in some of the near-fault ground motions might have resulted in unexpectedly high local displacement demands. A number of methods for estimating the local displacement demands of structures subjected to near-fault ground motions have been developed. Iwan(1997) have introduced the drift spectrum, a measure of local displacement demand imposed on structures. This drift spectrum was based on wave propagation analysis of a shear beam model. Gülkan and Akkar (2002) have proposed a simple method for

estimating the elastic ground story drift, based on the first mode response of a shear beam. Use of shear beam model may provide sufficiently good estimates for the ground story drifts of frames having beams relatively stiffer than columns (shear frames). However, for the frames having beams and slabs relatively more flexible than columns the use of shear beam model results in inaccurate estimates of the ground story drift. To overcome this inaccuracy, this study aims to introduce a set of modifying coefficients to the approximate equation proposed by Gülkan and Akkar (2002).

This study also presents an initial survey for estimating the inelastic displacement demands of structures subjected to near-fault ground motions. Estimation of inelastic displacement demands, based on the elastic analysis of structures subjected to near-fault ground motions would provide a useful tool for seismic engineering practice. Although a number of methods exists in the literature for estimating the inelastic demands based on elastic analysis, a method directly taking into account the intrinsic features of near-fault ground motions has not been proposed. This study is an initial survey for such a method. Furthermore, as it will be seen in Chapter 4, C_1 coefficient employed in FEMA356(2000), which is one of the most discussed technical documents on inelastic analysis, may provide alarmingly inaccurate estimates of inelastic displacements for the case of near-fault ground motions. A set of preliminary equations was established for estimating the inelastic displacement demands imposed on inelastic non-degrading SDOF systems subjected to near-fault ground motions based on elastic analysis of the systems.

Integration of the two procedures stated above would provide a useful tool for estimating the local inelastic displacement demands of moment resisting frames subjected to near-fault ground motions. However, it should be noted that such an integration process requires a comprehensive research on the effects of nonlinearity on the response of frame structures subjected to near-fault ground motions. Such a comprehensive research is beyond the scope of this study.

1.2 Review of Past Studies

Several researchers have performed experimental and analytical studies on the estimation of lateral displacements of building type of structures since the 1960s. A number of analytical procedures and computer programs have been developed for this purpose. Also a number of static and dynamic tests have been conducted for evaluating and further improving these methods. Some of the major studies on estimation of displacement demands, effects of near-fault ground motions and characteristic properties of near-fault ground motions are summarized below.

1.2.1 Past Studies on the Characteristics of Near-Fault Ground Motions

Somerville et al., (1997) studied the fundamental characteristics of near-fault ground motions. They stated that, when the velocity of rupture is close to the shear wave velocity of the rock near the source, a series of waves resulting from each dislocation are accumulated in the direction of rupture. Accumulation of pulses in the direction of rupture results in a single large pulse of strong ground motion at the beginning of the record. This pulse represents the cumulative effect of almost all of the seismic radiation from the fault. The resulting phenomenon, which is closely related to the Doppler effect in physics, is called forward directivity. The large pulse of motion is generally observed at the beginning of velocity or displacement traces of the near-fault strong motion records affected by forward directivity. Somerville et al. (1997), stated that forward rupture directivity effects are observed when the rupture front propagates through the site and the direction of slip on the fault is aligned with the site. Somerville et al. (1997) also stated that, according to the theory of seismic wave propagation, strike normal components of near-fault ground motions have greater damage-causing potential compared to other components. It should be noted that if most of the seismic energy is released at the beginning or end of rupture, directivity effects would not be significant. In other words, energy release through the rupture should be nearly uniform for directivity effects to be noticeable (Steward et al., 2001). Somerville et al., (1997)

noticed that when the rupture propagates away from the site, arrivals of seismic waves are distributed in time and named this phenomenon as backward directivity. They observed that backward directivity resulted in long duration motions having low amplitudes at long periods. Akkar and Gülkan (2002) examined the forward directivity effects in the near-fault strong ground motion records taken during the 17 August 1999 Kocaeli and 12 November 1999 Bolu-Düzce earthquakes. They observed that the ground motion component with highest displacement demands were not always in the fault normal direction. Akkar and Gülkan (2002) stated that the ground motion components in the maximum ground velocity direction does correlate better with the larger drift demands, compared to the strike normal component for the near-fault ground motion records taken from the 17 August 1999 Kocaeli and 12 November 1999 Bolu-Düzce earthquakes.

1.2.2 Past Studies on the Estimation of Displacement Demands Imposed on Frame Structures

Blume (1968) investigated the modal characteristics of a number of frames. He examined the effects of the various types of degrees of freedom, joint rotation, axial deformation of columns and base rocking, on the overall response of building type of structures. He established a set of equations and graphs for estimating the dynamic characteristics of frame type of buildings with joint rotation, overall flexure and base motion, using simple rigid-floor shear frame analysis. Diaz et al. (1994) examined the validity of alternate models (i.e., rigid frame model, equivalent shear-beam model and equivalent shear-frame model) of building frames by comparing the ductility demands found for two idealized buildings excited by five simulated ground motions. Results of the study showed that a model that neglects the joint rotations may produce significant errors in estimating the lateral drift demands of frame type of systems.

Heidebrecth and Stafford Smith (1973) studied the interaction of shear walls and frames and derived closed form solutions for lateral displacements. Using these closed

form solutions Miranda (1999) set up an approximate procedure for estimating the maximum lateral deformations, maximum roof displacement and maximum interstory drifts of frame type of structures with uniform stiffness. Miranda and Reyes (2002) further improved the approximate method proposed by Miranda (1999), by adding the capability of estimating the lateral displacements of frame structures with non-uniform stiffness distribution.

Anderson and Bertero in 1986 examined the significant displacement demands imposed on frame type of structures by near-fault strong ground motions. However, it was after the 1994 Northridge and 1995 Kobe earthquakes that engineering community recognized the inadequacy of current seismic design and evaluation methodologies for the case of near-fault excitations.

Chopra and Cruz (1986a) analyzed the accuracy of response spectrum analysis using a set of 5 story generic frames having various fundamental periods of vibration and beam-to-column stiffness ratios. Comparisons of the response quantities obtained from response spectrum analysis with the elastic response history analysis for 8 simulated ground motions showed tolerable errors. Making use of those results they proposed a method called Simplified Response Spectrum Analysis (Chopra and Cruz 1986b). This method involved a practical procedure to estimate the first two fundamental modes, periods of vibration and modal participation factors.

Realizing the fact that local displacements are of primary importance, particularly under near-fault excitations, researchers attempted to develop some practical tools for measuring local displacement demands. Iwan (1997) developed the drift spectrum concept which was summarized in Section 1.1. Iwan (1997) demonstrated that the single-degree-of-freedom (SODF) response spectrum is an inadequate tool for measuring the interstory drift demands, particularly for near-fault ground motions. Similarly, Heidebrecht and Naumoski (1997) developed an alternative method for establishing a drift spectrum. They utilized the shear-beam theory together with

approximate equivalent shear stiffness formula for portal frames, derived by Heidebrecht and Stafford Smith (1973). Heidebrecht and Rutenberg (2000) further improved this method by employing the approximate fundamental period formulas for frame structures. Gülkan and Akkar (2002) developed a simpler procedure, utilizing the shear-beam model, for constructing the drift spectrum.

Chopra and Chintanapakdee (2001a) compared the ground story drift ratios found from response spectrum analysis with that of drift spectrum analysis and stated that the difference is due to effects of higher modes. They also pointed out that a sufficient degree of accuracy may be obtained using response spectrum method, if at least five modes are included in the analysis.

1.2.3 Past Studies on the Estimation of Inelastic Displacement Demands Imposed on Single Degree of Freedom Systems

Estimation of inelastic displacement demands from elastic displacements is the most popular research area in earthquake engineering. Among these methods some are based on the modification of elastic spectral ordinates by functions of period (T) and ductility (μ) (Newmark and Hall, 1982; Nassar and Krawinkler, 1991; Vidic et al., 1994; Miranda, 2001). The displacement coefficients method employed in FEMA356 (2000) is based on the amplification of elastic displacements for estimating the inelastic displacement demands according to strength reduction factor, natural period and characteristic site period. FEMA356 (2000) employs the inverted form of an equation which was originally derived for constant ductility by Vidic et al. (1994). This inversion of the equation proposed by Vidic et al. (1994) from constant ductility form to constant strength form resulted in loss of accuracy. Aydınoğlu and Kaçmaz (2002) have addressed this inaccuracy and performed regression analysis directly on the spectral coefficients depending on R and T. It should be noted that all these studies were

primarily based on far-field ground motions whose characteristics are very different from near-fault excitations.

Baez and Miranda (2000) studied the inelastic displacement demands imposed on single degree of freedom systems by near-fault ground motions. They stated that structures subjected to ground motions with large velocity pulses may experience maximum inelastic deformations larger than those subjected to ground motions that do not have these pulses, even if the linear elastic ordinates in the short period spectral region are similar.

(Chopra and Chintanapakdee, 2001b) compared the responses of single-degree-of-freedom (SDOF) systems to 15 near-fault and 15 far-fault strong ground motions, they concluded that near-fault ground motions had much narrower velocity sensitive regions. Chopra and Chintanapakdee (2001b) further indicated that, the design equations proposed by Veletsos and Newmark (1960), which are mainly derived for far-field ground motions, are valid for near-fault ground motions also, as long as spectral regions are defined appropriately.

Another set of methods (Rosenblueth and Herera, 1964, Gülkan and Sözen, 1974, Iwan 1980) are based on equivalent linearization. In equivalent linearization methods maximum response of the inelastic system is approximated by the elastic response of a linear elastic system with increased damping and lowered stiffness. Capacity Spectrum Method is a method developed by Freeman et al. (1975), and based on the iterative use of equivalent linearization. Capacity spectrum method is employed in ATC-40 (1996), which is one of the most debated technical documents on inelastic analysis of structures.

All of these studies provided considerable information on the nature of near-fault ground motions, response of frame structures and inelastic displacement demands imposed on single degree of freedom systems by near-fault ground motions.

1.3 Object and Scope

This study examines the properties of near-fault ground motions and effects of ground motions containing pulses on the response of structures. Important characteristics of near-fault ground motions were studied for this purpose. Performances of various attenuation relationships were evaluated. Effects of various parameters on the characteristic properties of near-fault ground motions were examined.

Modal properties of frames having different overall lateral deformation patterns were analyzed. A set of idealized moment resisting frames having various numbers of stories and beam-to-column stiffness ratios was utilized for this purpose. A set of equations, estimating the elastic ground story and maximum interstory drift ratios for moment resisting frames, was established. Principles of modal analysis were utilized in the derivation of these equations. The equations were based on the equation proposed by Gülkan and Akkar (2002) for estimating ground story drift.

Another set of equations have been established for estimating the inelastic deformation demands of non-degrading SDOF systems, based on the maximum elastic displacement demand imposed on SDOF systems with the same natural period and damping. Equations for estimating the inelastic displacements were established by directly performing regression analysis on elastic to inelastic displacement ratio, natural period and strength reduction factor. This study is an attempt for establishing a direct link between the strength capacity of the structure and inelastic displacement demand. Such a methodology may serve as a convenient and practical tool for performance evaluation of existing structures excited by near-field earthquakes.

This thesis is composed of five main chapters and two appendices. Contents of each chapter may be summarized as follows:

Chapter 1 Statement of the problem and review of past studies on the estimation of the displacement demands imposed on structures, effects of near-fault ground motions on the response of structures and fundamental characteristics of near-fault ground motions.

Chapter 2 Inspection of some of the fundamental characteristics of near-fault ground motions records used in the study. Evaluation of performances of some of the attenuation relationships for the case of near-fault ground motions.

Chapter 3 Inspection of the effects of near-fault ground motions on moment resisting frames. Derivation of the equations for estimating the elastic ground story and maximum interstory drifts of moment resisting frames. Establishment of equations for estimating the maximum inelastic displacement demands imposed on non-degrading SDOF systems subjected to near-fault ground motions.

Chapter 4 Statistical study on the errors of the proposed equations. Comparison of the error ranges with other studies available in the literature.

Chapter 5 Summary and conclusions.

Appendix A List of the near-fault strong ground motion records used.

Appendix B Coefficients of the attenuation relationships referred to in Chapter 2.

CHAPTER 2

NEAR-FAULT GROUND MOTIONS

2.1 Ground Motion Records

A set of 148 near-fault ground motion records was utilized in this study. All the records had been recorded on dense or stiff soils, with average shear wave velocities in the upper 30 m ranging from 760m/s to 180m/s. Records utilized in this study were downloaded from the PEER Strong Motion Data Archive Website (http://peer.berkeley.edu/smcat/). The strong motion record set, comprised of horizontal components taken from 10 different earthquakes, covered a moment magnitude (M_w) range from 6 to 7.6. The nearest and farthest records used in the study were made at distances of 0.24 km and 20 km to the rupture surface, respectively. In order to examine the effects of strong long duration pulses on the elastic and inelastic response, the record set was sub-divided into two parts. A total of 56 records having both significant velocity pulses in their time history traces and corresponding sharp peaks in their pseudo-velocity spectra formed the "Records with Pulse" group. The remaining 92 strong motion records formed the "Records without Pulse" group. Basic properties of these ground motion records are listed in Table A.1 in Appendix A.

In Figure 2.1, moment magnitudes (M_w) and distances of the records are summarized. The horizontal crowding in the graph at M_w equal to 7.6 is due to numerical dominance of the 1999 Chi-chi earthquake records in the dataset. This earthquake, which was recorded by a very dense array of accelerographs, provided a useful group of data for near-fault strong ground motion studies. Indeed, 82 of the near-fault strong motion records used in this study have been recorded during the 1999 Chi-chi earthquake.

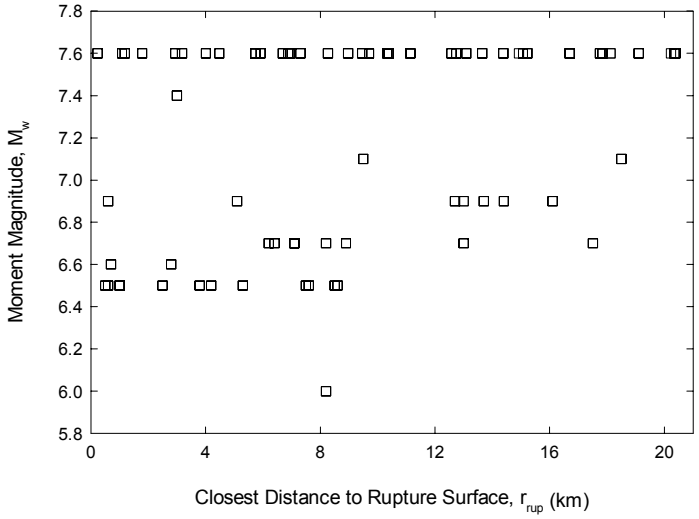

Figure 2.1 Moment Magnitude versus Distance Plot of the Record Set

2.2 Characteristics of Near-Fault Ground Motions

Understanding the nature of near-fault ground motions is crucial for establishing proper design methodologies for buildings situated in such conditions. In Figure 2.2, a near-fault and a far-fault ground motion records were plotted. The sample near-fault strong motion record on the left of Figure 2.2 was taken at a distance of 2.94 km to the rupture surface during 1999 Chi-chi, Taiwan Earthquake (M_w=7.6).

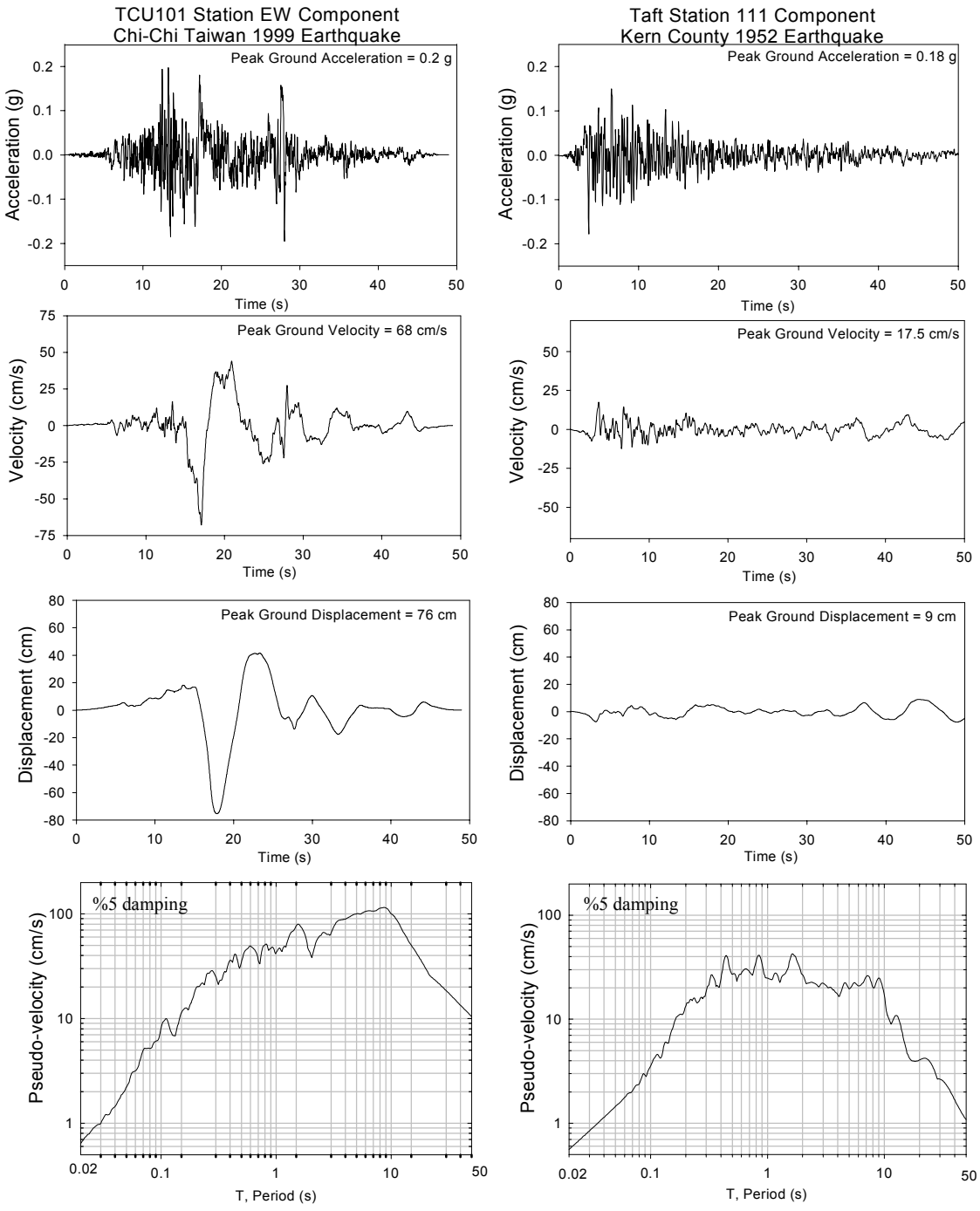

Figure 2. 2 A Sample Near-Fault Ground Motion Record with Pulse (1999 Chi-Chi Earthquake) and Far-Fault Ground Motion Record (1952 Kern County Earthquake)

A significant long duration pulse may easily be noticed in the velocity and displacement traces of this near-fault record. The sample far-fault strong motion record on the right side of Figure 2.2 was taken at a distance of 41 km to the rupture surface during 1952 Kern County Earthquake. It may easily be noticed that a significant long duration pulse, like the one seen in the velocity and displacement traces of the near-fault record, is not observed in the velocity and displacement traces of the sample far-field record. The pseudo-velocity spectra of the records seem to be different too. By examining the pseudo-velocity spectra of the sample near-fault and far-fault records, one may conclude that the sample near-fault has significantly higher spectral ordinates for the periods greater than 1 s. Dominance of the strong pulse seen in the velocity trace of the sample near-fault record is evident from the pseudo-spectral velocity diagram too.

2.2.1 Peak Ground Acceleration (PGA)

The most commonly used measure of amplitude of a particular ground motion is peak ground acceleration. It is simply the largest (absolute) acceleration in the strong motion record. Widespread use of PGA for characterizing strong ground motions comes from its straight-forward relationship with inertial forces. Although it is strongly related to the sampling rate of accelerogram and gives only an indication about the inertial forces acting on very stiff structures, it has been used widely for characterizing strong ground motions.

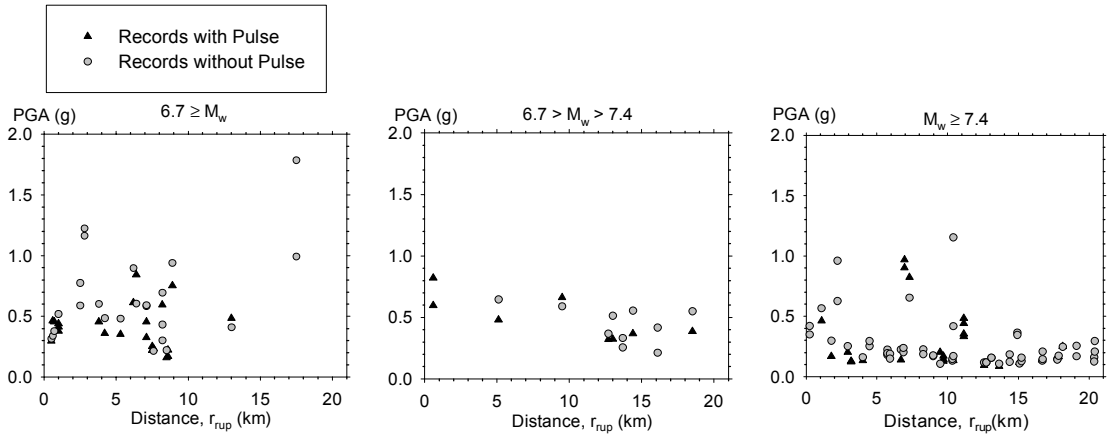

Figure 2.3 Peak Ground Acceleration versus Distance to Rupture Surface

Figure 2.3 shows the Peak Ground Acceleration (PGA) versus distance scatter plots of the record set grouped into M_w sets. Although a falling trend in PGA with increasing distance may easily be noticed from the $6.7 > M_w > 7.4$ and $M_w \geq 7.4$ graphs, such a trend is hardly noticed in the $6.7 \geq M_w$ graph in Figure 2.3. Especially the strong motion record taken at Tarzana Cedar Hill Nursery (CDMG 24436) during the 1994 Northridge (M_w=6.7) earthquake seems to be lying outside the rest of the measurements with a PGA of 1.78g at a distance of 17.5 km. The same plot shows that there is no significant relation between the velocity pulse content and PGA.

2.2.2 Peak Ground Velocity (PGV)

Velocity is the first integral of acceleration with respect to time. Therefore, unlike PGA, PGV is less sensitive to higher frequency components of the ground motion. Therefore, PGV is a more effective tool for characterizing ground motion's potential for damage to typical engineering structures. Wald et al. (1999) have developed regression relationships between the peak ground velocity and Modified Mercalli Intensity (Richter 1958). Modified Mercalli Intensity is the measure of damage caused by an earthquake at a site. Wald et al. (1999) have stated that peak ground

velocity is strongly related to the Modified Mercalli Intensity for the earthquakes having intensities larger than VII. Figure 2.4 shows the Peak Ground Velocity (PGV) versus distance distributions of the record set. A narrowing trend in PGV values with increasing distance from rupture surface may be noted in the $M_w \geq 7.4$ graph in Figure 2.4. In other words, strong motion records taken at closer distances have significantly wider ranges of PGV values compared to those recorded at more distant locations. Nevertheless, it should be noted that there exists a number of records taken at closer distances than 4 km and having relatively small PGV values. Additionally, PGV versus distance graph does not show a notable difference between records with and without significant pulses in their velocity traces.

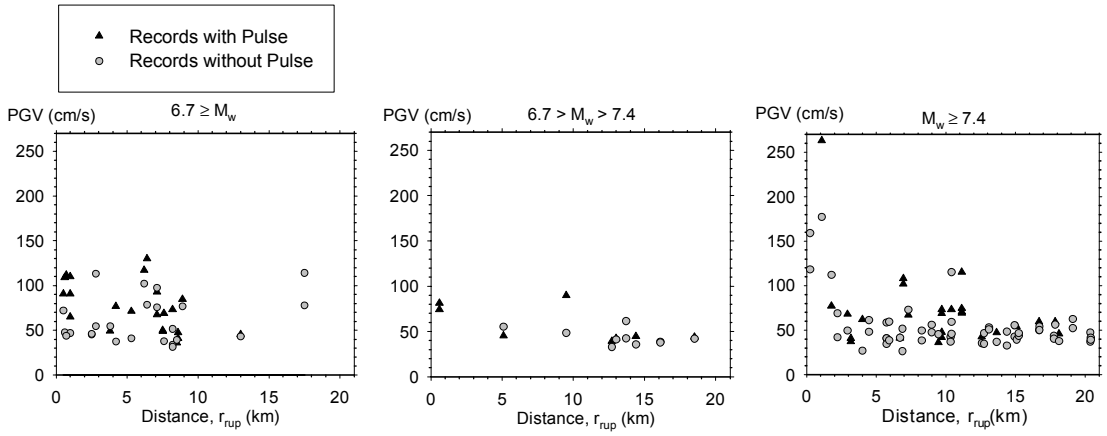

Figure 2.4 Peak Ground Velocity versus Distance to Rupture Surface

2.2.3 Arias Intensity

Despite the fact that they are popular ground motion characterization parameters, PGA and PGV only provide simple information about the amplitude of strong ground motion. For proper characterization of a strong ground motion for engineering purposes amplitude, frequency content and duration of the record should be reflected in the characterization parameter. Arias Intensity (Arias 1970), reflects the amplitude,

frequency content and duration of the ground motion. Arias Intensity proposed by Arias (1970), relates the cumulative energy per unit weight absorbed by an infinite set of single degree of freedom oscillators having fundamental frequencies uniformly distributed in the range (0,∞). In the case of oscillators with zero damping, Arias Intensity is defined as:

$$I_a = \frac{\pi}{2g} \int_0^{\infty} \left[a_x(t) \right]^2 dt \tag{2.1}$$

where I_a is the the Arias Intensity (in units of meter per second), a_x(t) is the acceleration time history of the strong motion record (in units of meters per second square) and g is the gravitational acceleration (9.81m/s^2).

Arias intensity is a simple and efficient index of damage for many structural and geotechnical engineering problems, such as dynamic response of stiff structures, earthquake induced liquefaction and seismic slope stability (Kayen and Mitchell 1997).

In Figure 2.5, variation of Arias Intensity with distance is presented. Similar outliers, like those in PGA versus distance plot (Figure 2.3), are observed in Figure 2.5. Two of these outliers in the $6.7 \geq M_w$ graph in Figure 2.5, with distances of 17.5 km are again the components of strong motion recorded at Tarzana Cedar Hill Nursery (CDMG 24436) during the 1994 Northridge earthquake (M_w = 6.7). The third outlier in the $M_w \geq 7.4$, with a distance of 10.4 km is the west component recorded by TCU084 station during 1999 Chi-chi earthquake. Leaving aside these three outliers, a narrowing trend in Arias Intensity with increasing distance may be seen. No significant difference may be observed between Arias Intensities of records with and without pulses.

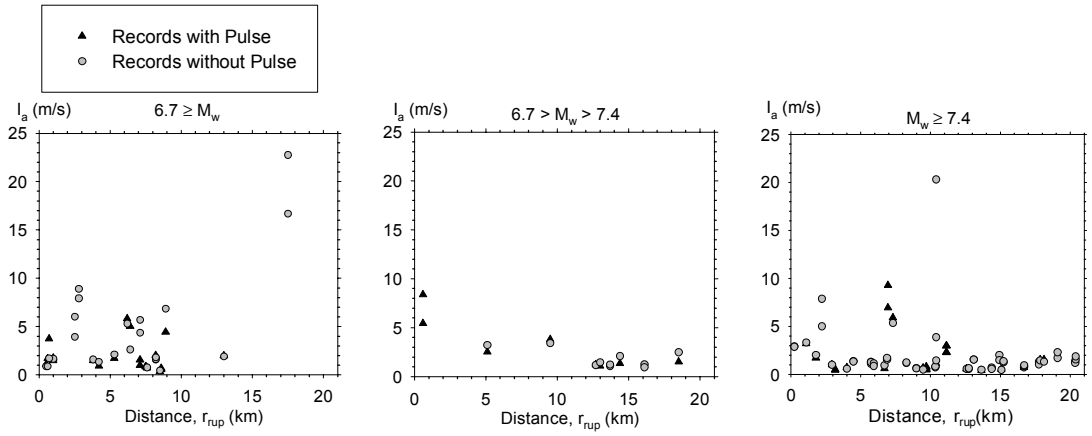

Figure 2.5 Arias Intensity versus Distance to Rupture Surface

2.2.4 Peak Ground Acceleration to Peak Ground Velocity Ratio (PGA/PGV)

Studies have indicated that the decrease of ground velocity with distance is generally slower than that of acceleration. Therefore it is generally expected that, the (PGA/PGV) ratio is relatively higher near the earthquake source and lower at larger distances from the source of energy release. Because the peak velocities and peak accelerations are usually associated with different frequencies, PGA/PGV should give information about the frequency content of the earthquake (McGuire, 1978). Zhu et al. (1988), using 36 strong motion records, studied the correlation between the inelastic displacement demand and maximum of the ground acceleration to velocity ratio computed for each time step of the strong motion record *max(a/v)*. It should be noted that although *max(a/v)* is not directly related to PGA/PGV. However, it provides a similar information about the strong motion record. Zhu et al. (1988) found that strong ground motion records with lower *max(a/v)* had higher inelastic displacement demands. They also found that records with low *max(a/v)* ratios had significantly higher hysteretic energy demands. Malhotra (1999), using 4 strong motion records, claimed that near-fault records having forward directivity effects, which were summarized in Chapter 1, tended to have lower PGA/PGV ratios.

The PGA/PGV versus distance scatters for different magnitudes were plotted in Figure 2.6. Through Figure 2.6, it is observed that for the ground motions taken from earthquakes with M_w<7.4 records with pulse on the average have lower PGA/PGV ratios than records without pulse.

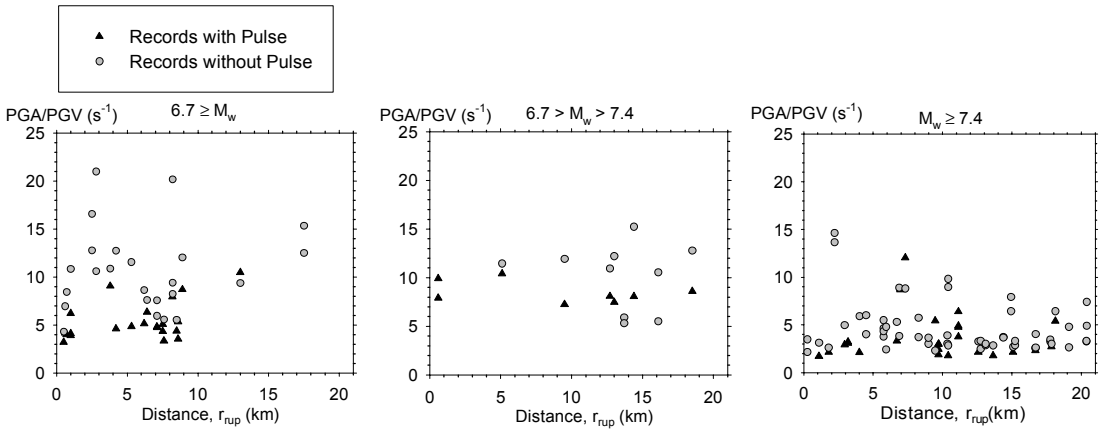

Figure 2.6 Ratio of Peak Ground Acceleration to Peak Ground Velocity versus Distance Plot

2.3 Near-fault Ground Motions and Attenuation Relationships

Estimation of the maximum level of ground acceleration that a structure will be subjected to during its service life constitutes an important part of force-based earthquake-resistant design. The ground motion parameters of interest, for common engineering applications, are peak ground acceleration (PGA), pseudo-spectral acceleration (PSA), pseudo-spectral velocity (PSV), and spectral displacement (SD). There exists more than 120 equations proposed by various researchers (Douglas 2001) for PGA alone. Another important parameter that has proven to be strongly correlated with the potential destructiveness of an earthquake is the Arias Intensity (Travasarou et al. 2003). Numerous studies have been made for capturing the effects of earthquake

magnitude, rupture mechanism, site characteristics and source to site distance on these strong motion parameters. In this section, the performance of two studies for predicting PGA (Boore et al. 1997, Sadigh et al. 1997) and one study for predicting Arias Intensity (Travasarou et al. 2003) will be evaluated.

2.3.1 Attenuation Relationships Predicting Peak Ground Acceleration

Boore et al. (1997), using a record set mostly based on California earthquakes, proposed the following empirical equation for estimating the PGA of the average horizontal component:

$$\ln(Y) = b_1 + b_2(M-6) + b_3(M-6)^2 + b_5 \ln(r) + b_V \ln\frac{V_s}{V_A} \qquad (2.2)$$

$$\text{where } r = \sqrt{r_{jb}^{\,2} + h^2}$$

where Y is the peak horizontal ground acceleration or pseudo-acceleration response (measured in g), r_{jb} is the closest distance to surface projection of rupture surface (the so-called. 'Joyner and Boore Distance'), M is the Moment Magnitude, V_S (m/s) is the average shear-wave velocity in the upper 30 m of the recording station, b_1, b_2, b_5, b_V, h and V_A are the coefficients to be found from weighted, two-stage, regression analysis. Coefficients and standard deviations associated with the above equation may be found in Appendix B.

Boore (2001) has compared predictions calculated with this equation with records obtained from 1999 Chi-chi earthquake (M_w=7.6). In his study, Boore (2001) concluded that, for periods less than 1 s, predictions on the average were about twice the recorded ground motions. Additionally, Boore (2001) observed that long duration wave trains present in the ground motions even at distances of 30-60 km produced spectral accelerations as much as five times larger than predictions made by this equation, in the

range of periods from 2 to 20 seconds. Boore (2001) expressed the view that these unexpected differences might be due to site and propagation effects.

Geometric means of the PGA's found from two components of strong ground motion records obtained from each station are plotted above the attenuation relationship proposed by Boore et al. (1997) in Figure 2.7. The moment magnitudes used in the generation of each attenuation curve have been indicated on the top right corner of the graphs in Figures 2.7, 2.9 and 2.10.

In their original study Boore et al. (1997) have directly incorporated the site effects using the average shear-wave velocity in the upper 30 m of the recording station. However, in this study only the NEHRP site classes of the strong motion stations were available. Hence, the V_s in Equation 2.2 was taken as equal to the recommended value by Boore et al. (1997) for each NEHRP site class. Closest distance to surface projection of rupture surface was not available for 6 stations in the record set, so, they are excluded from these curves.

In the topmost two curves in Figure 2.7, the principal representation is for near-fault strong motion records obtained from the 1999 Chi-chi earthquake (M_w=7.6). It is evident from these two graphs that there is a considerable overestimation for both C and D class sites. Additionally, it should be stated that a significant dispersion exists in the data.

The second row of curves in Figure 2.7 contains measurements of the strong motion records from 1992 Cape Mendocino (M_w = 7.1) and 1989 Loma Prieta (M_w = 6.9) earthquakes. Although there are too few points to draw a comment, it may be seen that all the points lie within the 84 percentile (mean plus one standard deviation) range.

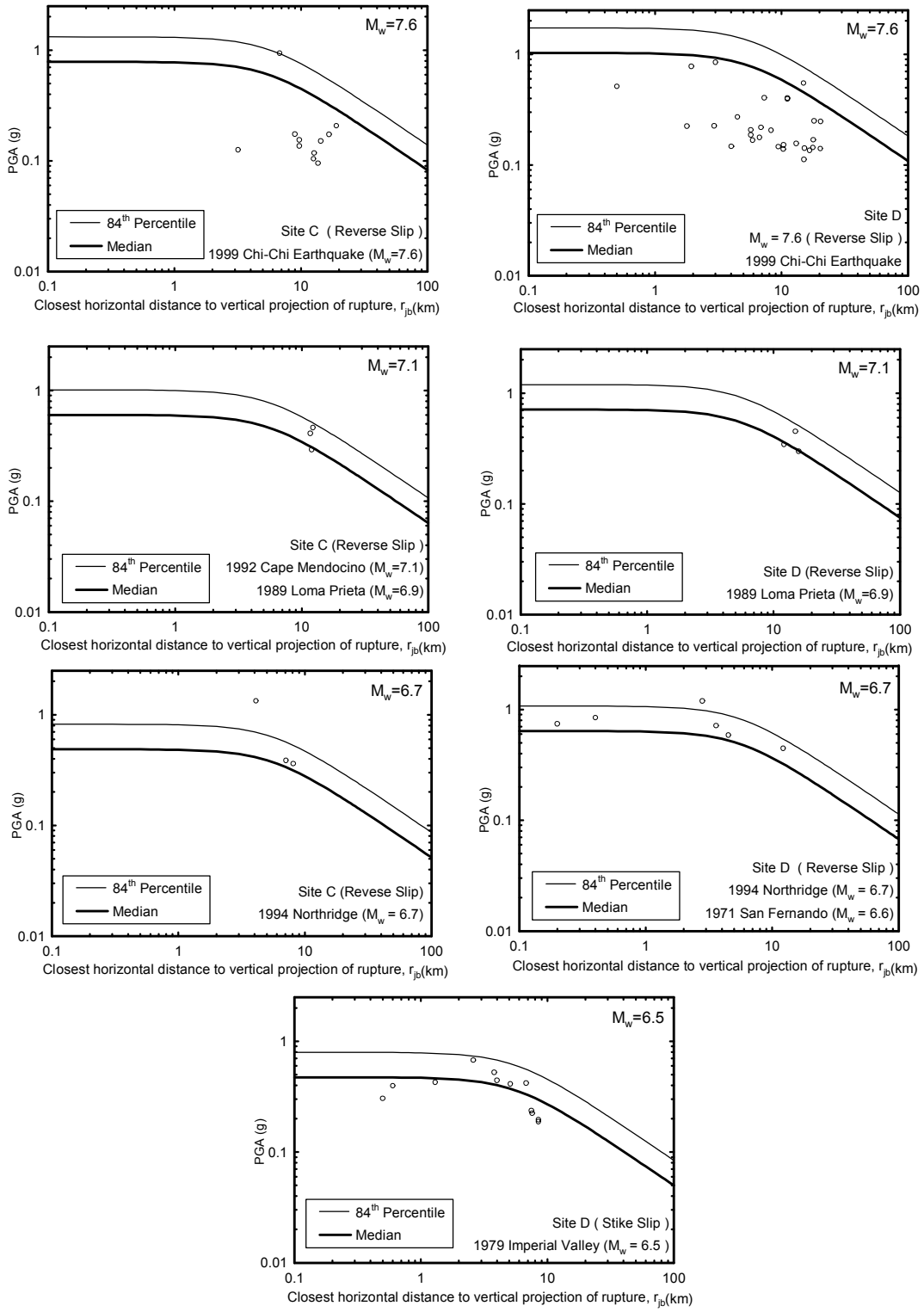

Figure 2. 7 Attenuation Relationship Proposed by Boore et al. (1997) and Scattergrams of Strong Motion Records Used in This Study

The third row of graphs in Figure 2.7 consists of strong motion records from 1994 Northridge (M_w = 6.7) and 1971 San Fernando (M_w = 6.6) earthquakes. Except for a few outliers, it is observed that the attenuation equation follow the trend of scatter points. Similar to the M_w = 7.1 graph, it seems that most of the data points are located between the mean and 84 percentile. This may be an indication that the strong motion records in the dataset have higher PGA's than the average near-fault strong motion records.

The single graph at the bottom of Figure 2.7 represents the strong motion records from 1979 Imperial Valley (M_w = 6.5) earthquake. It is clearly observable from the graph that, attenuation relationship by Boore et al. (1997) captures the individual values and trend of data very well.

A similar equation for estimating PGA's and PSA's, resulting from earthquakes with a moment magnitude range from 4 to 8, at distances up to 100 km, has been proposed by Sadigh et al. (1997). In this study, unlike Boore et al.(1997) all the ground motion records are grouped into two according to their site characteristics as "rock sites" and "deep soil sites". Sadigh et al. (1997) have stated that deep soil data has been collected from sites having greater than 20 m of soil over the bedrock. In the light of this statement, it may be assumed that record set used in this study was derived from "deep soil sites". The comparisons were made accordingly. Function and coefficients proposed by Sadigh et al.(1997) for the prediction of PGA are given in Appendix B. An important point to be noted is that, the attenuation relationship proposed by Sadigh et al. (1997) and Boore et al. (1997) have different distance definitions. The two site to source distances, namely closest distance to surface projection of the rupture surface (r_{jb}) used by Boore et al. (1997) and closest distance to rupture surface (r_{rup}) used by Sadig et al. (1997), are shown in the representative sketch in Figure 2.8.

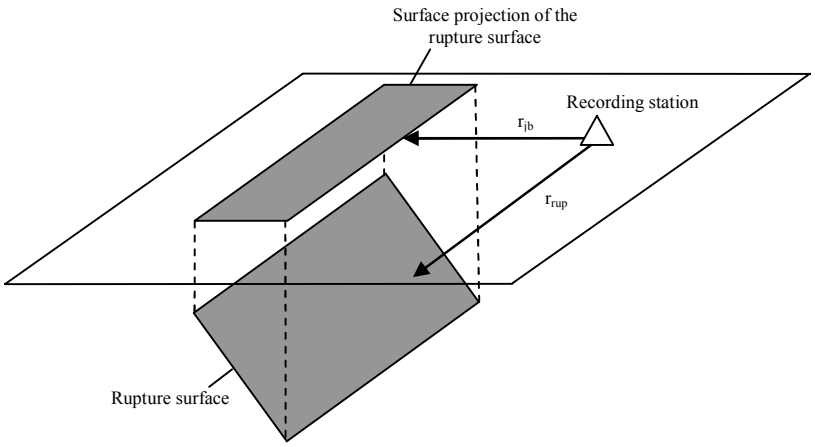

Figure 2.8 Sketch of r_{jb} and r_{rup}

Attenuation relationship proposed by Sadigh et al (1997) and measurement points of the strong motion records used in this study may be inspected in Figure 2.9. The graphs contain the same earthquakes as in Figure 2.7. Unlike Boore et al. (1997), there is some underestimation for the $M_w = 7.6$ graph. This underestimation is even more noticeable in the $M_w = 6.7$ graph. More importantly, a clear parallel trend can not be observed between the points and attenuation relationship.

In conclusion, it may be stated that according to dataset used in this study attenuation relationship proposed by Boore et al (1997) seems to capture the overall trend better than Sadigh et al (1997). This may be due to the difference of the distance definitions proposed for each relationship.

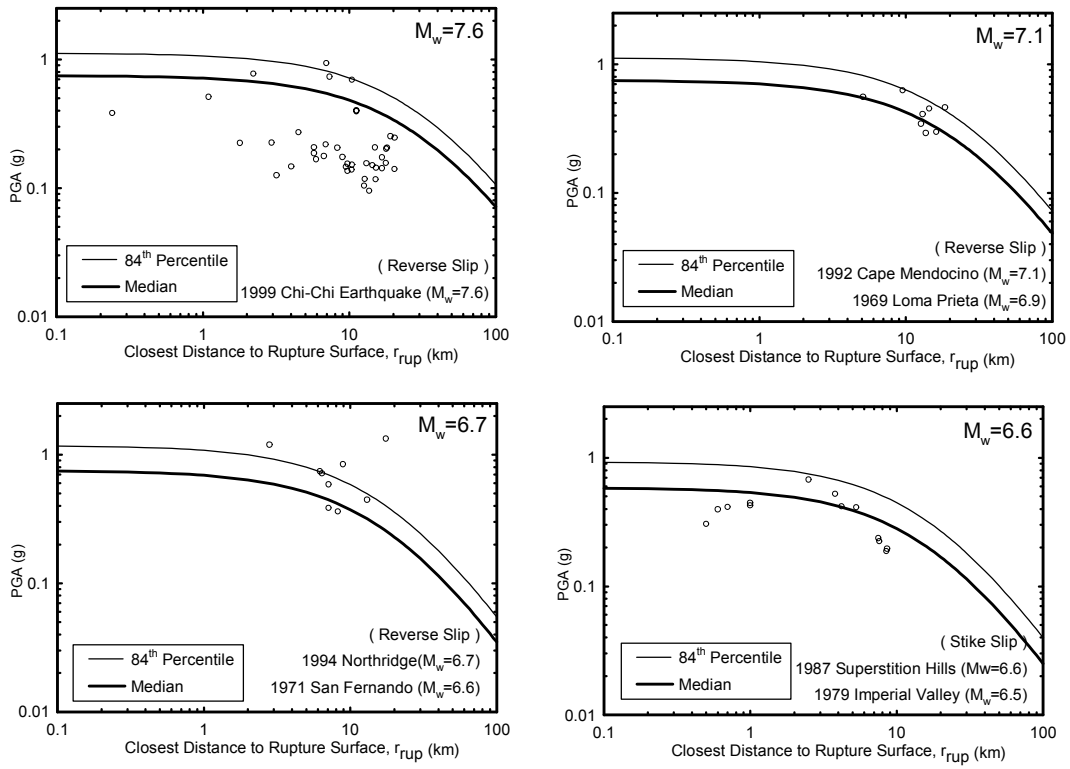

Figure 2. 9 Attenuation Relationship Proposed by Sadigh et al. (1997) and Scattergram of Strong Motion Records Used in This Study

2.3.2 Attenuation Relationships Predicting Arias Intensity

Emphasizing the fact that Arias Intensity is a useful measure for characterizing strong ground motions, Travasarou et al. (2003) proposed an attenuation relationship for estimating Arias Intensity. This relationship, which was derived from point-source model and the coefficients found from regression analysis on 1208 ground motion records, is given in Appendix B. It is stated that this relationship is applicable for earthquakes with moment magnitudes in a range from 4.7 to 7.6 and distances from 0.1 km to 250 km (Travasarou et al. 2003). It should be noted that the equation proposed by Travasarou et al. (2003) estimates the average of the Arias Intensities of the two components.

In Figure 2.10 this attenuation equation is plotted over the data obtained from the near-fault strong motion record set used in this study. Travasarou et al. (2003) have used the site classification scheme proposed by Rodrigez-Marek et al. (2001). This site classification scheme, unlike NEHRP(2000) site classification which is only based on the average shear-wave velocity of the soil profile in the upper 30 m, takes both the shear-wave velocity and depth of soil layer above the bedrock as parameters. Since the classification data of all of the stations according to this scheme was not available, plots have been prepared assuming all the sites were BRM -D class (which results in higher I_a values). It is seen from Figure 2.10 that the proposed attenuation relationship captures most of the measurement points very well. The same over estimation in M_w = 7.6 set and outliers in M_w=6.7 are seen in these graphs too.

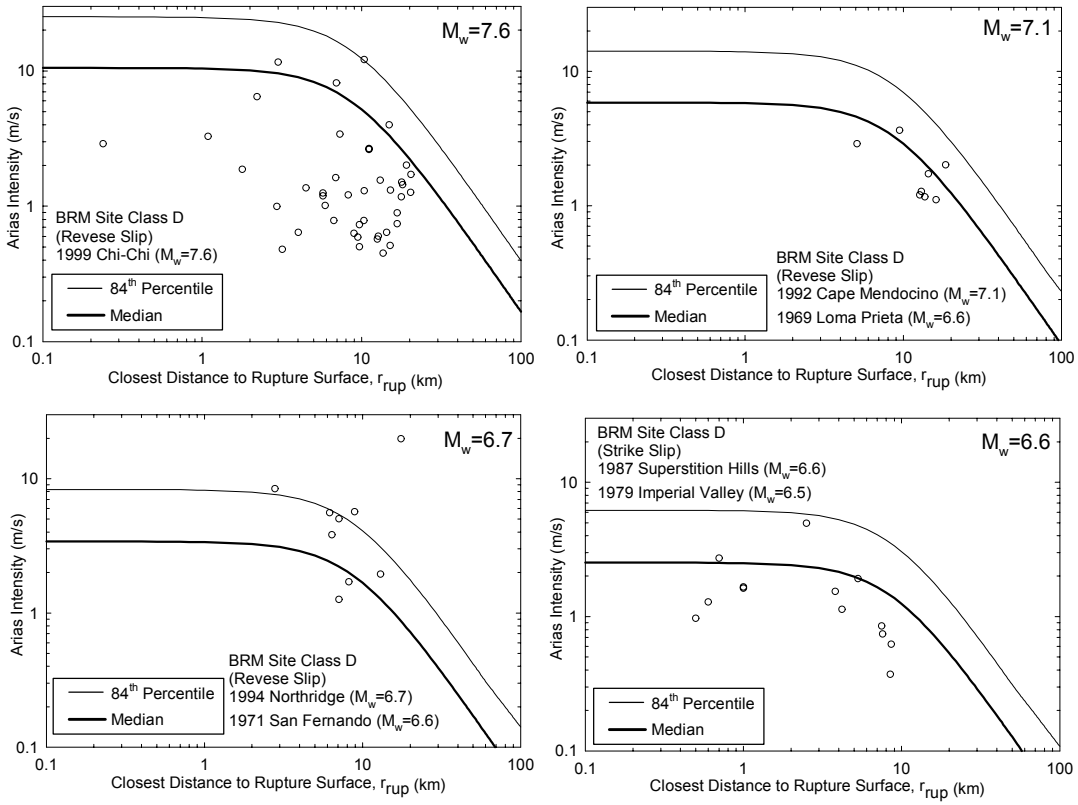

Figure 2.10 Arias Intensity Attenuation Relationship Proposed by Travasarou et al. (2003) and Plotted against Strong Motion Records Used in This Study

2.4 Correlation between the Pulse Period and the Predominant Period from Pseudo-Velocity Response Spectra

Two important parameters, characterizing the frequency content of near-fault records are pulse period (T_v) and predominant period from pseudo-velocity response spectrum ($T_{p\text{-}v}$). Pulse Period (T_v) is defined as the duration of the largest amplitude pulse in the velocity trace of the strong motion record. Starting and ending times of the pulse are either defined as zero crossing time or the time at which velocity is equal to 10 percent of the peak velocity (Stewart et al. 2001). Likewise, Somerville et al. (1999) define pulse period as the largest cycle of motion in the strong motion record. Predominant period in the pseudo-velocity response spectrum ($T_{p\text{-}v}$), as the name implies, is measured as the period corresponding to the peak at the pseudo-velocity response spectrum (Stewart et al., 2001). These two measures are capable of providing information about the frequency content and spectral shapes of near-fault strong motions, particularly for those affected by forward directivity.

Pulse period (T_v)'s of all of the near-fault records were measured by careful examination of velocity traces of near-fault strong motion records that had "significant" pulses in their velocity traces. Predominant period of the pseudo-velocity response spectrum ($T_{p\text{-}v}$) of each record were read from the response spectra of all strong motion records. A sample velocity trace and pseudo-velocity response spectrum for 5 percent damping, together with corresponding T_v and $T_{p\text{-}v}$ measurements are given in Figure 2.11.

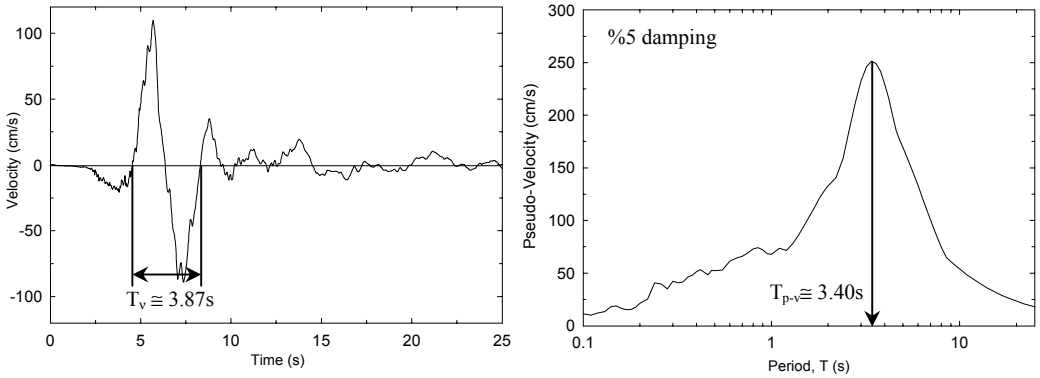

Figure 2.11 Determination of T_v and $T_{p\text{-}v}$ from 1979 Imperial Valley (M_w=6.5) Earthquake Strong Motion Record (Station: El Centro Array #6, Component 230)

Stewart et al. (2001) have stated that coincidence of T_v and $T_{p\text{-}v}$ for a strong ground motion indicates that velocity pulse contains energy in a narrow period band. In order to examine the correlation in between T_v and $T_{p\text{-}v}$, the plot given in Figure 2.12 was prepared, and coefficient of correlation was calculated. It is apparent from the figure and calculated correlation coefficient that there is a strong connection between T_v and $T_{p\text{-}v}$, especially for the periods shorter than 4 seconds. Mean and standard deviation of the ratio between T_v and $T_{p\text{-}v}$ were found to be 0.96 and 0.18, respectively. In a similar study Rodrigez-Marek (2000) found a mean ratio of 0.84 and a standard deviation of 0.28.

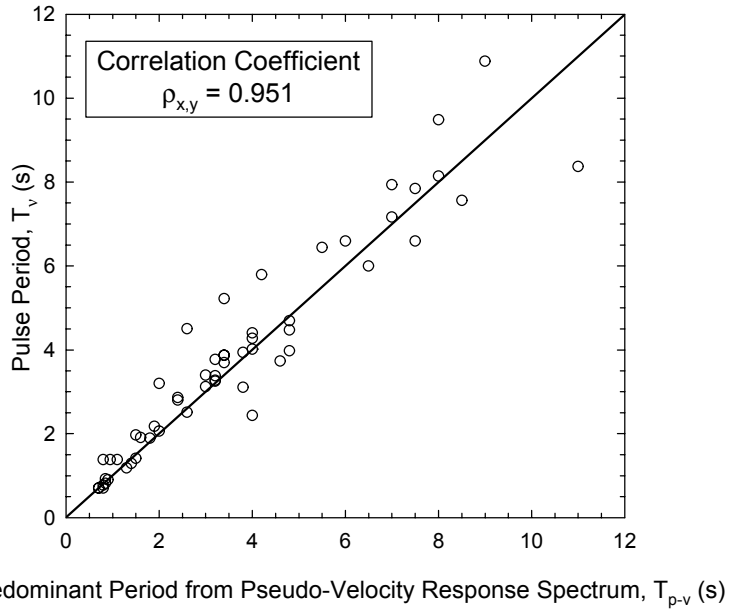

Figure 2. 12 Correlation between the Pulse Period and Predominant Period from Pseudo-Velocity Response Spectrum for the Records Used in This Study

Sommerville et al. (1999), utilizing large set of ground motion records from 15 earthquakes, proposed the following relationship for T_v:

$$\log_{10} T_v = -3.0 + 0.5M_w \tag{2.3}$$

where T_v is the pulse period (period of strongest pulse in velocity trace) in seconds and M_w is the moment magnitude of ground motion.

A similar study, both relating T_v and $T_{p\text{-}v}$ to magnitude, was presented by Rodrigez-Marek (2000). Using 48 strong motion records from 11 earthquakes, he proposed the following relationships:

$$\ln T_v = -5.81 + 0.97M_w \tag{2.4}$$

$$\ln T_{p\text{-}v} = -5.66 + 0.91M_w \tag{2.5}$$

where T_v is the pulse period (period of strongest pulse in velocity trace) in seconds and M_w is the magnitude of ground motion. Standard errors (σ_{total}) associated with Equations (2.4) and (2.5) were given as 0.51 and 0.61, respectively.

Alavi and Krawinkler (2001) proposed the following relation for $T_{p\text{-}v}$:

$$\log_{10} T_{p\text{-}v} = -1.76 + 0.31 M_w \tag{2.6}$$

where M_w is the moment magnitude.

T_v versus M_w and $T_{p\text{-}v}$ versus M_w relationships given above are plotted over the individual points found using the record set in Figures 2.13 and 2.14, respectively. It is evident from the two figures that although all relationships follow the trend observed in the data sets, they are not fully capable of predicting the applicable ranges for related variables. Additionally, the scatter in T_v-M_w graph (Figure 2.13) seems to be smaller compared to $T_{p\text{-}v}$-M_w graph (Figure 2.14). Large scatter seen in the figures may be due to other factors which are not taken into account in the proposed relationships.

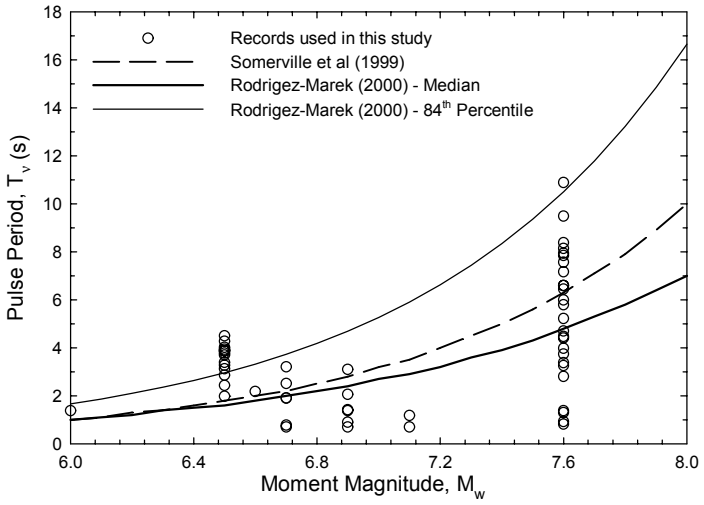

Figure 2. 13 Scatter Plot of the Records Used and T_v vs. M_w Relationships

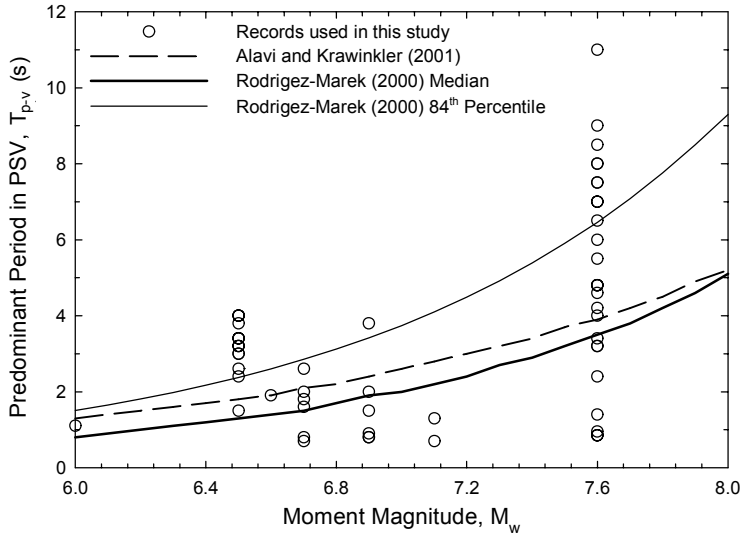

Figure 2.14 Scatter Plot of the Records Used and $T_{p\text{-}v}$ vs. M_w Relationships

In light of the observations stated above, it is reasonable to examine the variation in T_v with other parameters such as site to source distance and faulting mechanism. Variation of pulse period with distance may be inspected from the graph in Figure 2.15(a). A narrowing trend with increasing distance is hardly noticeable in this graph. Magnitude clusters significantly show the variation with magnitude which was selected as the governing parameter by other researchers. The graph in Figure 2.15(b) was prepared for making a rough comparison among pulse periods observed from events which have similar magnitudes but different faulting mechanisms. A rough conclusion that may be derived from this graph is that, for the data set used in this study, strike slip events tend to produce longer velocity pulses compared to reverse slip events.

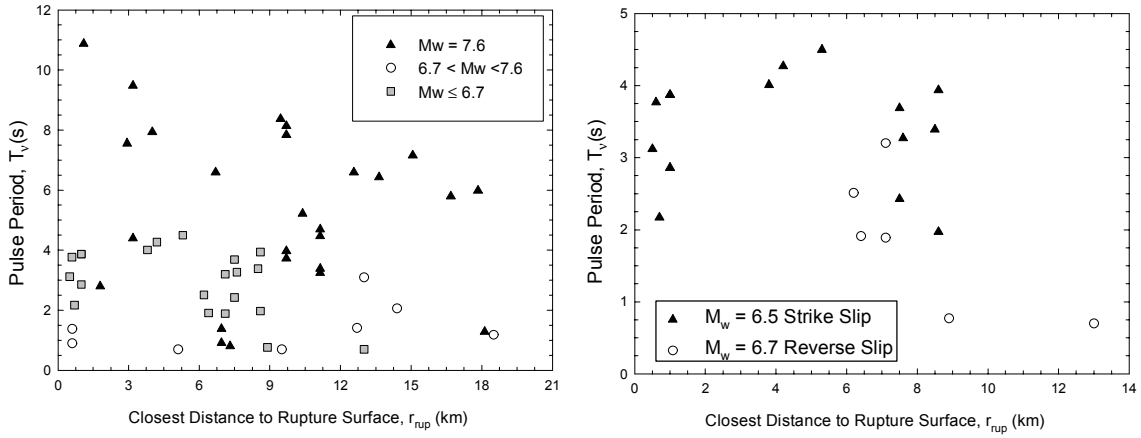

(a) (b)

Figure 2. 15 Variation of Pulse Period with Parameters Other than Moment Magnitude

2.5 Spectral Displacements of Ground Motion Components

Spectral displacements are the displacement demands imposed on the single degree of freedom structures by ground motions. Therefore, they are of primary importance for earthquake resistant design. Earthquake ground motion is a three dimensional motion. However, in common engineering applications only the two horizontal components are utilized. Using these two components, an infinite number of components in different directions, may be generated. Eventually, all these generated components would have different amplitude and frequency characteristics. As a result, they would have various different displacement spectra. Since it is not practical to analyze the structure under all these generated components, a severest component should be selected. In general, there is no such thing as "severest" component of a ground motion record if individual periods for maximum base shear are considered. Usually, for one period highest spectral displacement is observed in one direction, while for another period it is observed in another direction.

Somerville et al. (1997) state that, for the strong motion records showing effects of forward directivity, maximum spectral displacements are in the fault normal

component. However, for some cases the fault normal direction may not be readily available. Sometimes, a consensus on the layout of the fault can not be established or such information may not be reachable for a design engineer. Therefore, there is a need for a more practical method for finding the 'relatively' severest component of a near-fault ground motion.

In Figure 2.16, displacement spectra found by simple methods such as taking the arithmetic and geometric means of individual spectral displacements found from two recorded components are plotted. It is evident from the top four frames that there is no significant difference between taking the means and geometric means. Another important observation is that, records with pulse have noticeably higher spectral displacements compared to records without pulse. Akkar and Gülkan (2002) have studied the fault normal and maximum velocity direction components of near-fault strong motion records from 1999 Kocaeli (M_w=7.4) and 1999 Bolu-Düzce (M_w=7.2). Akkar and Gülkan (2002) pointed out that, the ground motion components in the maximum velocity directions, in general, have higher spectral drifts than other components. They have also stated that the maximum velocity direction does not always coincide with the fault-normal direction. In light of this study, spectral displacements in the maximum velocity direction are plotted in the two frames at the bottom of Figure 2.16. Noticeably, higher spectral displacements are seen in the maximum velocity direction components of strong motion records with pulse. It should also be noted that, such a difference is not observed in records without pulse.

In conclusion, when fault normal directions of the strong motion records are not readily available, a relatively severe component may be found in the maximum velocity direction.

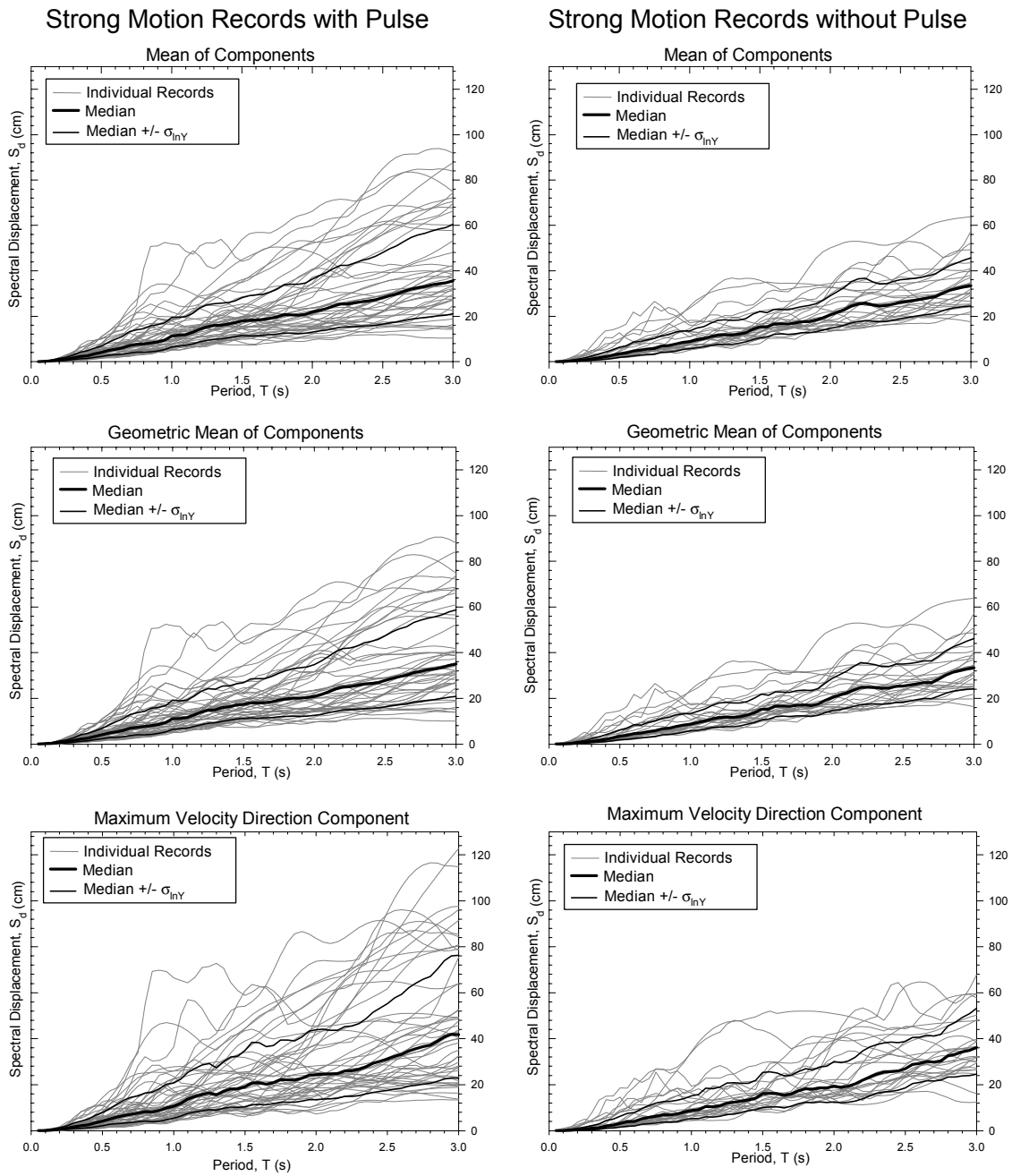

Figure 2.16 Comparisons among Spectral Displacements of Records with and without Pulse

Taking into account all of these observations it may be concluded that, near-fault ground motions have characteristics that are not observed in far-field ground motions. An in-depth understanding of these properties would eventually lead to development of reliable models for predicting demands imposed by near-fault ground motions on engineering structures. Such models are crucial both for designing earthquake resistant structures near-active faults and for reliable evaluation of existing structures affected by near-fault strong motions.

CHAPTER 3

BASIC THEORY AND DERIVATION OF EQUATIONS

3.1 Models and Analysis Procedures

In this chapter, elastic response of multi-degree-of-freedom (MDOF) systems and inelastic response of singe-degree-of-freedom (SDOF) systems subjected to near-fault ground motions will be analyzed. Despite the fact that, moment resisting frames are usually designed to yield under strong ground motion excitations, it is generally believed that analysis of the elastic response of these frames under near-fault excitations provides information on their response characteristics. During elastic MDOF response history analyses local displacement demands will be the main items of concern. In addition to examining the elastic response of conventional moment resisting frames, one of the main aims of this study is the enhancement of the simple drift estimation equation proposed by Gülkan and Akkar (2002). A set of coefficients will be introduced for further improving the predictive power of the equation by adding the capability of estimating the ground story drift ratios and maximum interstory drift ratios of frames having beams and slabs relatively more flexible than columns.

Response of a series of SDOF systems to the near-fault ground motions in the record set will be used to examine the fundamental characteristics of the response of

inelastic systems to near-fault ground motions. Using the results of these analyses, differences between the response of systems to records with and without pulse will be compared.

3.1.1 MDOF Models

3.1.1.1 Properties of the Idealized Frames

In order to capture the effects of different structural properties on the response, a set of idealized moment resisting frames were generated. Idealized frames were single-bay, rectangular plane frames, with a constant story height equal to 3 m and, bay width equal to 6 m. Structural configuration of a sample frame may be viewed in Figure 3.1. Only flexural deformations were considered in the structural members. P-delta effects were not taken into account in the analyses. The frames had uniform stiffness through their height. Moments of inertia of beams (I_b) were varied to investigate response characteristics of different frame systems, while moments of inertia of all the columns (I_c) were kept constant. The damping ratio for all modes of vibration was assumed to be equal to 5 percent of critical damping.

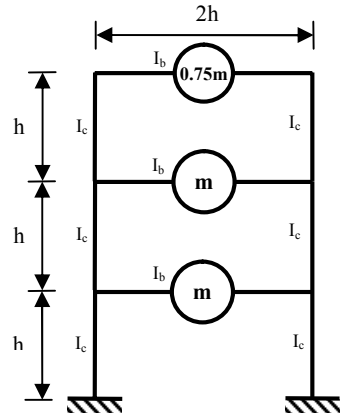

Figure 3.1 Representative Sketch of the Structural Configuration of Idealized Frames

The story masses were assumed to be concentrated at the floor levels and rotational inertias of stories were neglected. Mass of the roof story of each idealized frame was set to be 75% of the other stories. Story masses were adjusted so that the fundamental period T_n of the frames were equal to the period found from the approximate relation below:

$$T_n = 0.1N \qquad (3.1)$$

where N is the number of stories and T_n is the fundamental period in seconds.

Beam-to-column stiffness ratio (ρ), originally named as the joint rotation index by Blume (1968), is a parameter for quantifying the distribution pattern of lateral deformations in frames. ρ is calculated as follows:

$$\rho = \frac{\sum_{beams} \frac{I_b}{L_b}}{\sum_{columns} \frac{I_c}{L_c}} \qquad (3.2)$$

where I_b and L_b are the moments of inertia and lengths of the beams in the story closest to mid-height of the building, respectively, and I_c and L_c are the moments of inertia and heights of the columns, in the story closest to mid-height of the building, respectively. It should be noted that units of moments of inertia and lengths should be consistent. It is assumed that for a building with nearly uniform distributed stiffness, a representative value of ρ may be found by using the member properties of the elements in the mid-height of the building. For the case of idealized frames used in this study Equation 3.2 reduces to:

$$\rho = \frac{I_b}{4I_c} \qquad (3.3)$$

The parameter ρ is a measure of relative beam-to-column stiffness. It is directly related to the degree of frame action. When ρ equals to zero, indicating I_b equals to

zero, and beams do not impose any restraint to rotation of joints. As a result, system shows an overall lateral deformation pattern, like a vertical cantilever bending beam. Solid structural walls, with no considerable framing or effective spandrels, would portray such deformations. When, the ρ equals infinity, theoretically beams are infinitely stiff relative to columns and joint rotations are completely restrained. This frame model is named as shear building or shear frame in the literature (Ayre 1956, Paz 1985, Chopra 2000). Paz (1985) has stated that the name shear building has originated from the overall lateral deformation pattern of these frames which is similar to a shear beam deflected by shear forces. It should be noted that, for most of the time, the deformations taken into account in the analysis of shear buildings are only the flexural deformations of structural components. It should also be noted that in this study the deformations taken into account are only the flexural deformations of structural members. In the shear buildings, since all joint rotations are completely restrained, all the columns would bend in double curvature in the displaced configuration. Fundamental mode shapes of idealized four story frames, with various ρ values, are shown in Figure 3.2.

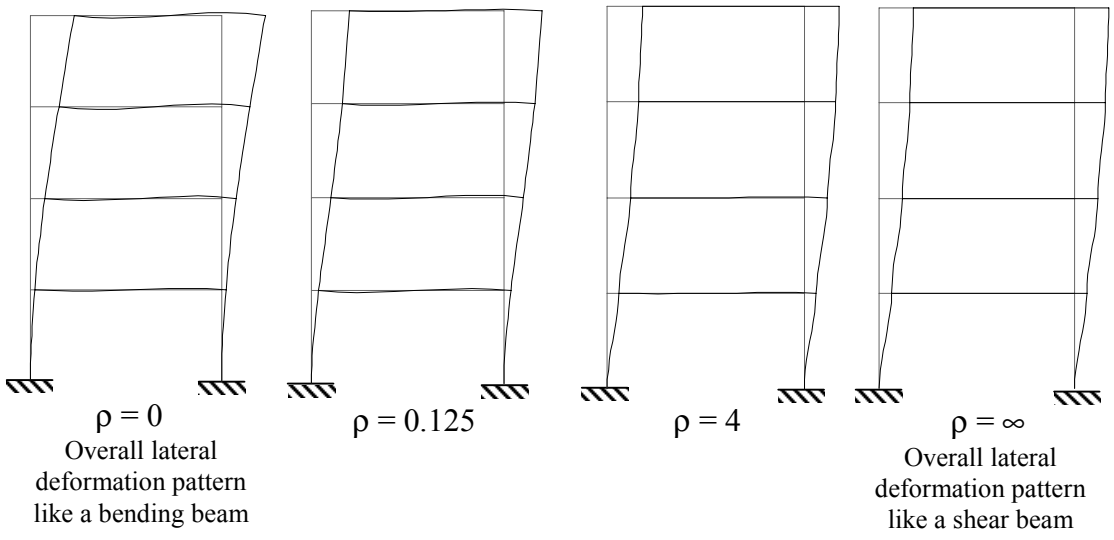

Figure 3.2 Fundamental Mode Shapes of Idealized Frames with Different ρ Values

Blume (1968) calculated ρ values, changing between 0.1 and 1.55, for 27 frames designed by several engineers. In the light of this observation, for the MDOF analyses in this study, moment resisting frames with ρ equal to 0.125, 0.25, 0.5, 0.75, 1, 1.5, 2, 3 and 4 were used. A separate case, utilizing shear-frame model with completely restrained joint rotations was included in the analysis ($\rho = \infty$).

A total of 190 moment resisting frames (corresponding to 19 different number of stories from 2 to 20 and 10 different ρ values) were used in the MDOF analyses. Studying such a wide set of moment resisting frames led to better understanding of various factors affecting the response of frames.

3.1.1.2 Analysis Procedure for MDOF Systems

For the elastic response history analysis and inspection of modal properties, a special MATLAB program was prepared. The program has the capability of generating any frame with the given number of story, fundamental period and ρ. The seismic response of frames was found by superposing the individual modal responses. Response in each mode was computed by exact solution of the response of linear system under the ground motion excitation, interpolated over each time step. This numerical procedure has proven to be useful, especially when the excitation is defined at closely spaced time intervals, such as the ground motion records used in this study (Chopra 2000).

Organization of the output file was arranged so that, it could be directly imported to common spreadsheet programs. This compatibility led to easier examination and processing of the output data.

3.1.2 SDOF Systems

3.1.2.1 Properties of the SDOF Systems

A set of inelastic SDOF systems was used for analyzing the basic response characteristics of yielding systems under near-fault ground motions. Natural periods of SDOF systems covered the range from 0.1 s to 3.0 s, with increments of 0.05s. In order to examine the significance of pulse period, which was defined in Chapter 2, on the inelastic displacement demands imposed on structures a series SDOF systems having natural period to pulse period ratios (T_n / T_v) between from 0.1 to 3 were generated for each strong motion record with pulse. Damping was set to be equal to 5 percent of critical. Elastoplastic load deformation model was used for simulating the inelastic behavior of SDOF systems. This load deformation model is commonly used for modeling the inelastic behavior of structural elements that display small strength or stiffness degradation. This is one of most widely used hysteretic models. Figure 3.3 shows the load deformation curve of a typical elastoplastic system and corresponding linear elastic system.

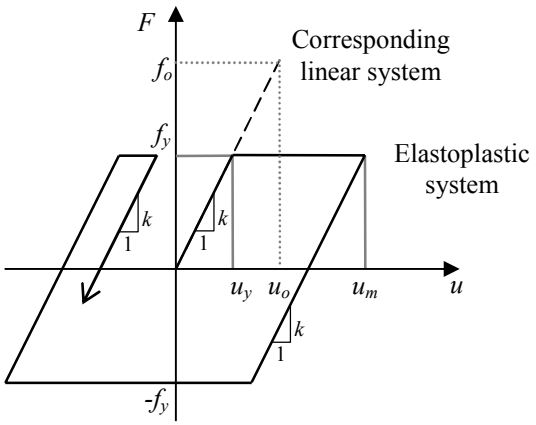

Figure 3.3 Elastoplastic Load Deformation Model and Corresponding Linear Elastic System

In Figure 3.3, F is the force applied on the system, k is the stiffness of the system in the elastic range, u_y is the yield displacement, f_y is the yield strength, f_o is the maximum earthquake force on the corresponding linear system, u_m is the maximum displacement of inelastic system and u_o is the maximum displacement of the corresponding linear system.

Strength reduction factor (R), is the ratio of the strength demand imposed on the linear elastic system to the strength capacity of corresponding inelastic system with the same natural period. It is formulated as follows:

$$R = \frac{f_o}{f_y} = \frac{u_o}{u_y} \qquad (3.4)$$

. R is a convenient parameter for normalizing the capacity of a system and it has been used as the main capacity parameter in this study. Inelastic response history analyses were performed for SDOF systems having R's equal to 1.5, 2, 3, 4, 5, 6, 7 and 8.

3.1.2.2 Analysis Procedure for SDOF Systems

A special FORTRAN program was prepared for performing elastic and inelastic response history analysis of SDOF systems. The program was based on Newmark's (1959) Linear Acceleration Method for Nonlinear Systems.

The special FORTRAN program had the capability of calculating the displacement response spectra for a given list of records and a given set of R_y values automatically for any range of periods.

3.2 Effects of Near-Fault Ground Motions on the Response of Elastic Moment Resisting Frames

Results obtained from the elastic response history analysis of the idealized frames subjected to near-fault ground motions provided a comprehensive data. In this section, observations made on the effects of strong ground motion pulses on the response of elastic moment resisting frames are presented. The importance of local displacement demands, particularly for the structures excited by near-fault ground motions, has been addressed by several studies (Iwan 1997, Alavi and Krawinkler 2001, Gülkan and Akkar, 2002). Studies by Alavi and Krawinkler (2001) have shown that high amplitude pulses observed in some of the near-fault ground motions result in significantly high local displacement demands. In light of this observation, ground story drift ratio (GSDR) and maximum interstory drift ratio (MIDR) were selected as the main displacement demand parameters in this study. Ground story drift ratio (GSDR) is defined as the lateral drift of the ground story normalized by the height of the ground story columns and maximum interstory drift ratio (MIDR) is defined as the maximum interstory displacement divided by the story height. $GSDR_{ALL}$ and $MIDR_{ALL}$ are short for ground story drift ratios and maximum interstory drift ratios found by considering the contributions of all modes, respectively. Similarly, $GSDR_1$ and $MIDR_1$ are the ground story drift ratios and maximum interstory drift ratios found by considering only the contribution of the first mode, respectively.

3.2.1 Effects of Pulse Period on Local Displacement Demands

In order to examine the effects of strong velocity pulses on the local displacement demands, ratio of fundamental period to pulse period (T_n/T_v) were computed for all the individual response history analyses of frames. $GSDR_{ALL}$ versus T_n/T_v points are plotted in Figure 3.4. It may be observed from these plots that, GSDR's are noticeably higher near $T_n/T_v=1$. In other words, for the frames with fundamental periods close to pulse period GSDR's are significantly higher, compared to frames with

longer or shorter fundamental periods. Strong correlation between the predominant period in the pseudo-velocity spectrum and the pulse period was examined in Chapter 2. Therefore, these high displacement demands observed in Figure 3.4 near $T_n/T_v=1$, are in confirmation of peaks observed in the pseudo-velocity spectra of near-fault ground motions with pulse. It should also be noted that, approximate GSDR and MIDR estimation equations developed in this study are based on spectral displacements. As a result, these equations inherently take into account the effects of strong velocity pulses on GSDR and MIDR.

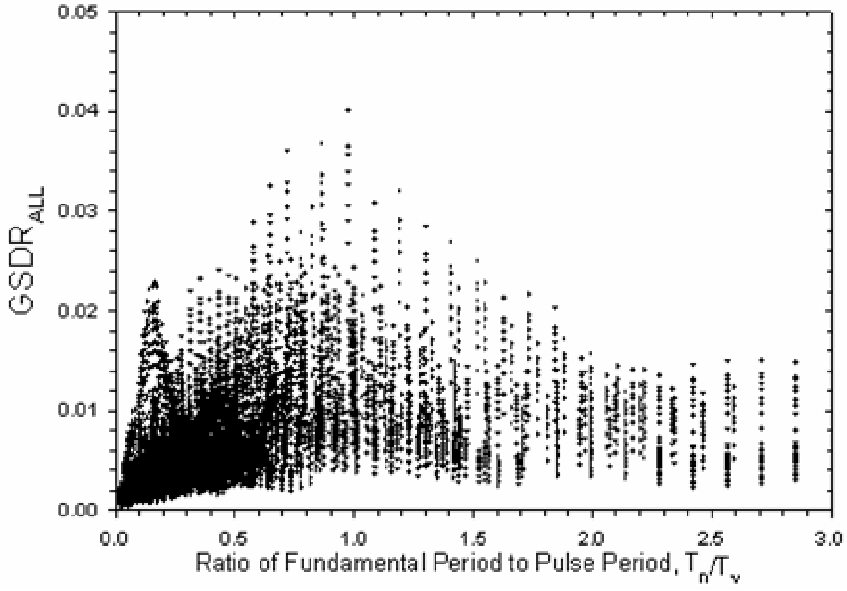

Figure 3.4 $GSDR_{ALL}$ versus T_n/T_v Scattergram

3.2.2 Effects of Pulse Period on the Contribution of Higher Modes

Alavi and Krawinkler (2001) have analyzed the effects of pulse-type of ground motions on frame structures. Results of those analyses have shown that, the displacement profiles for MDOF frames with fundamental periods larger than the pulse

were significantly different compared to the displacement profiles of frames with fundamental periods smaller than pulse period. They observed that for structures with T_n/T_v smaller than 1, the displacement profiles resembled the fundamental mode shape. However, for structures with T_n/T_v greater than 1, effects of higher modes on the overall response were observed to be more significant and displacement profiles showed traveling wave effects.

In order to examine the significance of these effects on the results obtained from the elastic MDOF response history analysis, the ratios of $GSDR_1$ to $GSDR_{ALL}$ and $MIDR_1$ to $MIDR_{ALL}$ were computed from all response history analyses. These ratios quantify the contribution of higher modes to overall response. Deviation of these ratios from one implies an increase in effects of higher modes on response. In order to visualize the average trend, mean of these ratios for each ρ and T_n/T_v was computed. It may be noticed from Figure 3.4 that an important part of the data points lie in the $T_n/T_v < 1$ region. This is a result of ground motions, in general, having significantly longer pulse periods compared to fundamental periods of idealized frames used in this study. It was thought that such a crowding in the $T_n/T_v < 1$ range might result in statistically questionable observations. To see the effect of this crowding on the mean curves, the same computations were repeated using only the strong motions records with $T_v < 2s$. This way the bulge in $T_n/T_v < 1$ range was eliminated to some degree.

In Figure 3.5, resulting mean curves found may be seen. It is evident from these graphs that elimination of records with $T_v > 2$ s did not affect the overall trend. It can be concluded from Figure 3.5 that for frames with fundamental periods shorter than twice the pulse period of ground motion, effects of higher modes on the overall response is, on the average, not very significant. However for the structures with $T_n/T_v > 2$ effects of higher modes on the response become more significant. A significant dependence between effects of higher modes and ρ may not be inferred from the mean lines related to GSDR in Figure 3.5. From the mean curves related to MIDR in Figure 3.5, it may be

concluded that effects of higher modes on the response are more significant for frames with higher ρ's.

These results are similar to the observations made by Alavi and Krawinkler (2001). The only difference is that, they had indicated the effects of contribution of higher modes to be significant for frames with $T_n/T_v > 1$, whereas results of this study show that the effects of higher modes become more noticeable for frames with $T_n/T_v > 2$. This difference may be a result of specific displacement demands, GSDR and MIDR, examined in this study.

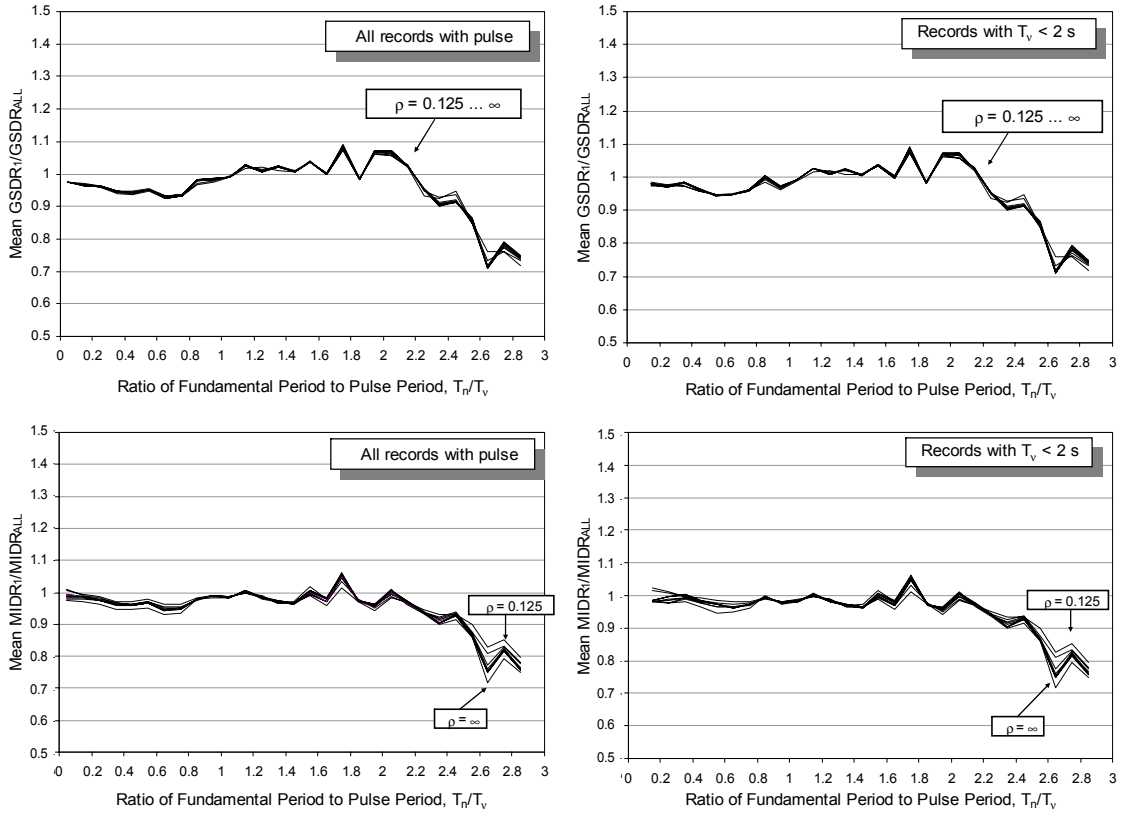

Figure 3.5 Effect of Ratio of Fundamental Period to Pulse Period on the Contribution of Higher Modes

In conclusion, response of frames to near-fault ground motions is affected by the ratio of fundamental period to pulse period. For the systems with $T_n/T_v<1$, the fundamental mode of vibration is dominant in the overall response, whereas for systems $T_n/T_v > 2$ contributions of higher modes significantly affect the overall response of systems.

3.2.3 Effects of Strong Motion Pulses on Lateral Displacement and Interstory Drift Profiles of Elastic Moment Resisting Frames

In order to examine the effects of strong ground motion pulses on the lateral displacement profiles of the idealized frames, maximum story displacements computed for each story were normalized with respect to roof displacement. Statistics associated with these normalized displacement profiles were computed so as to see the ranges of different lateral displacement profiles. In Figure 3.6, lateral displacement profiles computed for 10 and 20 story frames with ρ's equal to 0.125, 0.75 and ∞ are represented together with their fundamental mode shapes. It may be seen from Figure 3.6 that, in general, displacement profiles found for 10 story frames are very close to fundamental mode shapes. However, some deviation from the fundamental mode shape may be observed in the graphs associated with 20 story frames.

In order to examine the effects of near-fault records with pulse on the local displacement demands, interstory drift profiles of the frames were investigated. For this purpose maximum interstory drifts computed for all stories in each analysis were normalized with the maximum interstory drift. Statistical parameters associated with these interstory drift profiles were computed to analyze the overall trend. Results found for six sample frames are presented in Figure 3.7. On the left and right sides of Figure 3.7, ranges of interstory drifts are plotted for 10 and 20 story frames, respectively. It may be observed from Figure 3.7 that for the idealized frames with smaller ρ values location of maximum interstory drift shifts upwards. This trend may both be observed in the fundamental mode shapes and response history results.

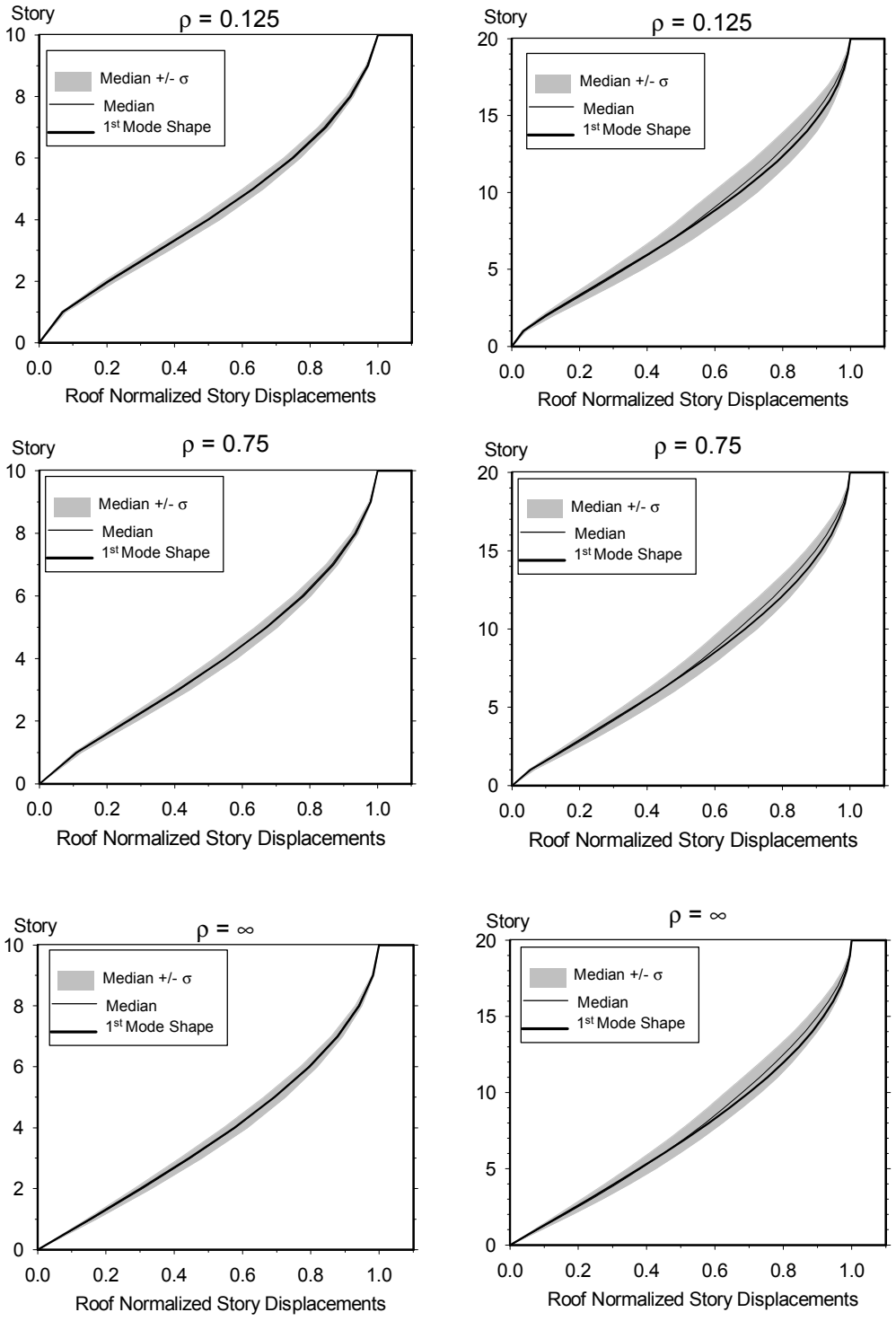

Figure 3.6 Displacement Profiles of Moment Resisting Frames Subjected to Near-Fault Ground Motions with Pulse

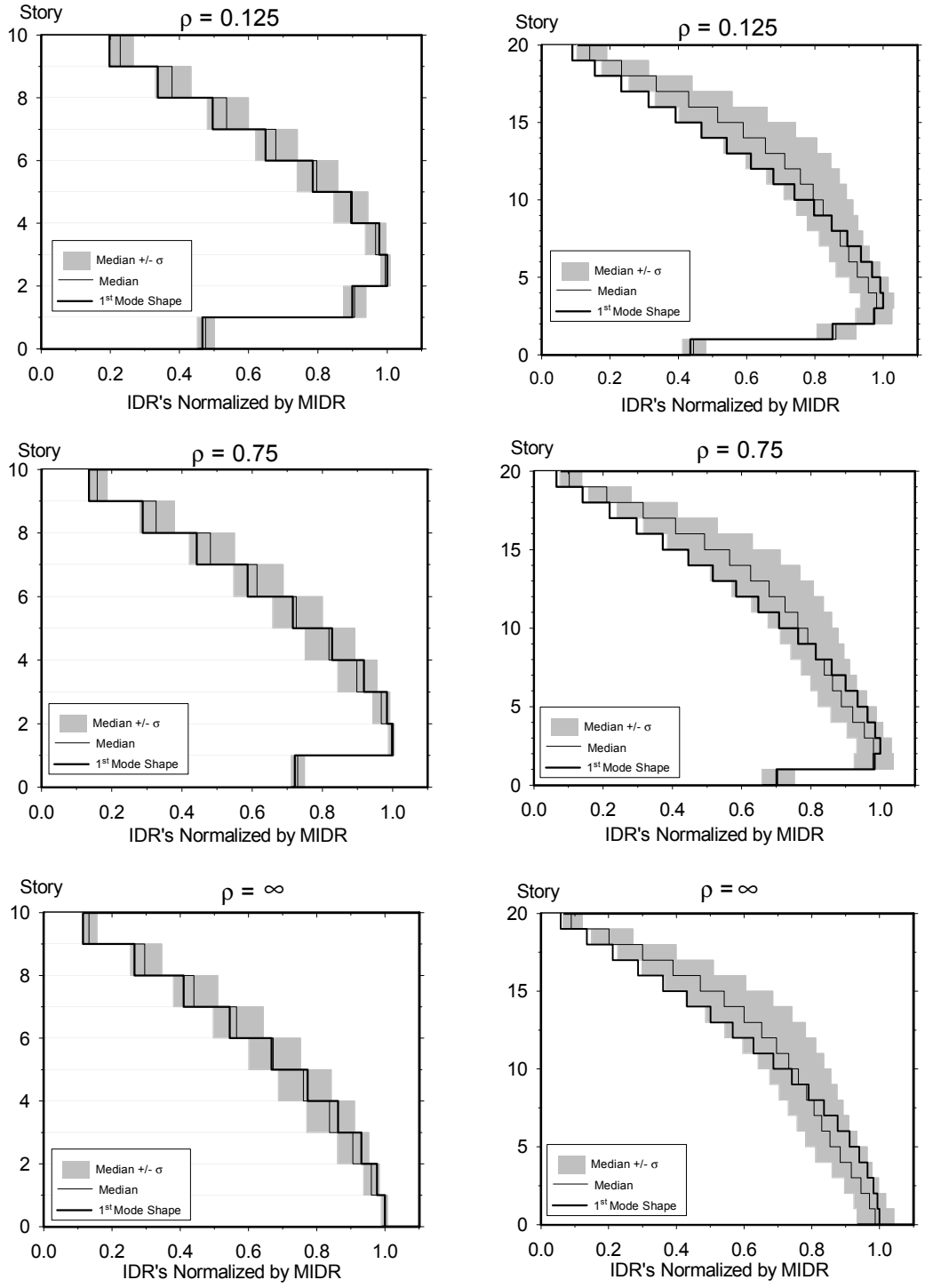

Figure 3.7 Interstory Drift Profiles of Idealized Moment Resisting Frames Subjected to Near-Fault Ground Motion with Pulse

Moreover, it may be seen that interstory drifts computed for upper stories are higher than those computed using only the fundamental mode shape; this is particularly more noticeable in the graphs related to 20 story frames. These deviations from the fundamental mode shape interstory drift profiles are results of higher mode effects.

In conclusion, higher mode effects cause some deviations in distribution of interstory drifts, particularly in the upper stories. However, when the location of maximum interstory drift is of concern, these deviations from the fundamental mode shape are not very significant. Also it should be noted that, the effects of higher modes on the magnitudes of ground story drift and maximum interstory drift will be further investigated in the following sections.

3.3 Derivation of the Equations Related to Elastic Response of Moment Resisting Frames

3.3.1 Equation for Estimating the Ground Story Drift Ratios of Moment Resisting Frames

Displacement-based design and evaluation methods emphasize estimation of displacement demands. Some of major studies, proposing approximate methods for the estimation of displacement demands, were summarized in Section 2.1. One of these studies was performed by Gülkan and Akkar (2002). They derived an approximate expression, based on the fundamental mode response of shear beam model, for estimating the ground story drift ratios of frames. The approximate equation for the ground story drift ratio based on the shear beam model ($GSDR_{SH}$) is given as follows:

$$GSDR_{SH} = 1.27 \frac{S_d(T,\xi)}{h} \sin\left(\frac{\pi}{2N}\right) \qquad (3.5)$$

where N is the number of stories, h is the height of the ground story columns, $S_d(T,\xi)$ is the displacement spectrum ordinate corresponding to the fundamental period T and

damping ratio in the fundamental mode, ξ. It should be noted that $S_d(T,\xi)$ and h should be in consistent units. Performance of Equation 3.5 was evaluated using a set of 25 near-fault ground motions by Gülkan and Akkar (2002) and it was found that Equation 3.5 provided sufficient accuracy for estimating the ground story drift of shear frames.

Since Equation 3.5 have been derived based on the shear beam model and it may be conveniently used for estimating the ground story drifts of frames having high ρ values (beams and slabs relatively stiffer than columns – shear frames). However for the case of moment frames having low ρ values (beams and slabs relatively more flexible than columns), Equation 3.5 may provide inaccurate estimates of GSDR. Such frames would portray overall lateral deformation patterns like a cantilever bending beam. As a result an expression solely based on the shear beam model is insufficient for estimating the ground story drifts of frames having low ρ values. One of the fundamental aims of this study is to introduce a set a modifying coefficients to be used with Equation 3.5 for estimating the GSDR's and MIDR's of general moment frames. This aim was achieved by establishing two coefficients as follows:

$$GSDR_{MF} = \gamma_{MF} GSDR_{SH} \quad (3.6)$$

$$MIDR_{MF} = \gamma_{MIDR} \gamma_{MF} GSDR_{SH} \quad (3.7)$$

where $GSDR_{MF}$ is the (approximate) ground story drift ratio of a general moment frame, γ_{MF} is the general moment frame GSDR to shear frame GSDR conversion coefficient, $MIDR_{MF}$ is the approximate maximum interstory drift ratio of the general moment frame and γ_{MIDR} is the ground story drift ratio to maximum interstory drift ratio conversion coefficient.

In the development of these approximate coefficients four assumptions were made:

1. Estimation of the first mode response results in an adequately accurate estimate of the total response.
2. Mass distribution in the structure is nearly equivalent to that of idealized frames
3. Stiffness is nearly uniform in structure.
4. Fundamental period of the system is nearly equal to the period calculated using Equation 3.1.

In order to verify the first assumption, modal response history analyses of each 190 idealized frame under 148 near-fault ground motions were made. GSDR's and MIDR's found from the modal response history analyses using all modes and only the first mode were calculated. Results of these 28120 response history analyses have provided an extensive data for verification of the first assumption. Results obtained for strong motion records with and without pulse were presented separately, so as to examine the effects of excitation type on the contribution of higher modes to the response.

In order to find the statistical parameters associated with the error introduced by considering only the participation of the first mode, following ratio was used:

$$Error_{GSDR} = \frac{GSDR_1}{GSDR_{All}} \qquad (3.8)$$

where $Error_{GSDR}$ is the error in GSDR for a single response history analysis, $GSDR_1$ is the contribution of the first mode to ground story drift ratio, $GSDR_{ALL}$ is the ground story drift ratio found by considering all modes. Ranges of $Error_{GSDR}$'s for the records with and without pulse may be inspected in Figures 3.8 and 3.9.

Similar to the computations performed for GSDR, error resulting from consideration of only the first mode contribution to MIDR was computed as follows:

$$Error_{MIDR} = \frac{MIDR_1}{MIDR_{All}} \qquad (3.9)$$

where $Error_{MIDR}$ is the error in *MIDR* for a single response history analysis, $MIDR_1$ is the maximum interstory drift ratio found considering the contribution of only the first mode, $MIDR_{ALL}$ is the maximum interstory drift ratio found by considering the contributions of all modes. Means and standard deviations of the errors may be inspected in Figures 3.10 and 3.11 for the records with and without pulse, respectively.

In all of those figures (Figures 3.8, 3.9, 3.10 and 3.11) effects of higher modes are more pronounced in the range of longer periods. Although there is an increasing trend in the underestimation, for periods less than 1.2 s error lies in acceptable ranges. Even for T_n = 2.0 s the error introduced by considering only the contribution of first mode to response is less than -20 percent with a probability of 84 percent. A significant dependence between ρ and error is not observed from the graphs. However, it may easily be noticed that contributions of higher modes to response are more effective for GSDR compared to MIDR. Furthermore, it may be noticed that contribution of higher modes are more effective on the response of structures excited by strong ground motions with pulse compared to those without pulse. The difference between the responses of the systems to records with and without pulse is more evident in the graphs related to MIDR (Figures 3.10 and 3.11)

In conclusion, by looking at Figures 3.8, 3.9, 3.10 and 3.11 it may be observed that, for the regular structures, such as the idealized frames used in this study, estimating only the contribution of first mode to response may provide a rough estimate of overall response. It should also be noted that, this conclusion has been derived for frame structures having fundamental periods between 0.2 and 2 s. Although Figures 3.8, 3.9, 3.10 and 3.11 have been developed for validating the first assumption, error ranges found from these figures may also be used as an estimate of the error associated with considering only the contribution of the first mode to overall response for regular frame structures in the given period range.

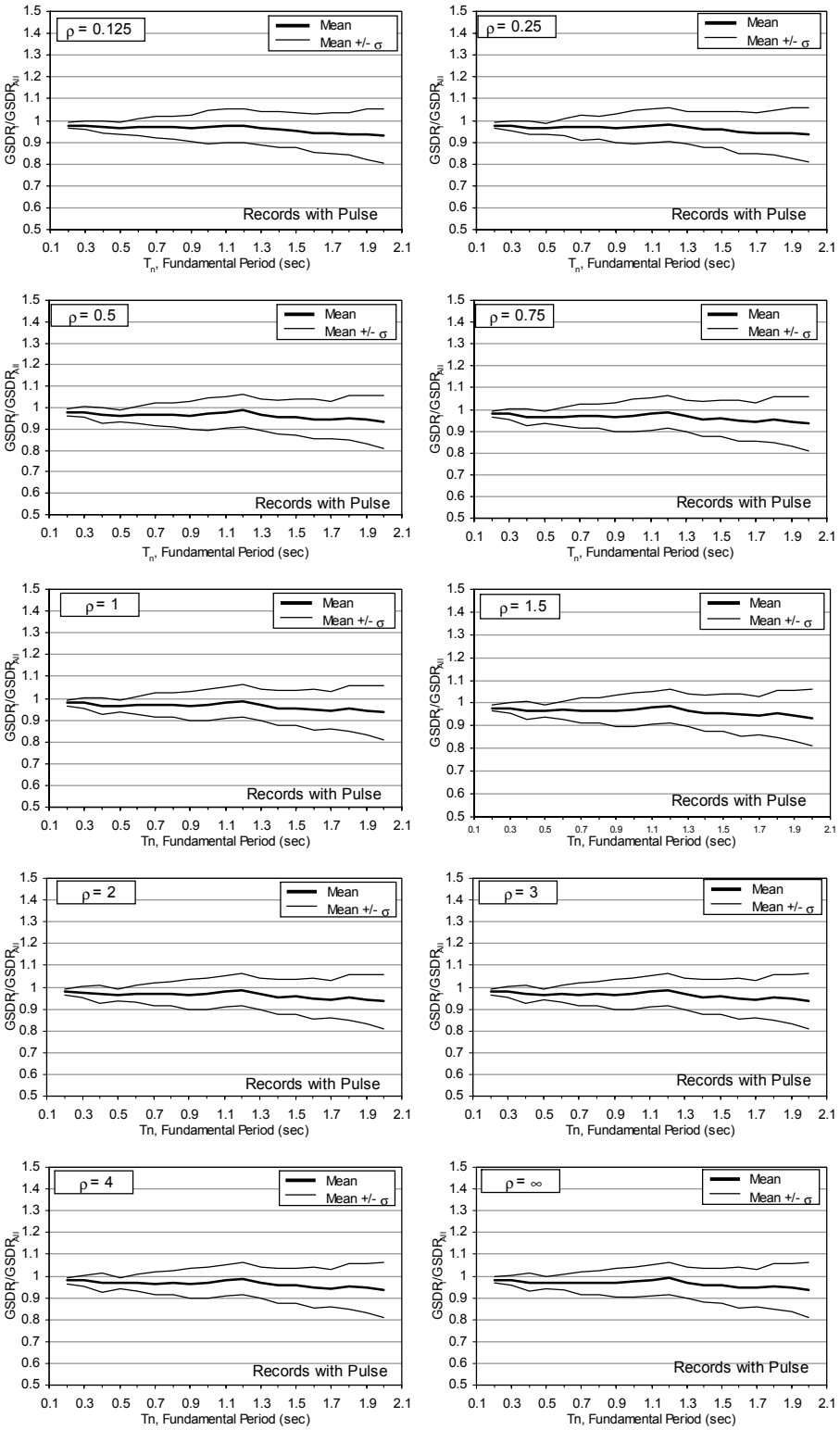

Figure 3.8 Error Statistics for Considering the Contribution of Only the First Mode to GSDR (Records with Pulse)

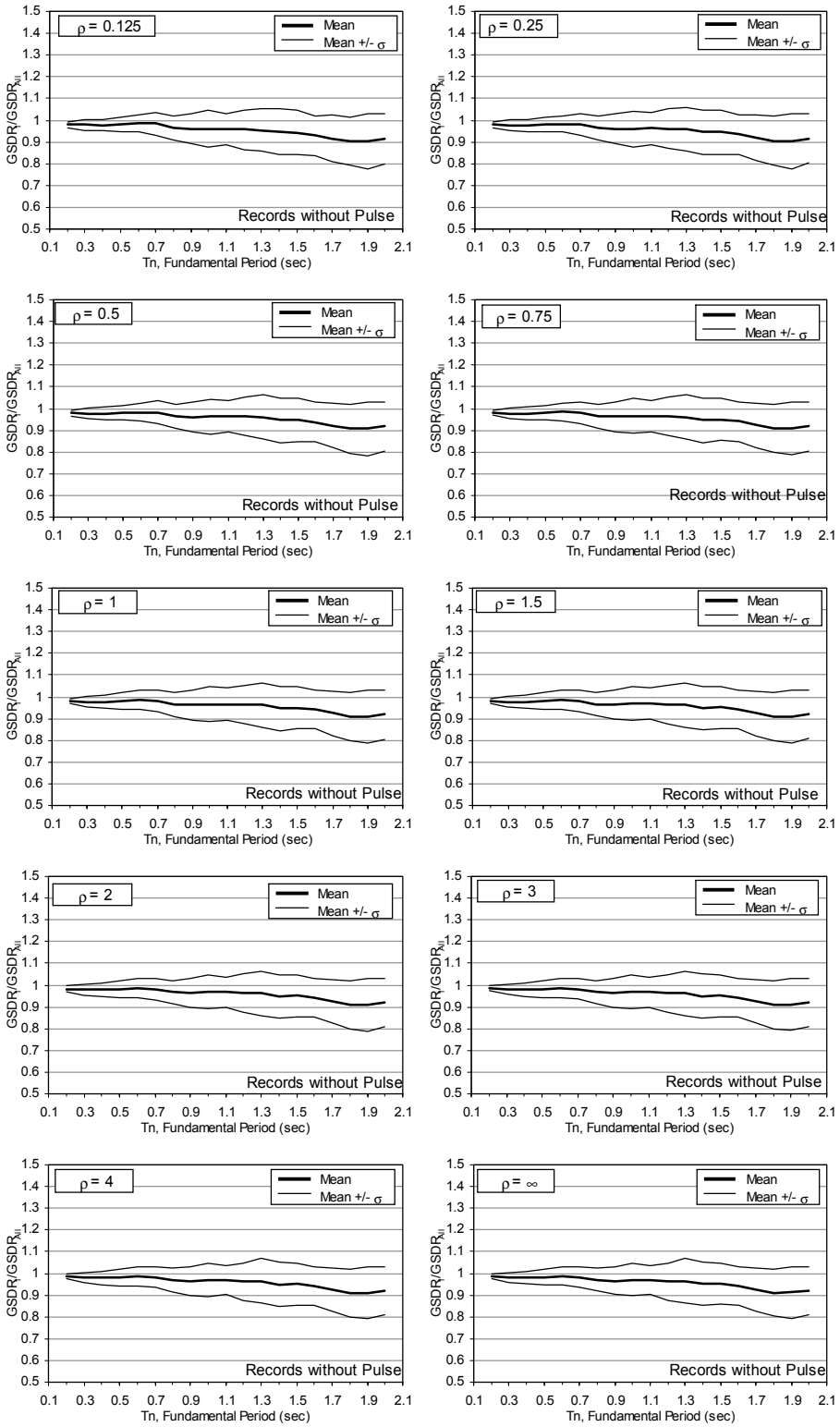

Figure 3.9 Error Statistics for Considering the Contribution of Only the First Mode to GSDR (Records without Pulse)

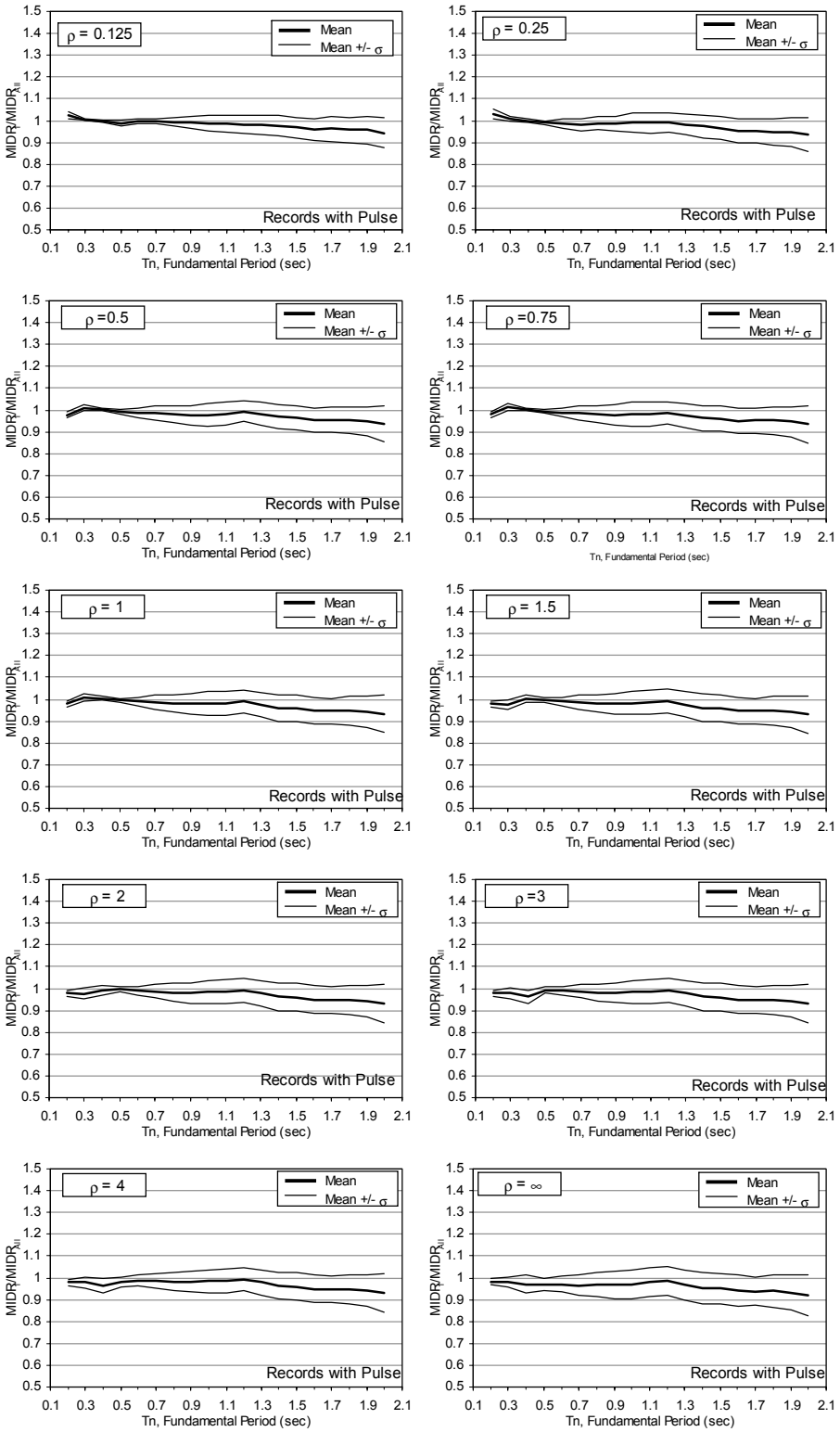

Figure 3.10 Error Statistics for Considering the Contribution of Only the First Mode to MIDR (Records with Pulse)

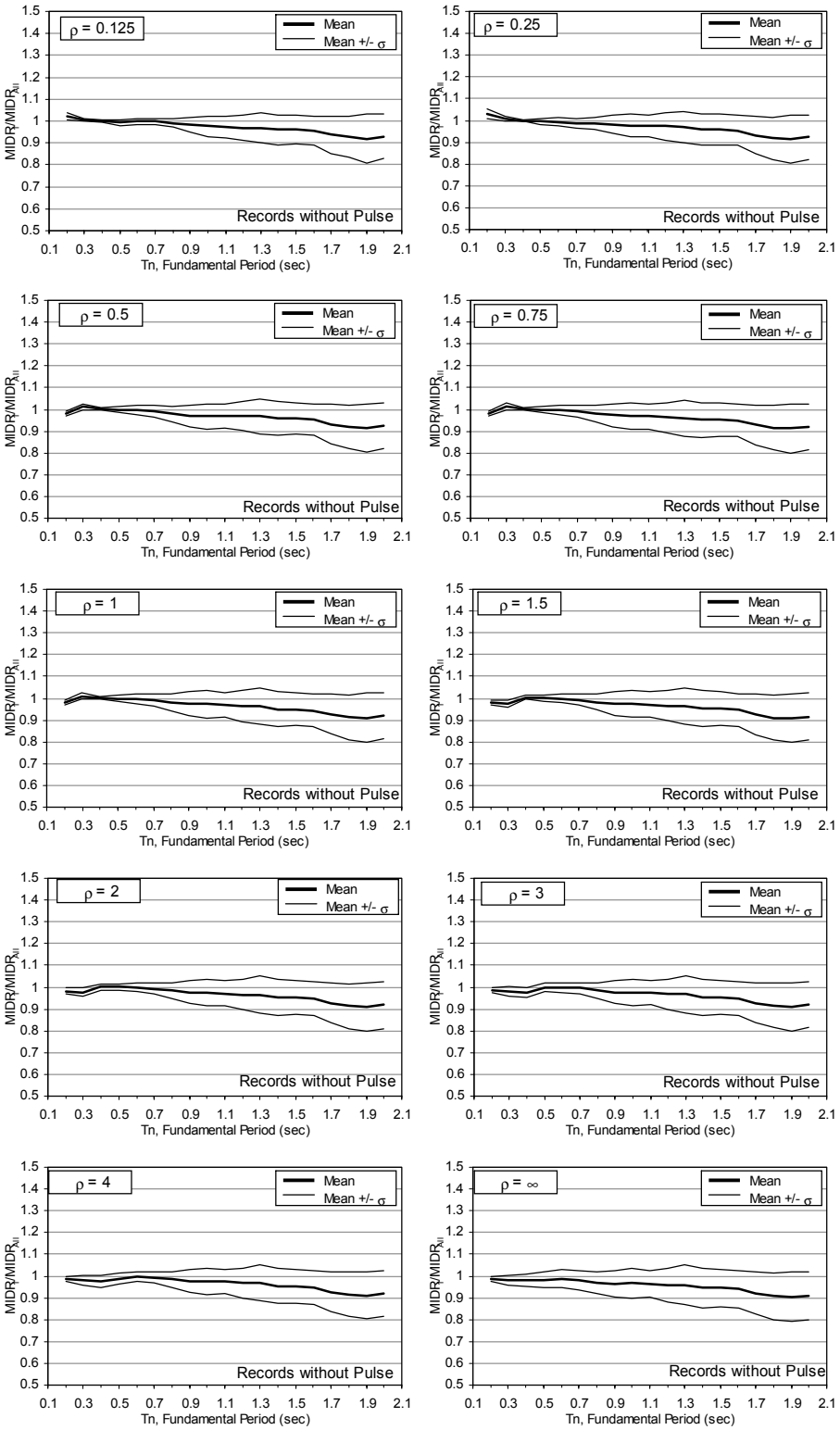

Figure 3.11 Error Statistics for Considering the Contribution of Only the First Mode to MIDR (Records without Pulse)

In order to establish equations for γ_{MF} and γ_{MIDR}, principles of modal analysis were employed. The theory underlying the modal analysis has been summarized by Chopra (1996). Principles of modal analysis states that the contribution of the n^{th} mode to nodal displacements ($u_n(t)$) may be found using the relationship below:

$$u_n(t) = \Gamma_n \phi_n D_n(t) \qquad (3.10)$$

$$\text{where} \quad \Gamma_n = \frac{\phi_n^T m \iota}{\phi_n^T m \phi_n}$$

where Γ_n is the modal participation factor of the n^{th} mode, ϕ_n is the n^{th} mode shape vector, m is the mass matrix of the system, ι is the influence vector and $D_n(t)$ is the displacement of the SDOF system with vibration properties, fundamental period T_n and damping ratio ξ_n, equal to properties of the n^{th} mode of the MDOF system, excited by the same ground motion. Since $D_n(t)$ for systems with the same period and damping are the same, γ_{MF} only depends on the first mode participation factors and the fundamental mode shapes of the moment frame and shear frame. γ_{MF} may be formulated as follows:

$$\gamma_{MF} = \frac{\Gamma_1^{MF} \phi_{1,1}^{MF}}{\Gamma_1^{SH} \phi_{1,1}^{SH}} \qquad (3.11)$$

where Γ_1^{MF}, Γ_1^{SH} are the first mode participation factors of the moment frame and shear frame, respectively, $\phi_{1,1}^{MF}$, $\phi_{1,1}^{SH}$, are the ground story drifts of the moment frame and shear frame in the first modal shapes. Equation 3.11 can be defined as the ratio of participation of the first mode to ground story drift of a moment frame to the participation of the first mode to the ground story drift of a shear frame.

The ratio in Equation 3.11 was computed for all the idealized frames used in the study. In Figure 3.12, results of Equation 3.11 for various T_n's and ρ's have been plotted. It can be seen that, γ_{MF} is significantly influenced by ρ. For small ρ values, such as $\rho = 0.125$, γ_{MF} even falls below 0.5.

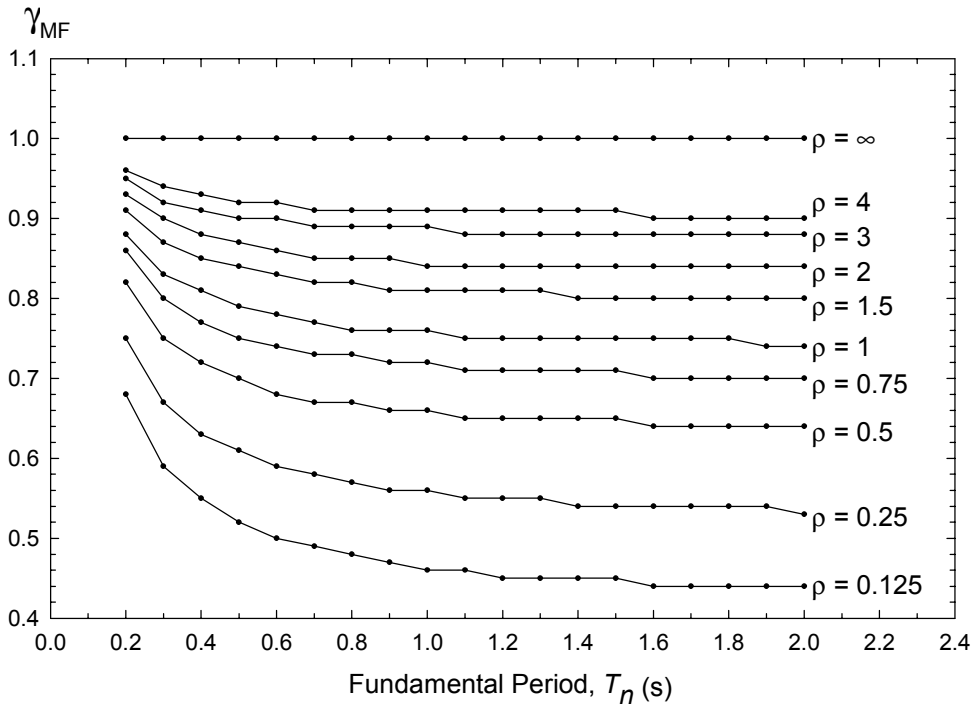

Figure 3.12 Variation in γ_{MF} with T_n and ρ

In order to take into account this difference and improve the estimates found using Equation 3.5, conversion factors found from Figure 3.12 may be utilized. Conversion factors for ρ values which are not given in the chart may be approximately found by linear interpolation. However, use of such a chart may not be practical for general design and evaluation purposes. An equation for finding γ_{MF}, based on ρ and T_n (or number of stories) would be much more useful. Regarding this fact, two stage nonlinear regression analyses, were performed on the curves in Figure 3.12. For all regression analyses performed in this study, a commercial curve fitting program (SYSTAT 2002) was used. This program employs the Levenburg-Marquardt algorithm for fitting non-linear equations. Sum of squares of residuals was selected as the fitting parameter in all fitting operations.

The following equation is the approximate expression found for γ_{MF}:

$$\gamma_{MF} = a_{MF}(\rho) + \frac{b_{MF}(\rho)}{T_n}$$
$$where \quad a_{MF}(\rho) = \frac{1}{1 + 0.35/\rho^{0.65}} \quad and \quad b_{MF}(\rho) = \frac{1}{8 + 25\rho^{0.4}} \qquad (3.12)$$

where T_n is the fundamental period and ρ is the beam-to-column stiffness ratio at the story closest to mid-height of the building. Theoretically, γ_{MF} should approach to 1 for all periods as ρ approaches infinity. It may easily be seen that for $\rho = \infty$ a_{MF} in Equation 3.12 equals 1 and b_{MF} equals zero. Hence, Equation 3.12 satisfies the theoretical boundary condition.

Deviation of the approximate γ_{MF} values found using Equation 3.12 from the theoretical analysis may be seen in Figure 3.13. It may be observed from Figure 3.13 that for the range of ρ and T_n values considered, deviation from theoretical value is between +5 percent and -2 percent. As a result, these values are accurate enough for a simple estimation. Nonlinearity of the deviation may be understood from the ρ values indicated in Figure 3.13.

In conclusion, when Equation 3.12 is used together with Equation 3.5 as a coefficient, approximate estimates of GSDR of conventional moment resisting frame structures may be obtained. Error statistics associated with the estimates obtained from Equations 3.12 and 3.5 will be evaluated in Chapter 4.

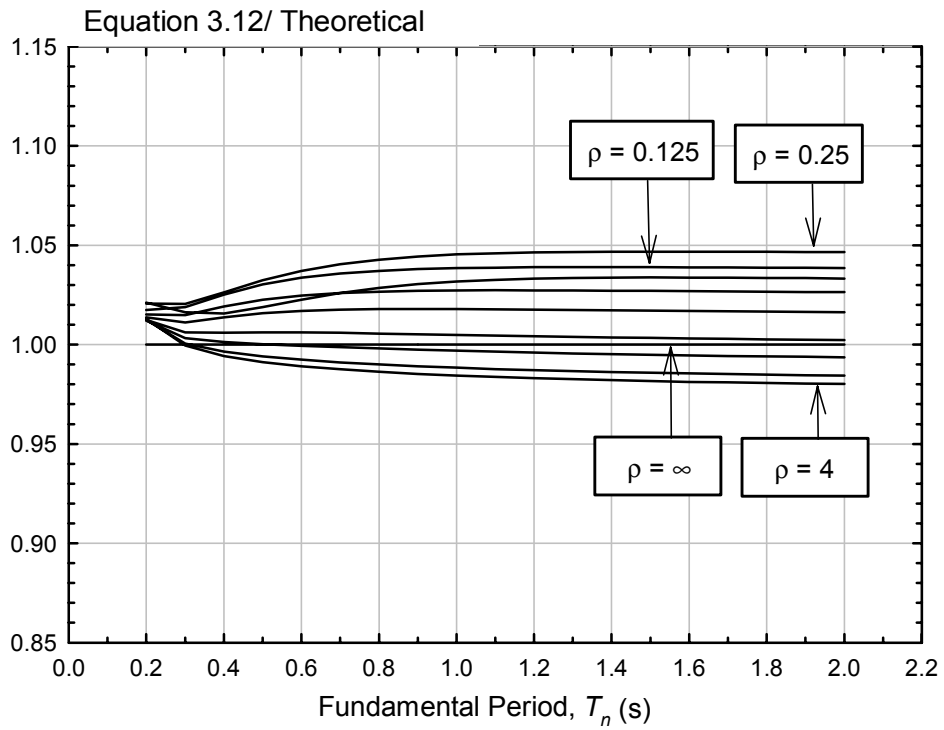

Figure 3.13 Deviation from Theoretical γ_{MF} and the Value Found Using Equation 3.12

3.3.2 Equation for Estimating the Maximum Interstory Drift Ratios of Moment Resisting Frames

Similar to γ_{MF}, principles of modal analysis were utilized in the development of the coefficient (γ_{MIDR}) for estimation of MIDR. According to principles of modal analysis, for a MDOF system, contribution of the 1st mode to the interstory displacement at the nth story, $\Delta_{1,n}$ may be computed as follows:

$$\Delta_{1,n} = \Gamma_1 \left(\phi_{n,1} - \phi_{n-1,1} \right) D_1(t) \qquad (3.13)$$

where Γ_1 is the modal participation factor of the fundamental mode, $\phi_{n,1}$ and $\phi_{n-1,1}$ are the drifts of nth story and the story below nth story in fundamental mode shape, respectively. The ratio of maximum interstory drift to ground story drift in the fundamental mode may be defined as follows:

$$\gamma_{MIDR} = \frac{\max\left[\Delta_{1,n}\right]}{u_{1,1}} \qquad (3.14)$$

where max[$\Delta_{1,n}$] is the contribution of the first mode to maximum interstory drift (n is the story at which the interstory drift is maximum in the fundamental mode shape), $u_{1,1}$ is the contribution of the fundamental mode to ground story drift. After Equations 3.10 and 3.13 are substituted into Equation 3.14 and simplifications are made, the following relationship is obtained:

$$\gamma_{MIDR} = \frac{\max\left[\phi_{1,n} - \phi_{1,n-1}\right]}{\phi_{1,1}} \qquad (3.15)$$

where max[$\phi_{1,n} - \phi_{1,n-1}$] is the maximum interstory drift in the fundamental mode and $\phi_{1,1}$ is the ground story drift in the fundamental mode shape. The ratio in Equation 3.15 has been computed for all idealized moment frames and results are plotted in Figure 3.14

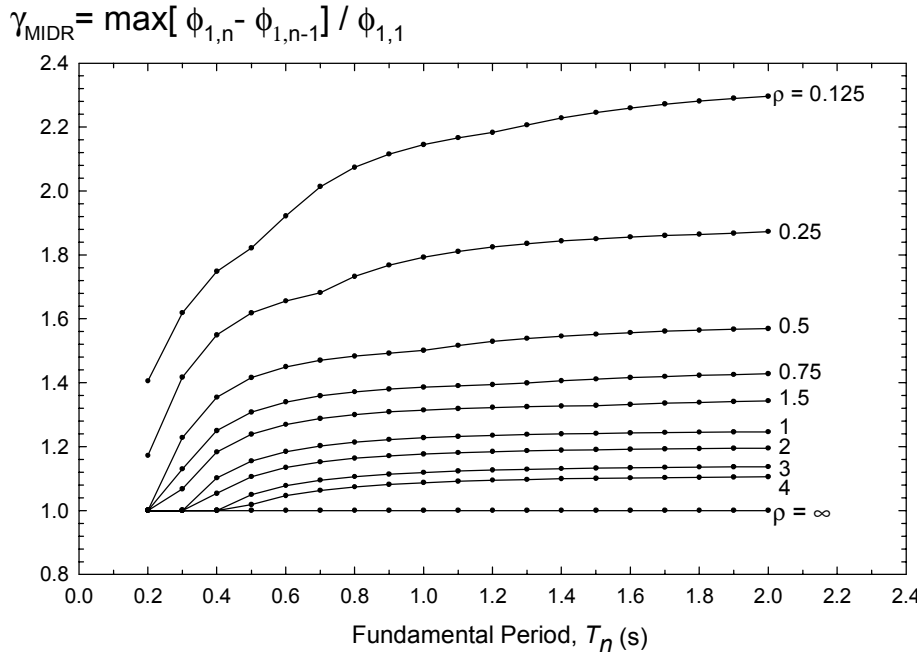

Figure 3.14 Variation in γ_{MIDR} with T_n and ρ

Similar to the nonlinear regression analyses performed for γ_{MF}, an equation for estimating γ_{MIDR} was found using the same regression techniques. The only difference was the abrupt change in the slope of the curves at γ_{MIDR}=1. Since such a change could not be modeled with a simple function, a piecewise function was introduced. As a result of the nonlinear regression analyses the following piecewise equation was found for the approximate amplification factor for finding the MIDR from GSDR (γ_{MIDR}):

$$\gamma_{MIDR} = \max\left\langle \exp\left(a_{MIDR} - b_{MIDR}/T_n\right), 1\right\rangle$$

$$\textit{where} \quad a_{MIDR}(\rho) = \frac{1}{2\rho + 0.9} \quad b_{MIDR}(\rho) = \frac{0.07}{\rho^{0.25}} \qquad (3.16)$$

where γ_{MIDR} is the maximum of the $\exp(a_{MIDR}-b_{MIDR}/T_n)$ and 1, T_n is the fundamental period and ρ is the beam-to-column stiffness ratio at the story closest to mid-height of the building. Theoretically, γ_{MIDR} should be equal to 1 for $\rho=\infty$, because maximum interstory displacement in first mode of shear frames is always at the ground story. It can easily be seen that as ρ approaches infinity, both a_{MIDR} and b_{MIDR} approach zero; as a result γ_{MIDR} approaches to 1.

Deviations of the γ_{MIDR}'s found using Equation 3.16 from the theoretical values, may be viewed in Figure 3.15. It is evident from Figure 3.15 that Equation 3.16 provides approximate values for γ_{MIDR} with an acceptable degree of accuracy for a wide range of periods. Maximum deviation from the theoretical values are observed for frames with T_n = 0.2 s which changes between +12 percent and -6 percent. For idealized frames with $T_n \geq 0.3$ s deviation is much smaller; it varies in the range of +5 percent to -2 percent.

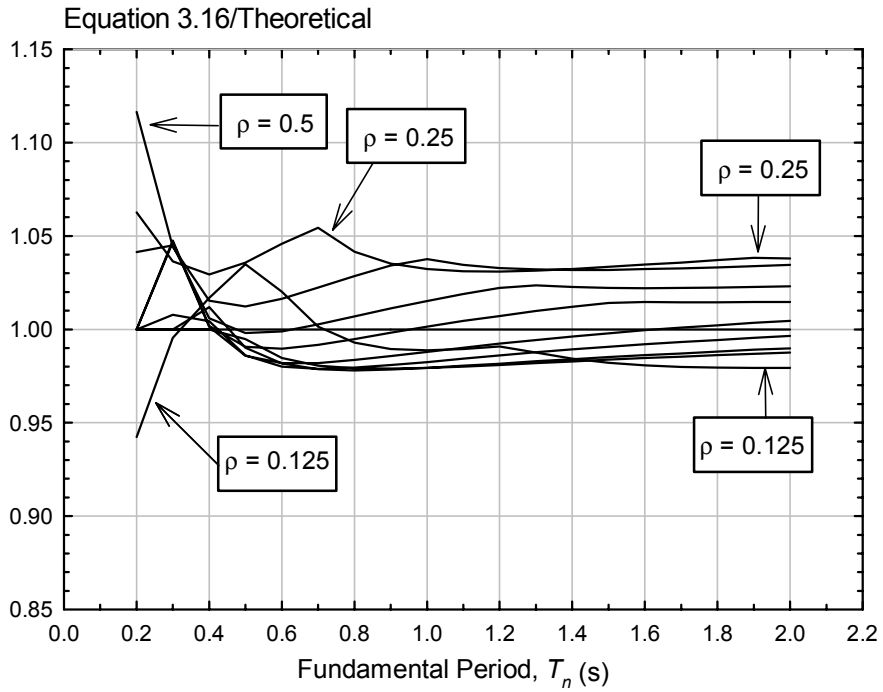

Figure 3.15 Deviation from Theoretical γ_{MIDR} and the Value Found Using Equation 3.13

In brief, Equations 3.12 and 3.16 provide the conversion factors needed for estimating GSDR's and MIDR's of general moment resisting frame structures. It should be noted that, γ_{MF} and γ_{MIDR} are essentially based on the first mode response of idealized regular moment resisting frames, and may not provide good estimates for irregular frames. Performance of Equations 3.5, 3.12 and 3.16, for the case of near-fault ground motions, will be evaluated in Chapter 4.

3.4 Estimating Inelastic Displacement Demands for SDOF Systems

3.4.1 Regression Analysis on the u_m/u_o-R-T Curves

Estimation of inelastic displacement demands imposed on structures is one of the key challenges of displacement based performance evaluation and design. A number of methods have been developed for the estimation of inelastic response spectra by

modifying the elastic response spectra. Major studies on this subject were summarized in Section 1.2.

Ductility and normalized yield strength are two important parameters that define the inelastic capacity of a structure. Yield strength was defined in Section 3.1.2.1. Ductility ratio (μ) of a system is the ratio of maximum displacement to yield displacement of a system. μ is formulated as follows:

$$\mu = \frac{u_m}{u_y} \qquad (3.17)$$

where u_m is the maximum displacement of a system and u_y is the yield displacement of the system. Ductility ratio is an important factor representing the energy dissipation of capacity of a system.

After substituting equation 3.17 into 3.4 the following relationship is obtained:

$$\frac{u_m}{u_0} = \frac{\mu}{R} \qquad (3.18)$$

where u_m is the maximum displacement of the inelastic system and u_o is the maximum displacement of the corresponding elastic system. The ratio in Equation 3.18 is also known as the inelastic displacement ratio and the functions used for estimating this ratio are named displacement modification factors.

There are two main approaches for estimating the inelastic displacement ratio: constant ductility approach and constant strength approach. Constant ductility approach, as the name implies, is based on assessing the required strength for a fixed specified ductility factor. This approach is particularly useful in the design of new structures with predefined ductility capacities. However, implementation of ductility based approaches in post-earthquake evaluation of structures requires a series of iterations and is not practical. On the contrary, constant strength approach is based on estimation of inelastic displacement demands imposed on structures consistent with their relative strength capacities. After the inelastic displacement demands are estimated, required ductility

capacities of members are checked. Application of constant strength approach in post-earthquake evaluation of structures is much easier compared to constant ductility approach.

A total of 69856 inelastic displacement ratios were computed (corresponding to 148 ground motions, 59 periods and 8 strength reduction factors). In order to include the effects of strong ground motion pulses on the inelastic displacement demands of SDOF systems, inelastic displacement ratios of the records with and without pulse were examined separately. Medians and standard deviations of natural logarithms, also known as dispersions, of inelastic displacement ratios were computed for each period and strength reduction factor. Medians $(u_m/u_o)^*$ and dispersions $\delta(u_m/u_o)$ in this study were computed according to the equations below:

$$\left(u_m/u_o\right)^* = \exp\left[\frac{\sum_{i=1}^{n}\ln\left(u_m/u_o\right)_i}{n}\right] \qquad (3.19)$$

$$\delta\left(u_m/u_0\right) = \left[\frac{\sum_{i=1}^{n}\left[\ln\left(u_m/u_o\right)_i - \ln\left(u_m/u_o\right)^*\right]}{n-1}\right]^{1/2} \qquad (3.20)$$

where $(u_m/u_o)_i$ are the individual inelastic displacement ratios computed for each ground motion and n is the number of ground motions analyzed. It should be noted that a dispersion equal to $\delta(u_m/u_o)$ means, 84th percentile of u_m/u_o corresponding to median $(u_m/u_o)^*$ may be calculated as $(u_m/u_o)^*\exp(\delta(u_m/u_o))$.

Figure 3.16 shows the variation in median inelastic displacement ratio with the fundamental period and strength reduction factor. It is evident from Figure 3.16 that the inelastic displacement ratios for the systems with short period ($T \leq 0.3$ s) are significantly higher compared to those with longer periods. For the structures with long periods ($T > 2.5$ s) inelastic displacement ratios for all strength reduction factors

approaches 1. This trend has been named as "equal displacement rule" by Newmark and Hall (1982). However, in the range of short periods inelastic displacement ratios are significantly affected from strength reduction factors. This phenomenon has been explained by Newmark and Hall (1982) as equal energy rule. Equal energy rule states that weaker structures tend to dissipate energy primarily by yielding, as a result they attain significantly larger displacement compared to elastic systems with the same natural period and damping. Comparing the two graphs in Figure 3.16, it may be concluded that inelastic displacement amplifications for records with strong pulses are higher than those without strong pulses.

Although the median inelastic displacement ratio curves are helpful for inspecting effects of various parameters on the inelastic displacement demands, it is also important to know the scatter associated with these inelastic displacement ratios. Dispersions of inelastic displacement ratios computed for each R have been plotted in Figure 3.17. Similar to the trend observed in the medians of inelastic displacement ratios, a decreasing trend in the dispersion with the increasing period may be seen in Figure 3.17. Although for the R's ranging from 1.5 to 4 dispersion of inelastic displacement ratios increase significantly with increasing R, such a significant increase can not be seen for R's higher than 4. Dispersions found for the short period range seem to be significantly higher compared to those found for longer periods. Also the dependence of dispersion to period seems to be more effective for smaller R's. Comparing the dispersions of inelastic displacement ratios found for records with and without pulse, it may be concluded that dispersions found using records with pulse are larger than those found using records without pulse in the period range from 0.5s to 2s. It should be noted that a dispersion equal to 0.6 means, 84^{th} percentile of u_m/u_o is $1.65(=e^{0.6})$ times median u_m/u_o. This is an indication of the large scatter in the u_m/u_o values for a single R and T.

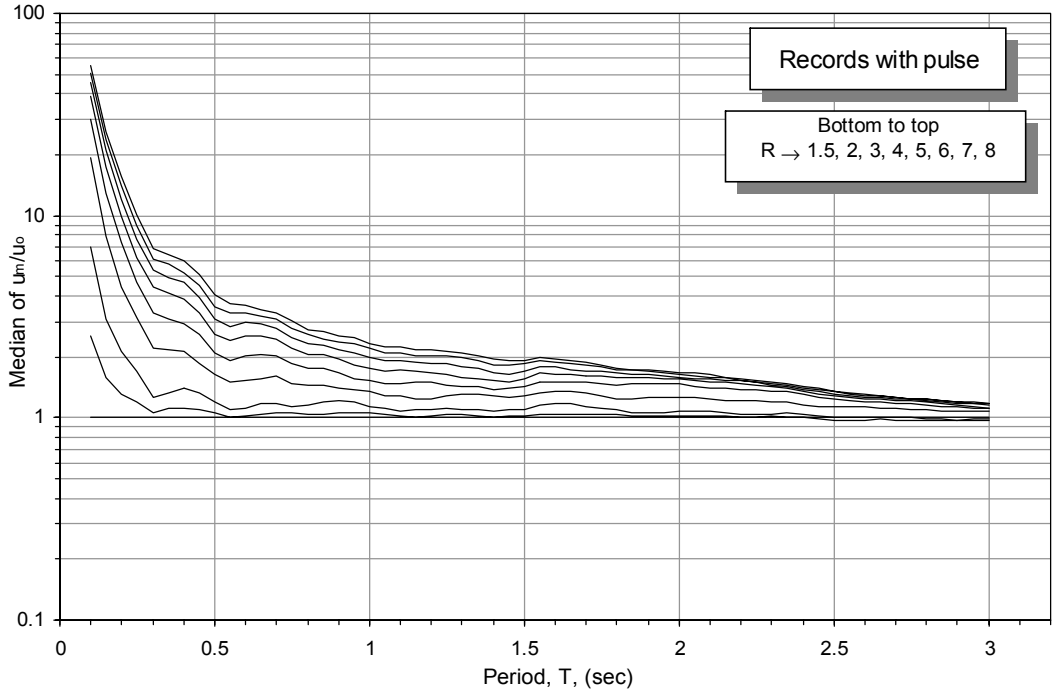

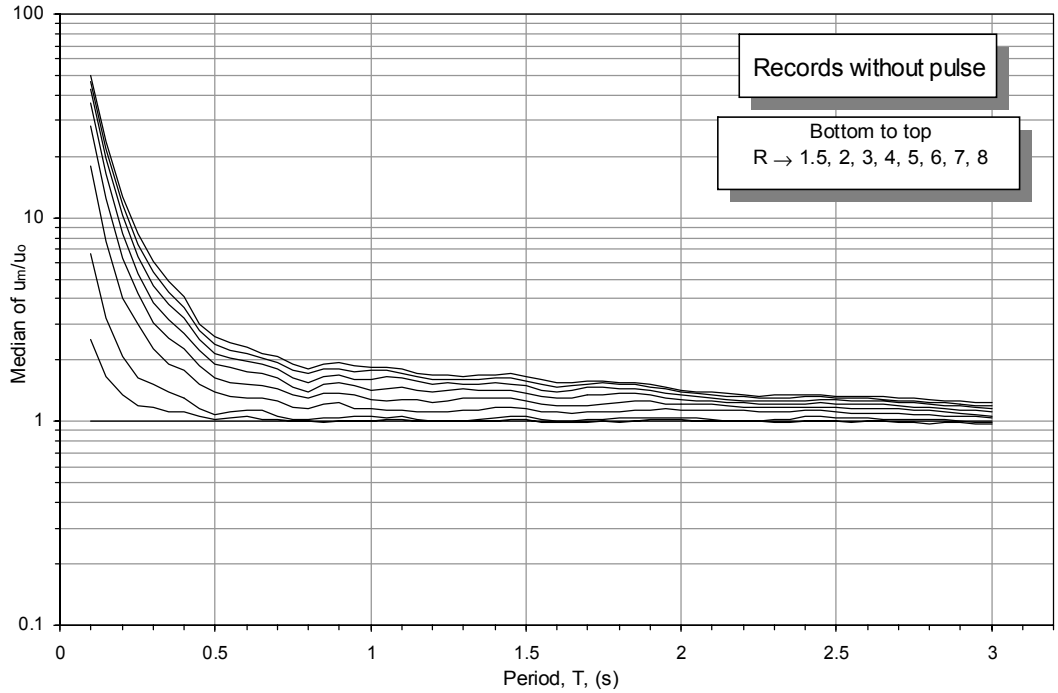

Figure 3.16 Median Curves for Inelastic Displacement Ratio versus Period

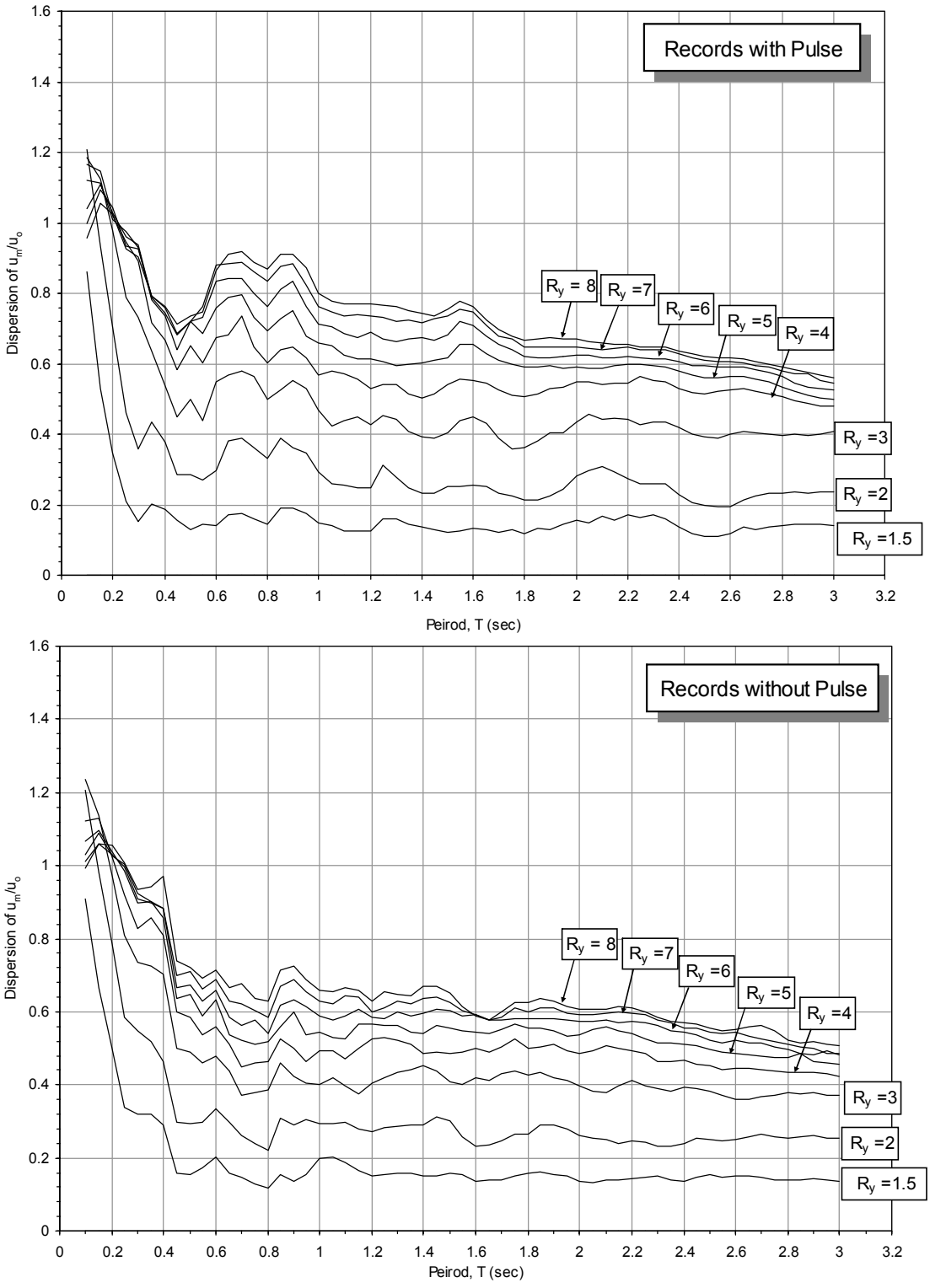

Figure 3.17 Dispersion of Inelastic Displacement Ratio versus Period

Although, Figures 3.16 and 3.17 may conveniently be used for estimating inelastic displacement ratios for structures with specified periods and strength reduction factors, it would be much more desirable to have a simplified expression for finding the inelastic displacement ratios. Considering this, equations for estimating the inelastic displacement ratios have been found using two stage nonlinear regression analyses. Since a single equation for estimating the inelastic displacement ratios both for records with and without pulse together might result in significant errors, two separate equations were established. Regressions for each set of median curves were performed in two stages. For the first stage the following equation, a slightly modified form of R-μ equation proposed by Osteraas and Krawinkler (1990), was employed:

$$\frac{u_m}{u_o}(R) = \frac{1}{R}\left(\frac{R^a - 1}{b} + 1\right) \qquad (3.21)$$

where R is the strength reduction factor, a and b are the coefficients to be determined by nonlinear regression analysis. Values for a and b making the sum of squares of residuals minimum were found for each period. Second stage of regression was performed on the a-R and b-R pairs. As a result the following equations were found for estimating inelastic displacement ratios (u_m/u_o) :

$$\frac{u_m}{u_o}(R,T) = \frac{1}{R}\left(\frac{R^a - 1}{b} + 1\right) \qquad (3.22)$$

for records with pulse

$$a(T) = \frac{1}{1 - 0.67\exp(-0.83T)} \quad b(T) = \frac{1}{1 + 0.15 \cdot T_n^{-1} - 1.4\exp(-1.3T)} \qquad (3.23a)$$

for records without pulse

$$a(T) = \frac{1}{1 - 0.7 \cdot \exp\left(-1.1 \cdot T^{0.9}\right)} \quad b(T) = \frac{1}{1 + 0.009 \cdot T^{-2} - 0.55 \cdot \exp(-0.8T)} \qquad (3.23b)$$

where T is the period . It should be noted that constants in Equation 3.22 were adjusted by trial and error so that the range of error of the estimation is a minimum, and numbers have meaningful precision. Theoretically, Equation 3.22 should satisfy the following conditions:

$$u_m/u_o(R\rightarrow 1, T)\rightarrow 1 \qquad (3.24)$$

$$u_m/u_o(R, T\rightarrow \infty)\rightarrow 1 \qquad (3.25)$$

It can be seen that Equation 3.22 satisfies both of these conditions. Furthermore, error statistics of Equation 3.22 and a similar equation utilized in FEMA356 (2000) has been evaluated in Chapter 4.

3.4.2 Derivation of the Equation Based on Natural Period to Pulse Period Ratio

Several studies (Iwan et al 2000, Baez and Miranda 2000) have shown that strong pulses observed in some near-fault ground motions affect the inelastic displacement ratios significantly. Iwan et al (2000) stated that inelastic displacement ratios for structures with periods shorter than the pulse period were significantly larger than those found for the structures having longer periods than the pulse period. In order to capture the effect of elastic period to pulse period ratio on the inelastic displacement ratio, 26432 inelastic displacements (corresponding to 56 ground motions with pulse listed in Appendix A, 59 elastic-period-to-pulse-period ratios from 0.1 to 3 with the increments of 0.05 and 8 R's values) were computed. In this study the term natural period is used to define the period of the inelastic SDOF systems in the elastic range. Medians and dispersions of inelastic displacement ratios for each natural period to pulse period ratio and R have been computed. Median curves for inelastic displacement ratios for each R have been plotted in Figure 3.18. From these curves it may be seen that inelastic displacement ratio is controlled by the ratio of natural period to pulse period. Moreover, it may be observed from Figure 3.18 that median curves for inelastic displacement ratios, fall below unity for systems having periods longer that 0.8 times the pulse period. This observation is similar to Iwan et al (2000). In Figure 3.18 it may be seen that the decrease in median inelastic displacement ratio was more effective for

systems with higher strength reduction factors. Similar to the Figure 3.16, for long period structures median inelastic displacement ratio curves in Figure 3.18 approach unity also. As a result, it may be concluded that, equal displacement rule may be observed from the median curves in Figure 3.18, too.

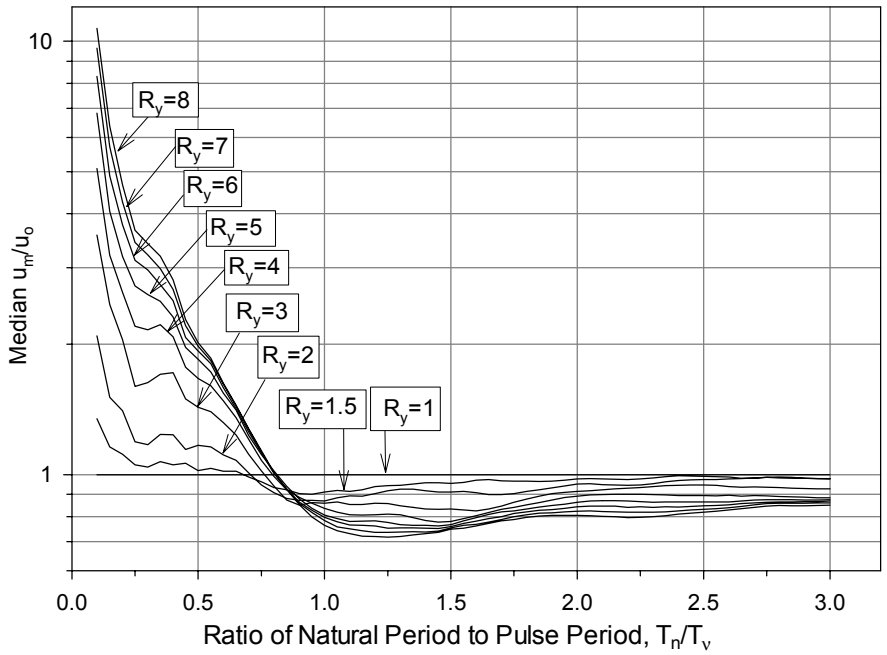

Figure 3.18 Median Curves for Inelastic Displacement Ratio versus Ratio of Natural Period to Pulse Period

Median inelastic displacement ratios versus ratio of natural period to pulse period curves provide information about the variation of inelastic displacement demands with various parameters. However, the dispersions associated with inelastic displacement ratios provide equally important information. In Figure 3.19, dispersion of inelastic displacement ratio versus elastic period curves has been plotted. From Figure 3.19 it may be concluded that dispersion of inelastic displacement ratios for systems with elastic periods shorter than 0.8 times the pulse period is significantly larger compared to systems with longer natural periods. Dispersion curves in Figure 3.19 seem to be nearly

constant in the range $T_n/T_v > 1$. Comparing Figures 3.19 and 3.17, it may be concluded that dispersion of inelastic displacement ratios found for each period on the average is larger than those found for each elastic period to pulse period ratio.

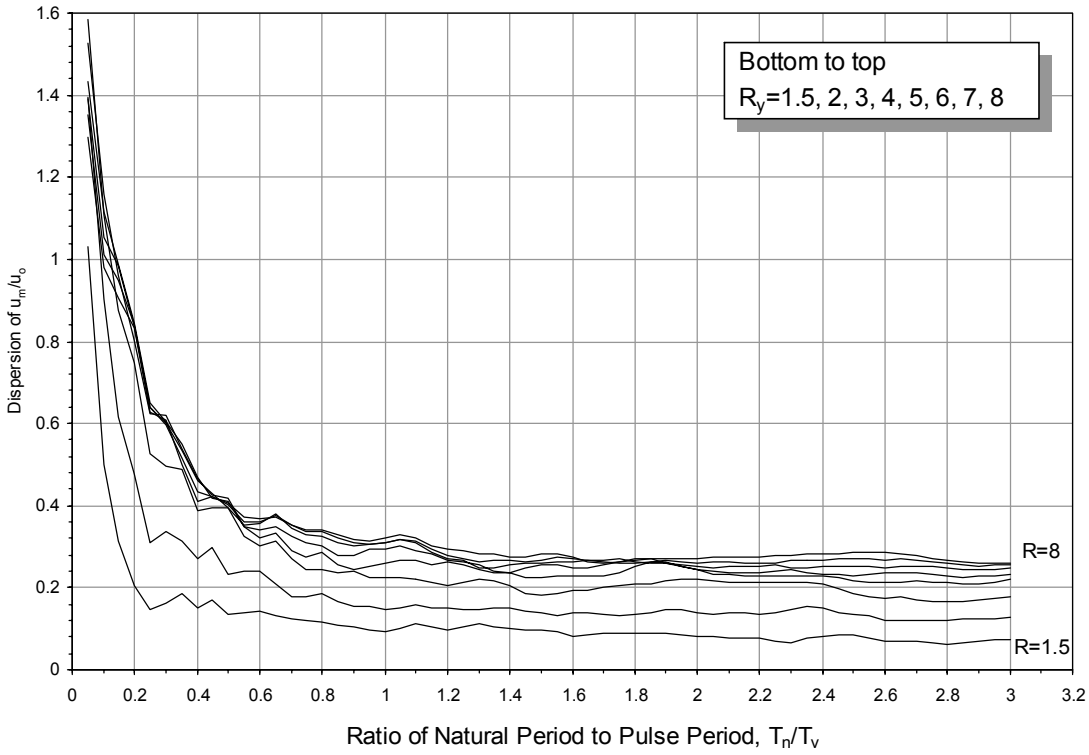

Figure 3.19 Dispersion of Inelastic Displacement Ratios versus Ratio of Natural Period to Pulse Period

In order to establish relationships for estimating the inelastic displacement ratios, two stage nonlinear curve fitting analysis was performed on the median inelastic displacement ratio versus natural period curves. As a result, the following equation was found:

$$\frac{u_m}{u_o}\left(R, T_n/T_v\right) = \frac{1}{R}\left(\frac{R^a - 1}{b} + 1\right)$$

$$a\left(T_n/T_v\right) = \frac{-2.5\left(T_n/T_v\right)^3 + 1.5}{\exp\left(2.4\,T_n/T_v\right)} + 1 \quad b\left(T_n/T_v\right) = \exp\left(\frac{\frac{-0.055}{T_n/T_v} + 1.4}{\exp\left(3.8\,T_n/T_v\right)}\right) \qquad (3.26)$$

where R is the strength reduction factor, T_n/T_v is the ratio of natural period to pulse period. Theoretically, Equation 3.26 should satisfy the following conditions for a specific T_v:

$$u_m/u_o(R \rightarrow 1,\ T_n/T_v) \rightarrow 1 \qquad (3.27)$$

$$u_m/u_o(R,\ T_n/T_v \rightarrow \infty) \rightarrow 1 \qquad (3.28)$$

It can be seen that Equation 3.26 satisfies both of these conditions.

In depth study of the error statistics of Equation 3.26 will be presented in Chapter 4.

CHAPTER 4

VERIFICATION

4.1 Verification of the Approximate Methods for Estimating the GSDR and MIDR

In this chapter, accuracy of the approximate equations developed for estimating the elastic GSDR's and MIDR's will be investigated. The approximate GSDR's and MIDR's found using Equations 3.5, 3.12 and 3.16 have been compared to those computed using the modal response history analysis. Hereafter, the values computed using the response history analysis will be referred as "exact" and the values found using the proposed approximations will be referred as "approximate". In order to quantify the performance of the proposed function approximate-to-exact-ratio (A/E) was used. A/E being greater than one implies that the approximate method overestimates the exact response. Similarly, an A/E smaller than one implies approximate method underestimates the exact response. It should also be noted that A/E is directly related to error as follows:

$$Error = \left(A/E \right) - 1 \tag{4.1}$$

where A is the value found using the approximate method and E is the exact value computed using modal response history analysis.

4.1.1 A/E Statistics for GSDR and MIDR

Selection of a proper theoretical distribution model is the key step for appropriate statistical analysis of observational data. Once the distribution function is found or assumed the statistical parameters associated with the data may be computed. Chi-square goodness-of-fit test provides a numerical way for evaluating the adequacy of different theoretical distribution functions (Ang and Tang, 1975). In this study, validity of normal (Gaussian) and log-normal distributions for modeling the probabilistic distribution of A/E was evaluated. The sample A/E sets used in the chi-square test are shown in Figure 4.1. Selection of these sample clusters was arbitrary. It was assumed that distribution characteristics of these sample clusters represented all the A/E's.

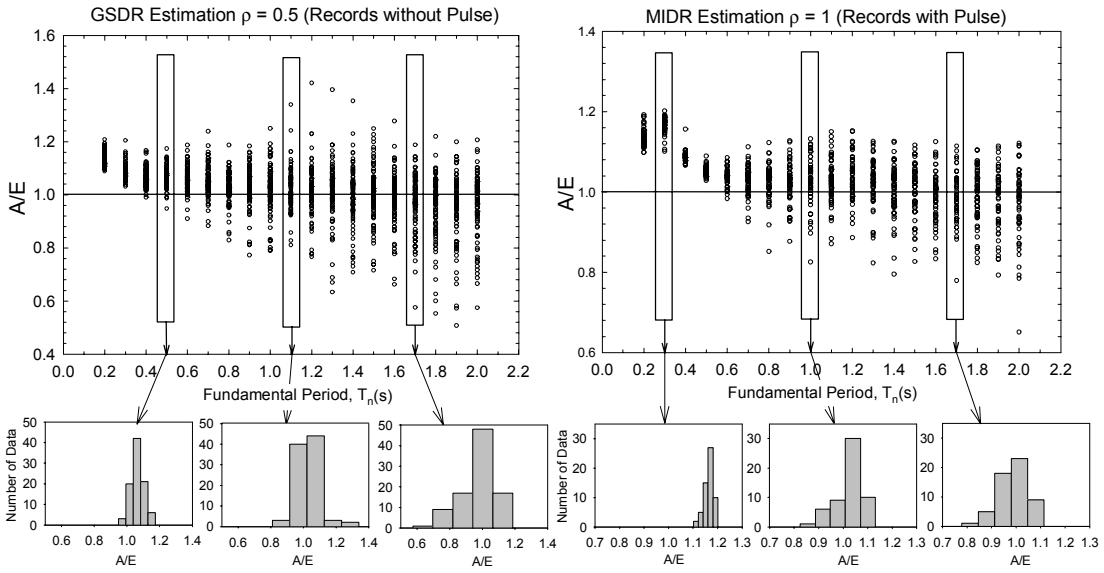

Figure 4.1 Scattergrams and Histograms of the Sample GSDR and MIDR A/E Sets used for Chi-Square Test

Chi-square (χ^2) values computed using the A/E sets shown in Figure 4.1 is presented in Table 4.1. It may easily be noticed from Table 4.1 that, for most of the sets

χ^2 values found for normal and log-normal distributions are very close. However, from the 3rd row of Table 4.1 it is seen that normal distribution has a significantly lower χ^2 compared to log-normal. This indicates the superiority of normal distribution over log-normal for modeling the A/E values related to GSDR estimation. For a significance level (α) of 0.05 (which the commonly used value), χ_{cr}^2 is given as 5.99. χ^2 being smaller than χ_{cr}^2 shows that the selected distribution function fits the data sufficiently (Ang and Tang, 1975). It should also be noted that, all the χ^2 values associated with normal distribution in Table 4.1 are all smaller than 5.99. As a result, normal distribution provides a sufficient degree of accuracy for analyzing the statistical parameters associated with A/E values related to GSDR and MIDR estimation.

Table 4.1 Chi-Square (χ^2) Values Computed for the Sample A/E Sets for GSDR and MIDR

		χ^2	
	T_n(s)	Normal	Log-normal
GSDR (ρ = 0.5)	0.5	1.25	0.90
	1.1	5.71	5.06
	1.7	5.97	10.64
MIDR (ρ = 1)	0.3	2.99	3.31
	1	5.43	6.14
	1.7	2.00	2.41

Mean and mean +/- standard deviation curves for A/E values related to GSDR and MIDR estimation may be seen in Figures 4.2 and 4.3. It may easily be noticed from Figures 4.2 and 4.3 that Equations 3.5, 3.12 and 3.16 provide, on the average, acceptably accurate estimates. It should also be noted that A/E graphs related to $\rho=\infty$ essentially show only the accuracy of the Equation 3.5, estimating the GSDR's of shear frames, proposed by Gülkan and Akkar (2002).

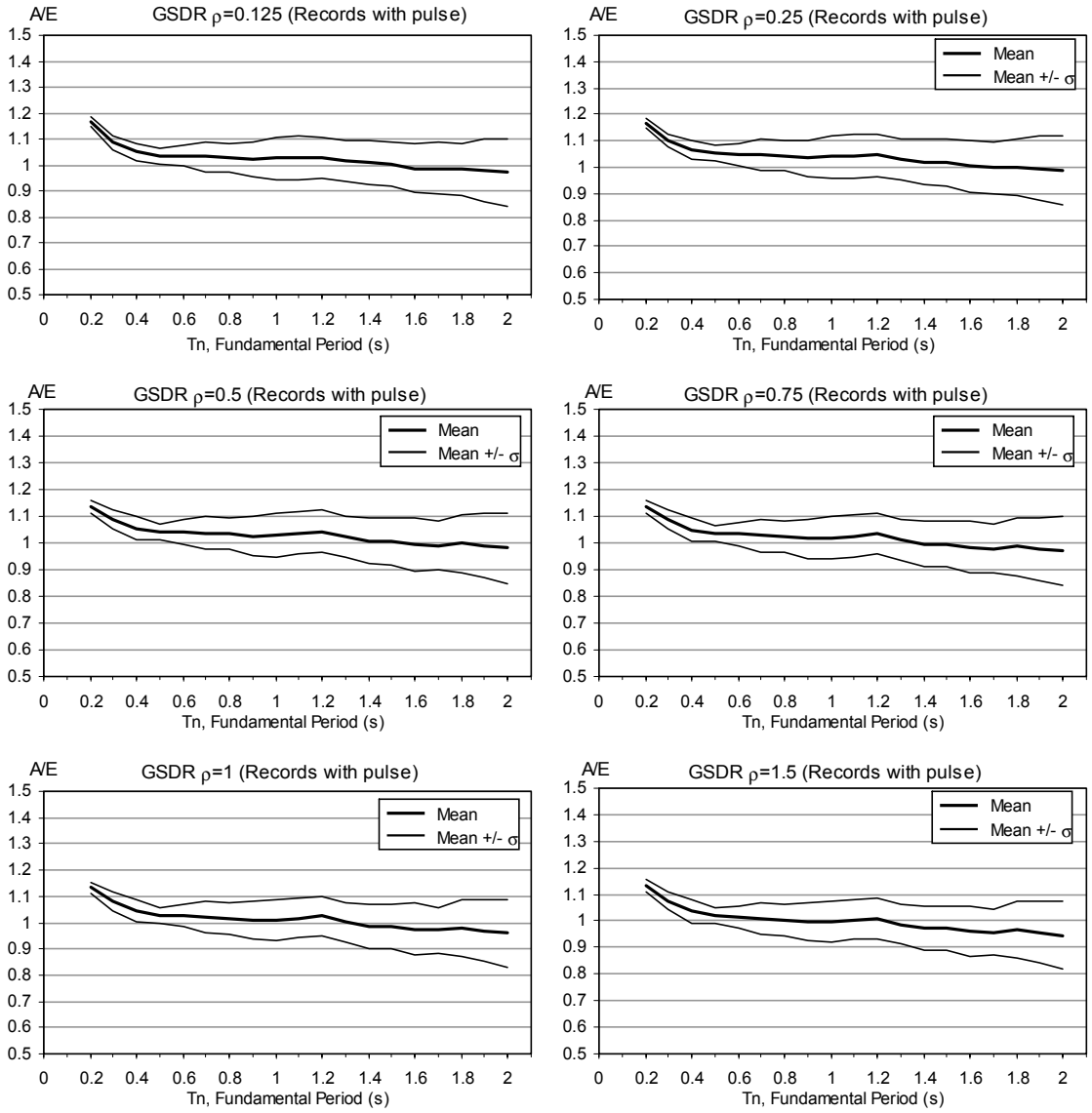

Figure 4.2 (a) A/E Statistics for GSDR Estimation ρ = 0.125 – 1.5 (Records with Pulse)

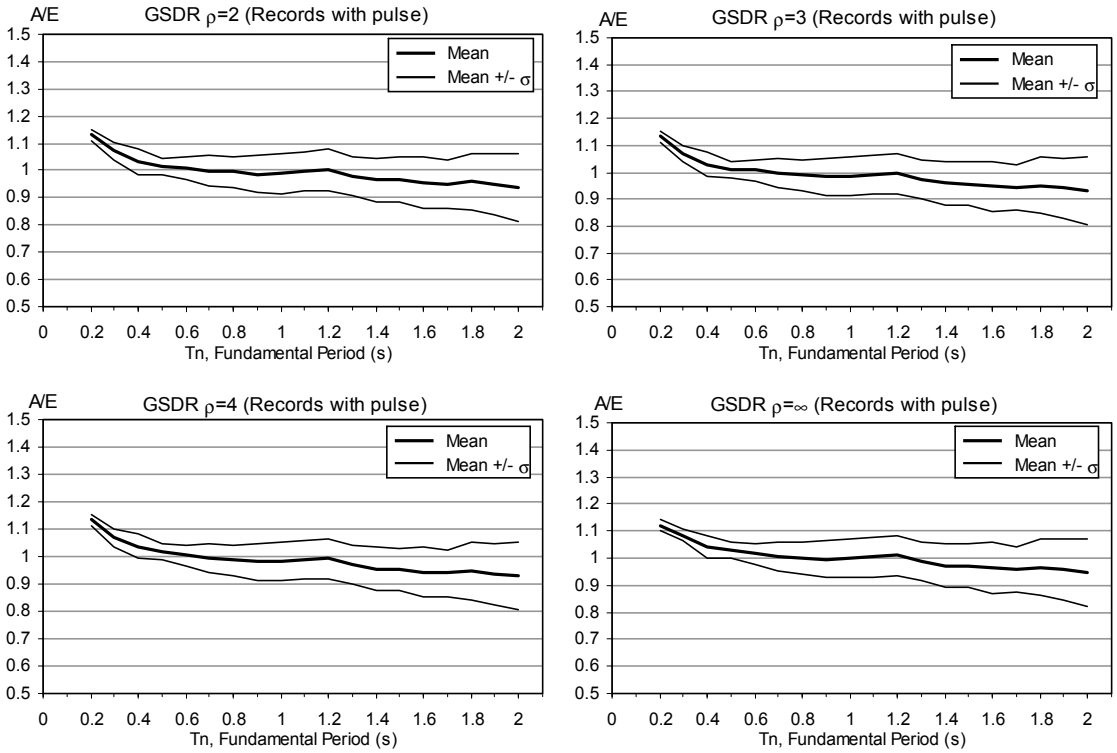

Figure 4.2 (b) A/E Statistics for GSDR Estimation ρ=2-∞ (Records with Pulse)

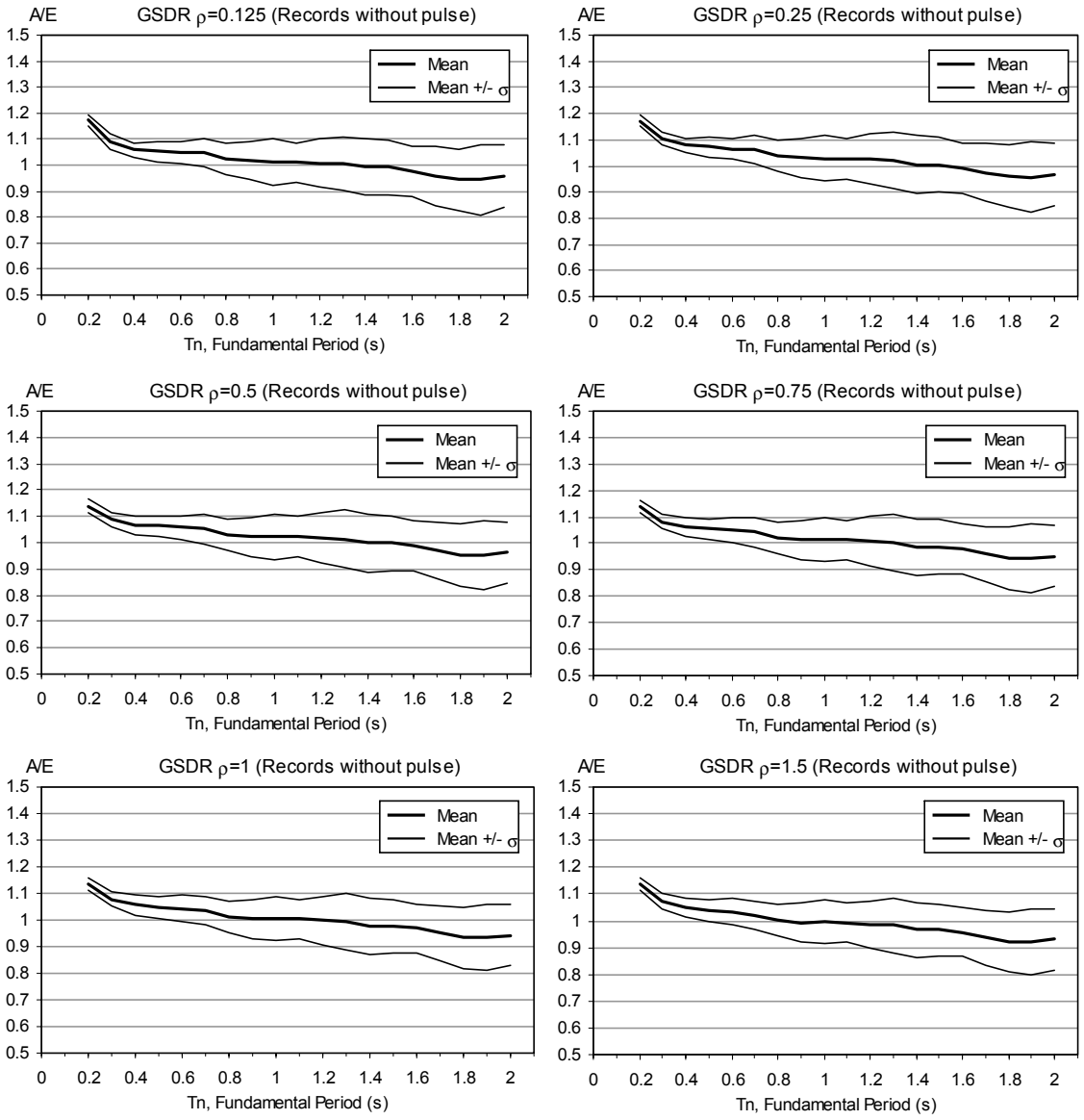

Figure 4.2 (c) A/E Statistics for GSDR Estimation ρ = 0.125 – 1.5

(Records without Pulse)

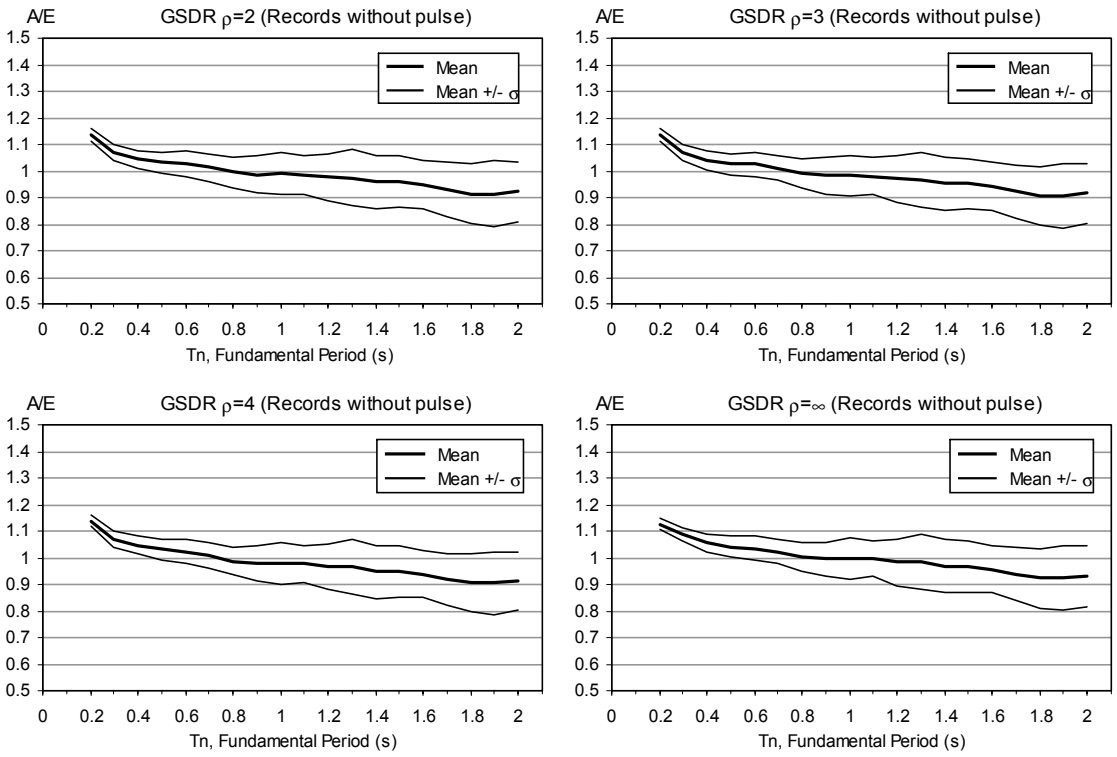

Figure 4.2 (d) A/E Statistics for GSDR Estimation ρ = 2 - ∞ (Records without Pulse)

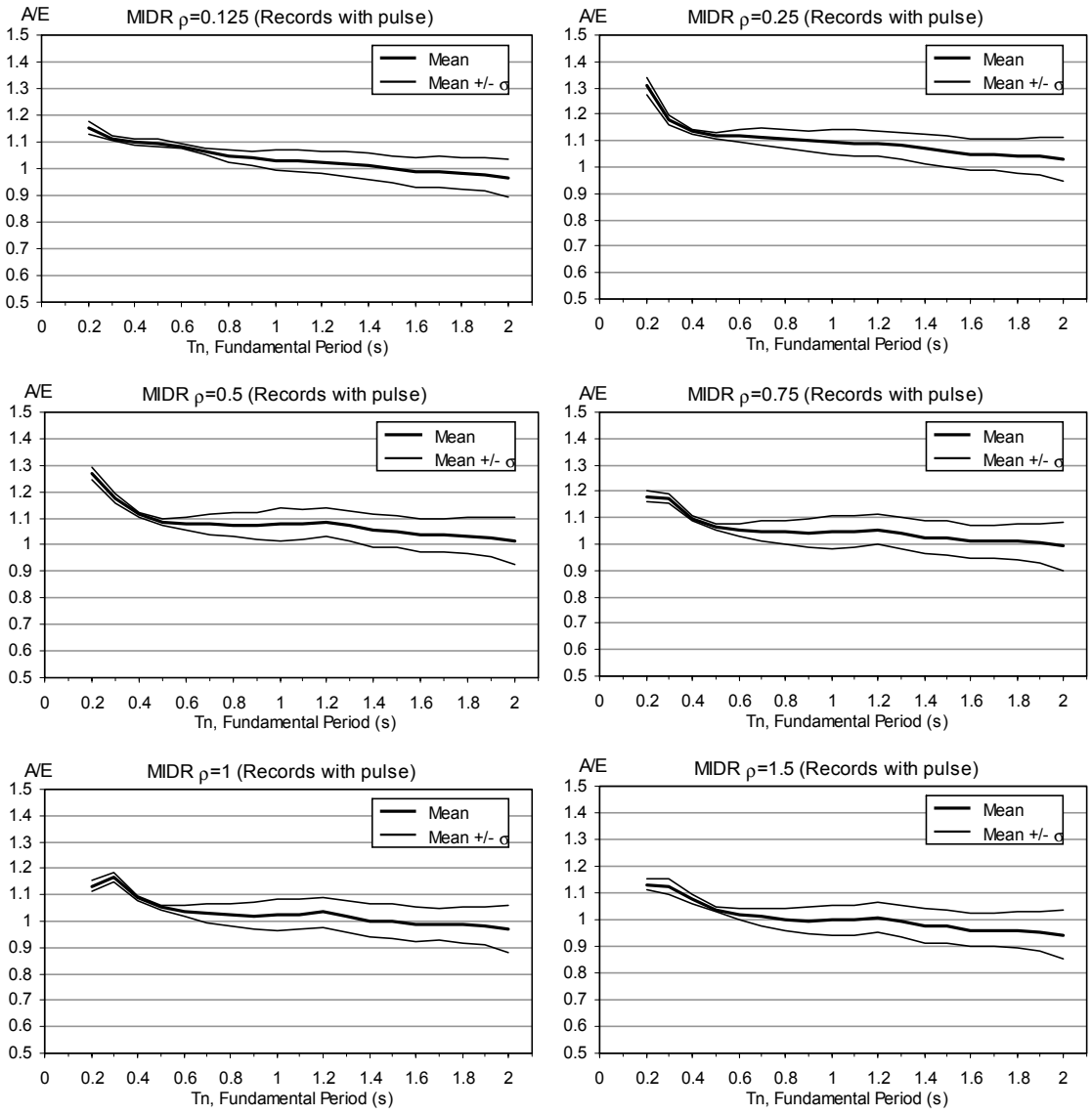

Figure 4.3 (a) A/E Statistics for MIDR Estimation ρ = 0.125 – 1.5

(Records with Pulse)

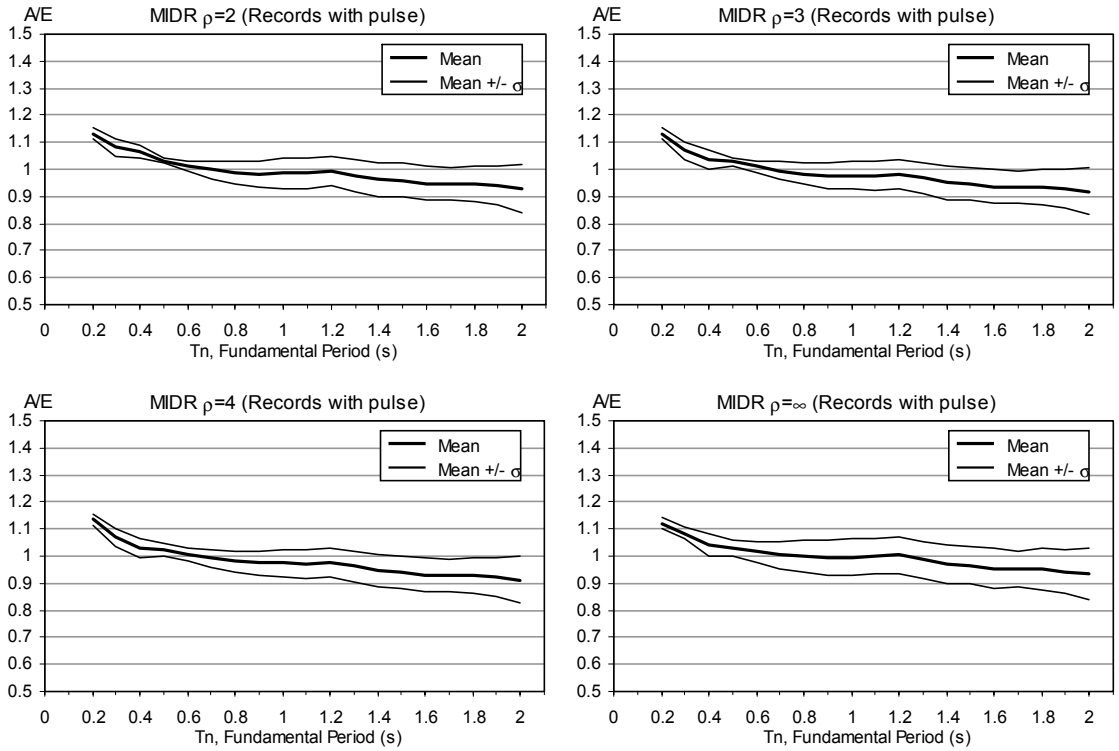

Figure 4.3 (b) A/E Statistics for MIDR Estimation $\rho = 2 - \infty$

(Records with Pulse)

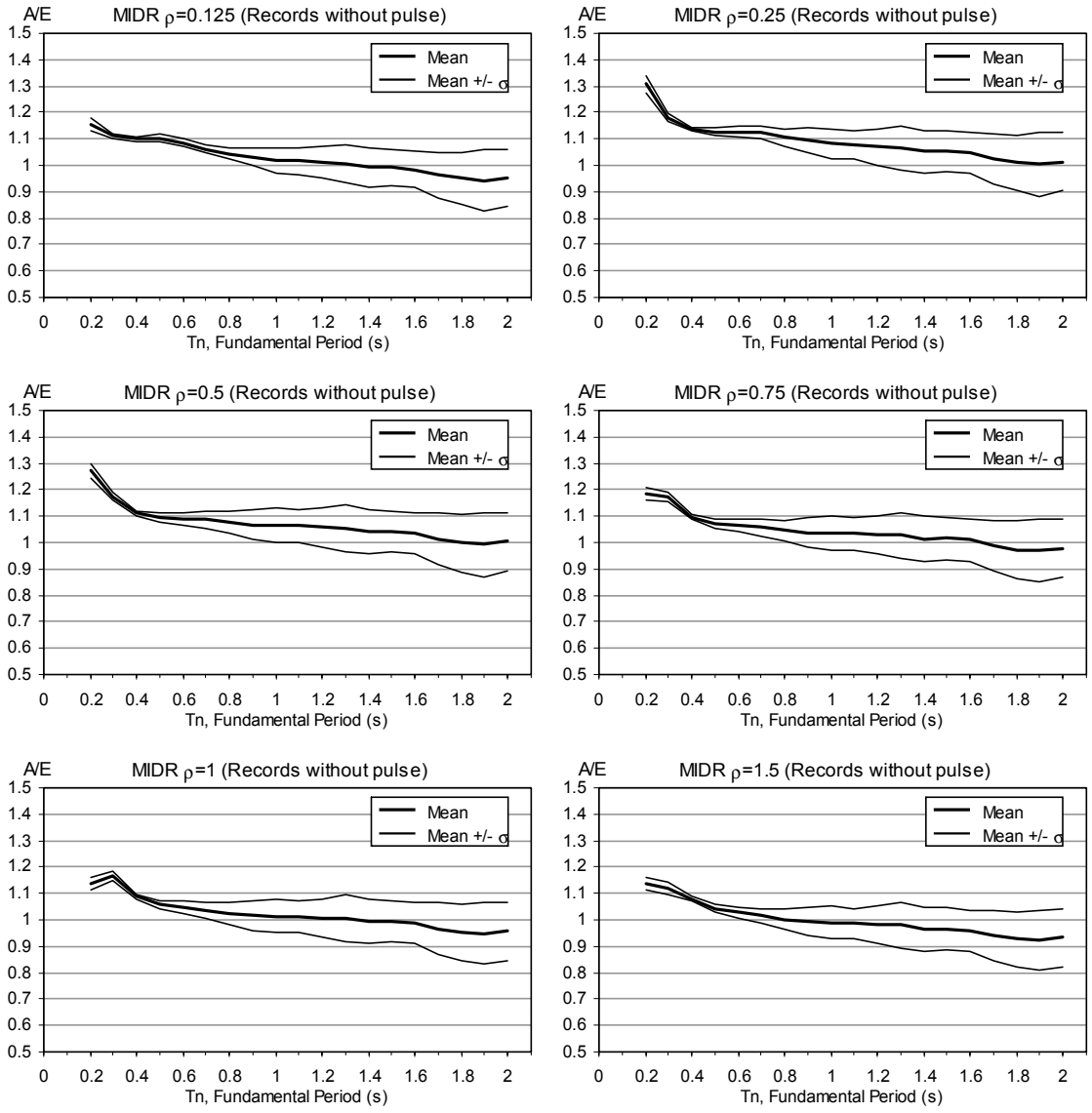

Figure 4.3 (c) A/E Statistics for MIDR Estimation ρ = 0.125 – 1.5

(Records without Pulse)

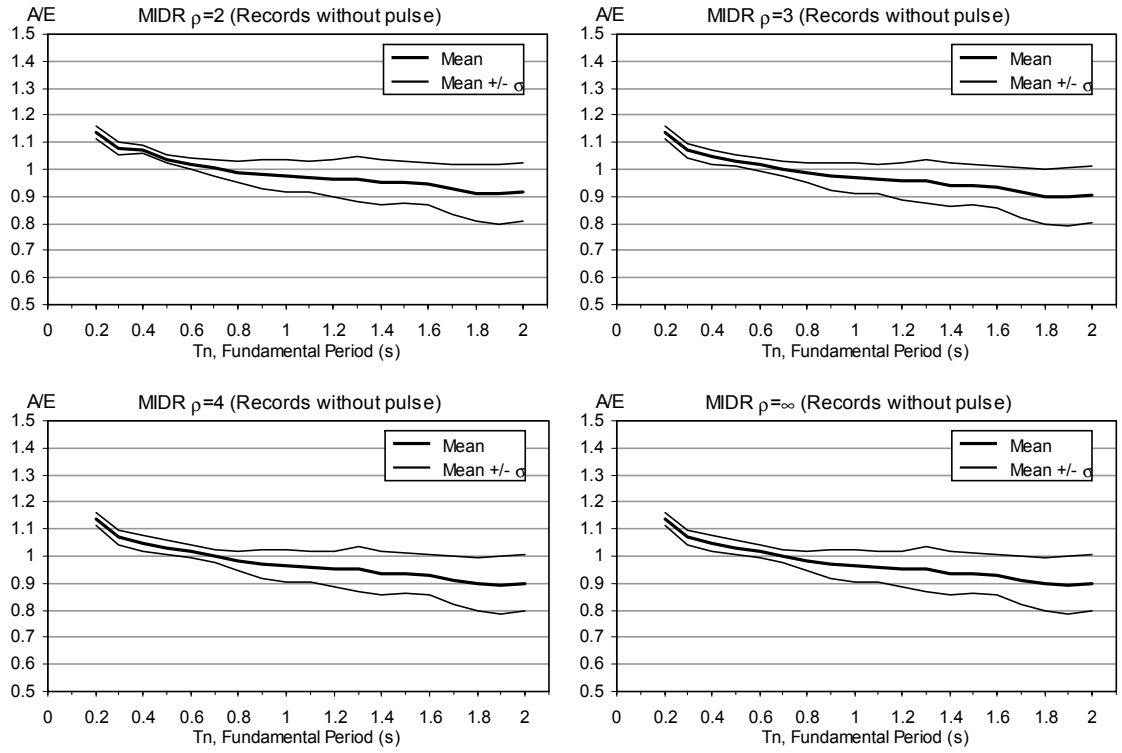

Figure 4.3 (d) A/E Statistics for MIDR Estimation $\rho = 2 - \infty$
(Records without Pulse)

It may be seen from Figures 4.3(a),(b),(c) and (d) that for the frames having $T_n < 0.6$ s A/E ranges are greater than 1. This indicates for frames having T_n <0.6 s Equations 3.5, 3.12 and 3.16 overestimates the GSDR and MIDR. For the frames having $T_n > 0.6$ s underestimations are observed. However this underestimation is limited to an acceptable degree for the frames having 0.6 s $< T_n <$ 1.2 s. The underestimations are generally smaller than 10 percent at that range. At the extreme case $T_n = 2$ s, underestimation reaches to –20 percent.

4.1.2 Comparison of the Proposed Method with Other Approximate Methods

In order to compare the performance of the approximate method proposed in this study with other studies in the literature, A/E's related to the method proposed by

Miranda (1999) were computed. Miranda (1999) utilizes an equivalent continuum structure consisting of a combination of a flexural cantilever beam and a shear cantilever beam. Approximate mode shape in Miranda (1999) is obtained using the relation below:

$$\psi(z) = \frac{C_1 \sinh\alpha \frac{z}{H} + C_2 \cosh\ \alpha \frac{z}{H} + C_3 e^{-az/H} + C_4 \left(\frac{z}{H}\right)^2 + C_5 \frac{z}{H} + C_6}{C_1 \sinh\alpha + C_2 \cosh\ \alpha + C_3 e^{-a} + C_4 + C_5 + C_6} \tag{4.2}$$

$$C_1 = \frac{\alpha^2 e^{-a} - a^2 e^{-a} - a^3 + a\alpha^2 - \alpha^2}{a\alpha^3 (a^2 - \alpha^2)}$$

$$C_2 = \frac{a^2 e^{-a} - \alpha^2 e^{-a} + a^3 - a\alpha^2 + \alpha^2}{a\alpha^3 (a^2 - \alpha^2)} \frac{\sinh\alpha}{\cosh\alpha} + \frac{\alpha^2 e^{-a} + a^2 - \alpha^2}{\alpha^4 (a^2 - \alpha^2)} \frac{1}{\cosh\alpha}$$

$$C_3 = \frac{-1}{a^2 (a^2 - \alpha^2)}$$

$$C_4 = \frac{-1}{2\alpha^2}$$

$$C_5 = \frac{a^2 e^{-a} - \alpha^2 e^{-a} + a^3 - a\alpha^2}{a\alpha^2 (a^2 - \alpha^2)}$$

$$C_6 = \frac{\alpha^2 e^{-a} - a^2 e^{-a} - a^3 + a\alpha^2 - \alpha^2}{a\alpha^3 (a^2 - \alpha^2)} \frac{\sinh\alpha}{\cosh\alpha} + \frac{1}{a^2 (a^2 - \alpha^2)} - \frac{\alpha^2 e^{-a} + a^2 - \alpha^2}{\alpha^4 (a^2 - \alpha^2)} \frac{1}{\cosh\alpha}$$

where a is the dimensionless parameter controlling the shape of loading (typically taken as 0.01 for triangular loading), α is the parameter controlling the participation of shear and flexural deformations, z is the height of story and H is the total height of the building. Miranda (1999) uses Equation 4.2 to compute the approximate participation factors.

In essence the parameter α is very similar to ρ. Smaller α's indicate that the overall lateral displacement profile of the frame is similar to displacement profile of a bending cantilever beam, whereas higher α's indicate an overall lateral displacement

profile similar to the displacement profile of a shear beam. Miranda (1999) states that, the α value should be computed as follows

1) Normalized roof displacement profile should be found from elastic analysis of the frame under triangular lateral loading with an arbitrary intensity.
2) The proper α value minimizing the differences between the displacement profiles found in Step 1 and the approximate mode shape found using Equation 4.2 should be found.
3) The α value obtained from Step 2 should be substituted into the set of equations presented by Miranda (1999). As a result of a series of computations maximum interstory and ground story drifts are found.

Therefore, unlike ρ the computation of α as it is proposed in Miranda (1999) involves a series of iterations. A subsequent article by Miranda and Reyes (2002) stated that α, without any iteration, may be taken as equal to 10 for typical frame buildings. However, as it will be shown in the preceding paragraphs using a constant α for all frame buildings may result in significant errors.

A/E's found using both methods (Miranda 1999, Miranda and Reyes 2002) have been evaluated in this study. In order to find the proper α values for 190 idealized frames using the method proposed in Miranda (1999) a special MATLAB program was prepared. For finding the proper α values a constrained optimization algorithm, namely Golden-search method, was utilized in the program.

The ranges of A/E's found for frames with ρ = 0.125, 0.75, 2 and ∞ using the former method (Miranda, 1999), by finding the α iteratively are shown in Figure 4.4. As it may be seen from Figure 4.4(a), the former method (Miranda, 1999) underestimates the ground story drift. For the case of maximum interstory drift some

overestimation may be observed in the T_n<0.6 s range in Figure 4.4(b). However for the extreme case T_n=2 s mean underestimation is -20 percent.

Similarly, ranges of A/E's found for frames with ρ = 0.125, 0.75, 2 and ∞ using the latter method (Miranda and Reyes, 2002), by taking α to be equal to 10 for all cases, are shown in Figure 4.5. Comparing Figures 4.4(a) and 4.5(a), it may be concluded that selection of a proper α value is critical for acceptably accurate estimation of GSDR. An approximate value of α equal to 10, as given in Miranda and Reyes (2002), may provide unsafe GSDR estimates. However, for the case of MIDR, there is no significant difference between the A/E's found using iterated α's and those found using α=10.

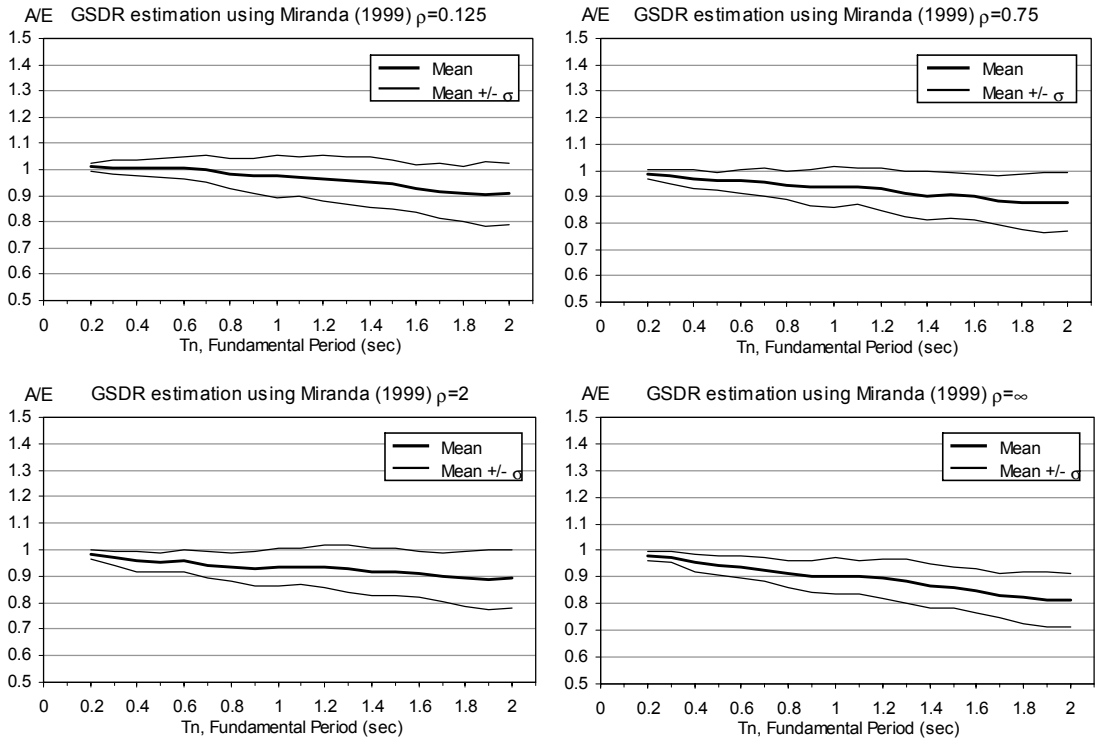

Figure 4.4 (a) A/E Statistics of GSDR Estimation Using the Method by Miranda (1999)

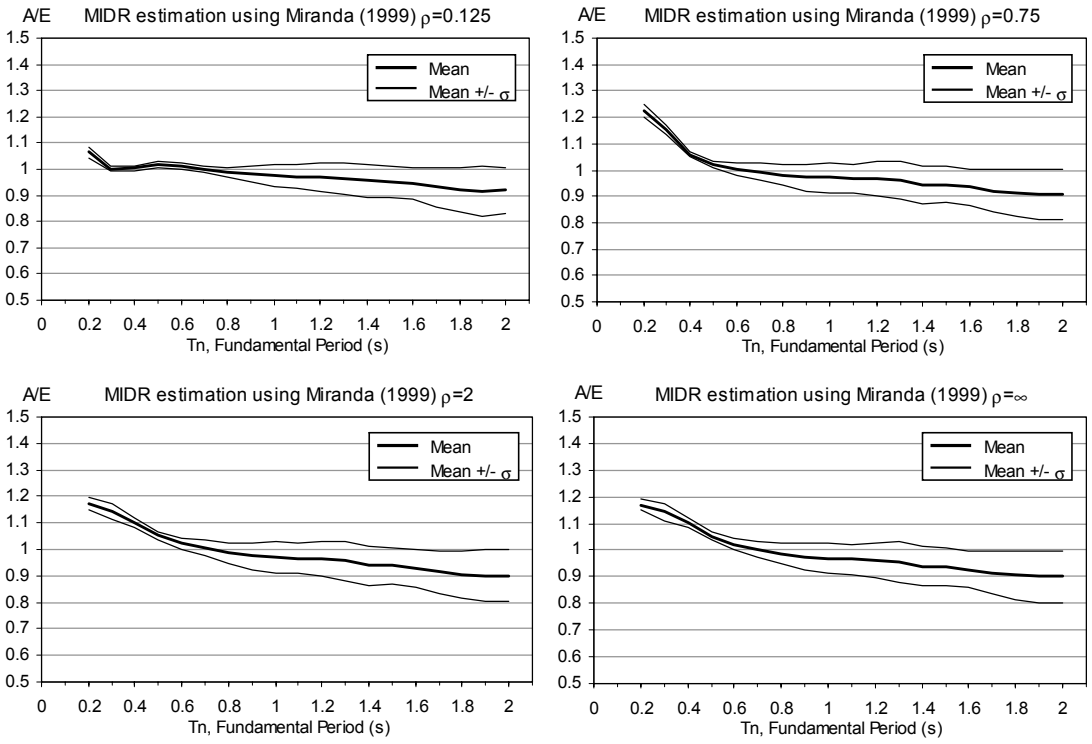

Figure 4.4 (b) A/E Statistics of MIDR Estimation Using the Method by Miranda (1999)

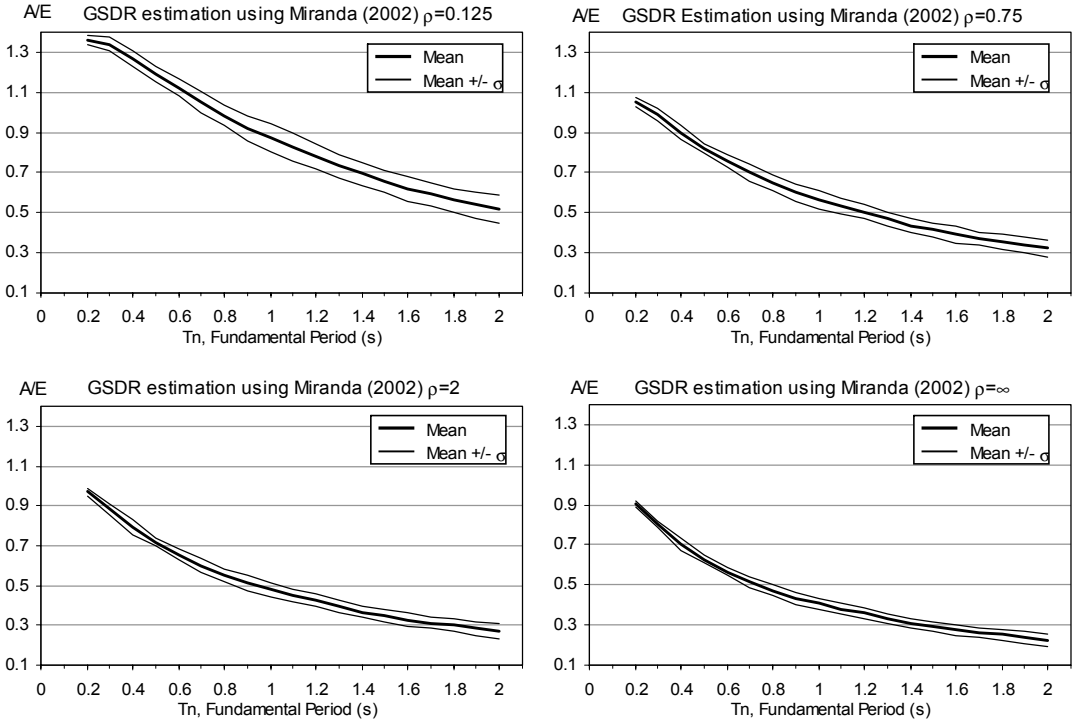

Figure 4.5 (a) A/E Statistics of GSDR Estimation Using the Method by Miranda and Reyes (2002)

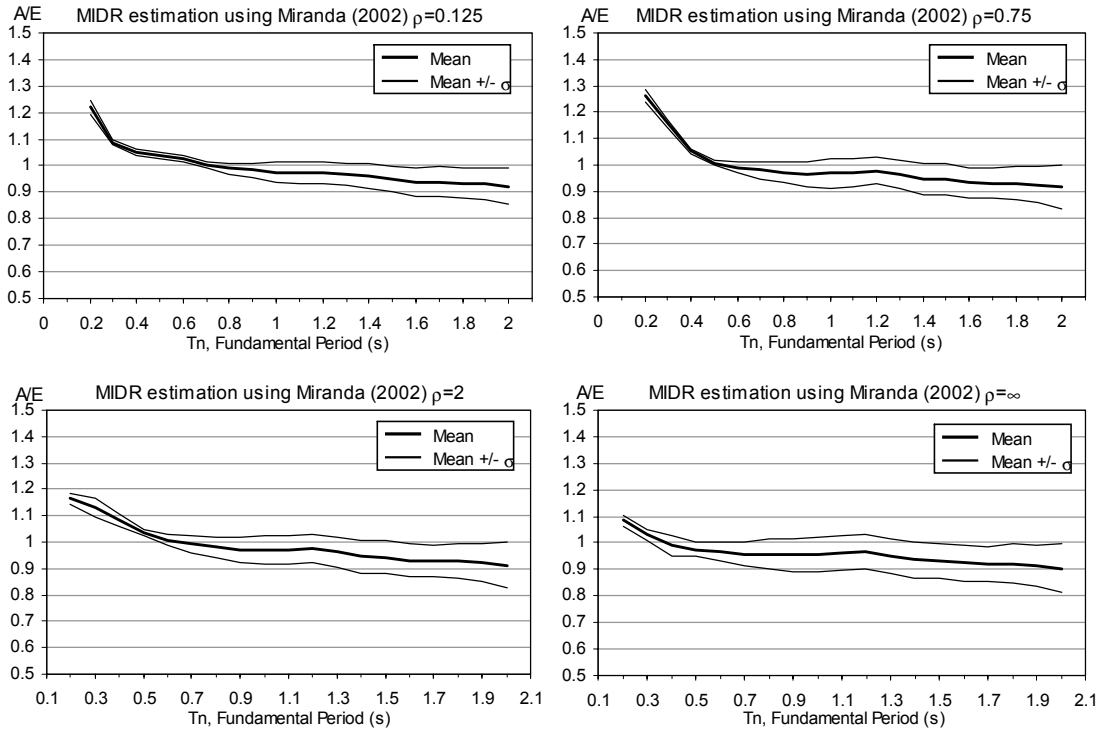

Figure 4.5 (b) A/E Statistics of MIDR Estimation Using the Method by Miranda and Reyes (2002)

4.2 Verification of the Approximate Equations for Estimating the Inelastic Displacement Ratio

4.2.1 A/E Statistics for Inelastic Displacement Ratio

In order to find the proper theoretical distribution function for modeling the distribution of A/E's associated with Equations 3.22 and 3.26, chi-square tests were performed. Performances of normal and log-normal distributions for modeling A/E's were evaluated. Sample sets for evaluating the validity of the distribution functions were selected arbitrarily. In Figure 4.6 the A/E's selected for evaluation were plotted. It was assumed that the A/E sets employed in the analysis represents the distribution characteristics of all A/E's. In Table 4.2, χ^2's computed are presented. It is evident

from Table 4.2, that χ^2 associated with the log-normal distribution are significantly smaller than those associated with normal distributions. This indicates the superiority of log-normal distribution over normal for modeling the A/E values related to estimation of inelastic displacement ratio. As a result, log-normal distribution was used for analyzing the statistical parameters associated with the A/E values related to inelastic displacement ratio estimation equations.

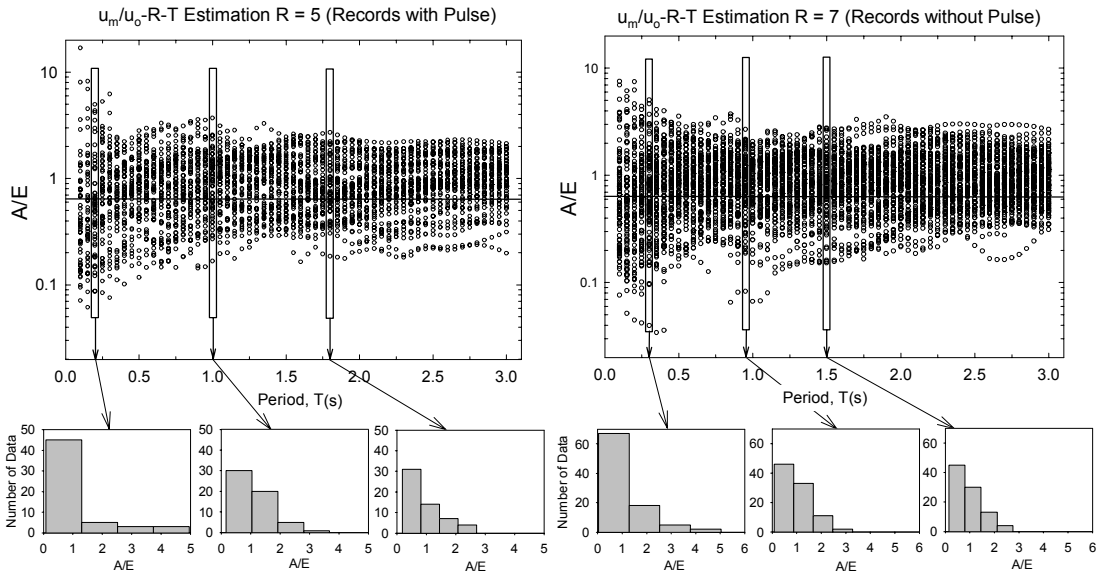

Figure 4.6 Scattergrams and Histograms of the Sample u_m/u_o-R-T Estimation A/E Sets used for Chi-Square Test

Table 4.2 Chi-Square (χ^2) Values Computed for the Sample A/E Sets for u_m/u_o

		χ^2	
	T(s)	Normal	Log-normal
u_m/u_o (R=5) (Records with pulse)	0.2	32.04	2.38
	1	6.34	0.98
	1.8	11.27	1.82
u_m/u_o (R=7) (Records without pulse)	0.3	37.35	0.95
	0.9	5.99	3.61
	1.5	7.79	1.39

In Figures 4.7, 4.8 and 4.9, A/E statistics for the u_m/u_o-R-T and u_m/u_o-R-T_n/T_v equations (Equations 3.22 and 3.26) may be inspected. As a result of the large dispersion associated with the inelastic displacement ratio, the A/E statistics related the estimation of inelastic displacement ratio (Equations 3.22 and 3.26) was found to be widely scattered in the T<0.5 s range (Figures 4.6 and 4.7). Although some underestimation is observed in the T<0.5 s range, for longer periods Equation 3.22, on the average, provides acceptably accurate estimates for inelastic displacement ratio (Figures 4.7 and 4.8). A similar underestimation in the T<0.5 s is observed for the estimates obtained using Equation 3.26 (Figure 4.8). Dispersion of the A/E associated with Equation 3.26 is much smaller compared to A/E's associated with Equation 3.22.

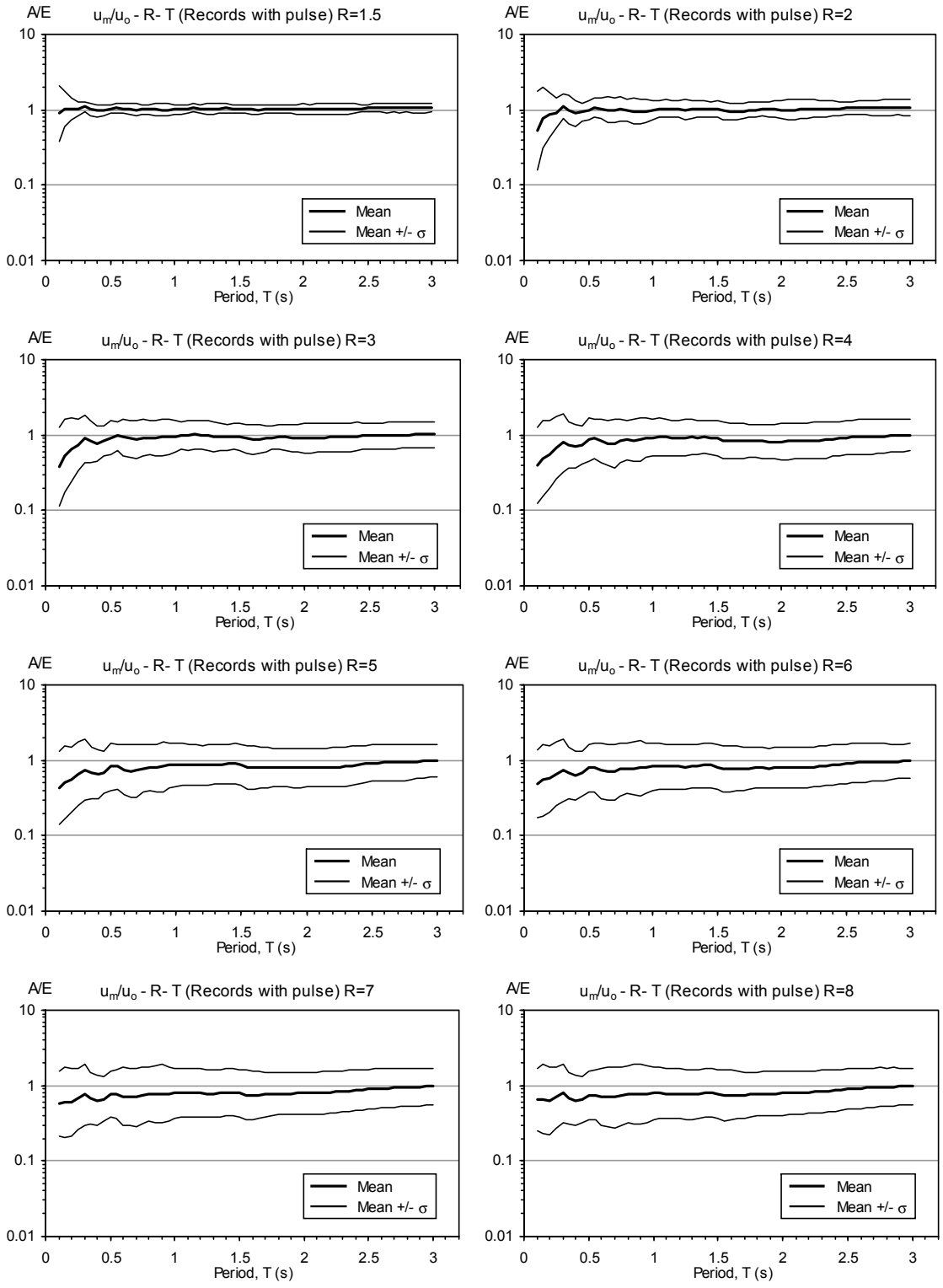

Figure 4.7 A/E Statistics for u_m/u_o-R-T Equation for Records with Pulse (Equation 3.22)

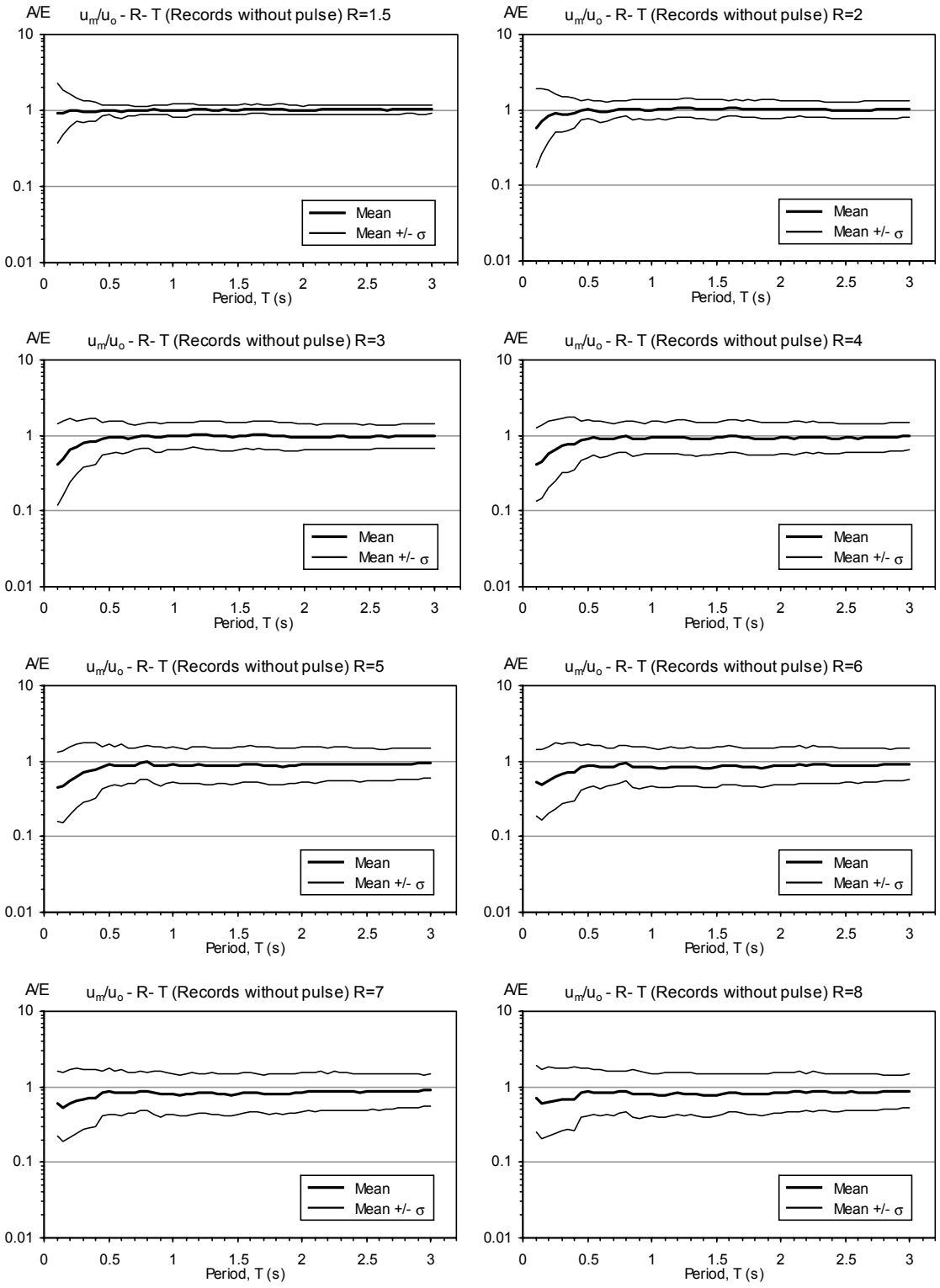

Figure 4.8 A/E Statistics for u_m/u_o-R-T Equation for Records without Pulse (Equation 3.22)

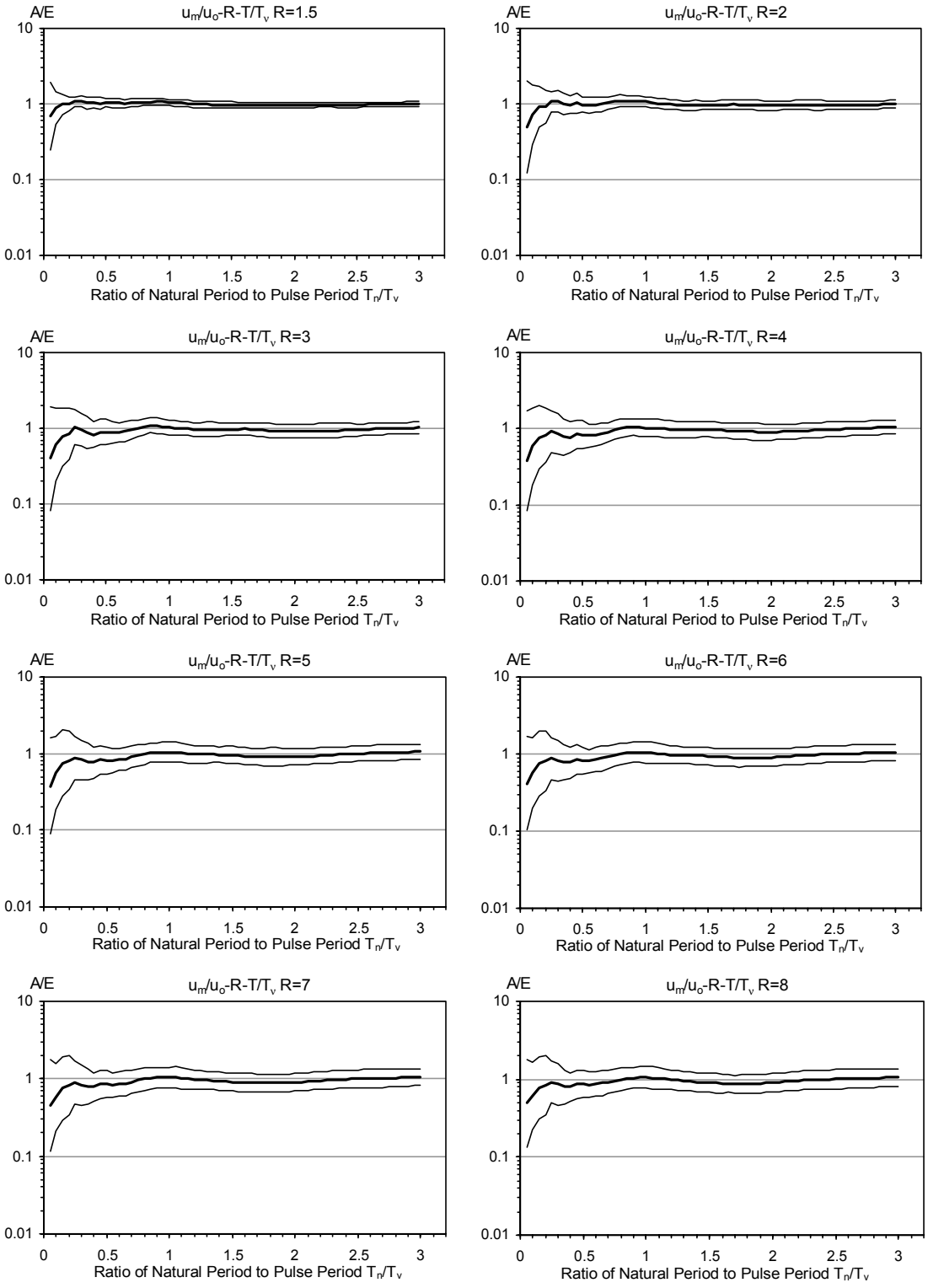

Figure 4.9 A/E Statistics for u_m/u_o-R-T/T_v Equation (Equation 3.26)

4.2.2 Comparison of the Proposed Method with Other Approximate Methods

Displacement modification factor (C_1) utilized in FEMA356 relates the maximum inelastic deformation of the non-degrading SDOF system to the maximum elastic deformation of the corresponding SDOF system with the same elastic period and damping. Like Equations 3.21 and 3.22, C_1 is an approximate factor for estimating the inelastic displacement ratio (u_m/u_o). The formula for C_1 in FEMA356 is given as follows:

$$C_1 = \begin{cases} 1.0 & for\ T_e \geq T_s \\ \left[1.0 + (R-1)T_s/T_e\right]/R & for\ T_e < T_s \end{cases} \tag{4.3}$$

where T_e is the natural period of the SDOF system, T_s is the characteristic period of the response spectrum and R is the ratio of the elastic strength demand to yield strength of the inelastic system (strength reduction factor).

A/E statistics associated with the C_1 coefficient are plotted in Figures 4.10(a) and (b). It should be noted that characteristic periods (T_s) were found individually for each ground motion record in the record set using the procedure stated in FEMA356. It is evident from Figures 4.10(a) and (b) that C_1 significantly underestimates the inelastic displacements. This underestimation is more noticeable for the records with pulse.

Comparing Figures 4.9 and 4.10(b) it may be concluded that estimation of inelastic displacement ratios according to natural period to pulse period ratio (T/T_v) provides more accurate results compared to natural period to characteristic period ratio (T/T_s).

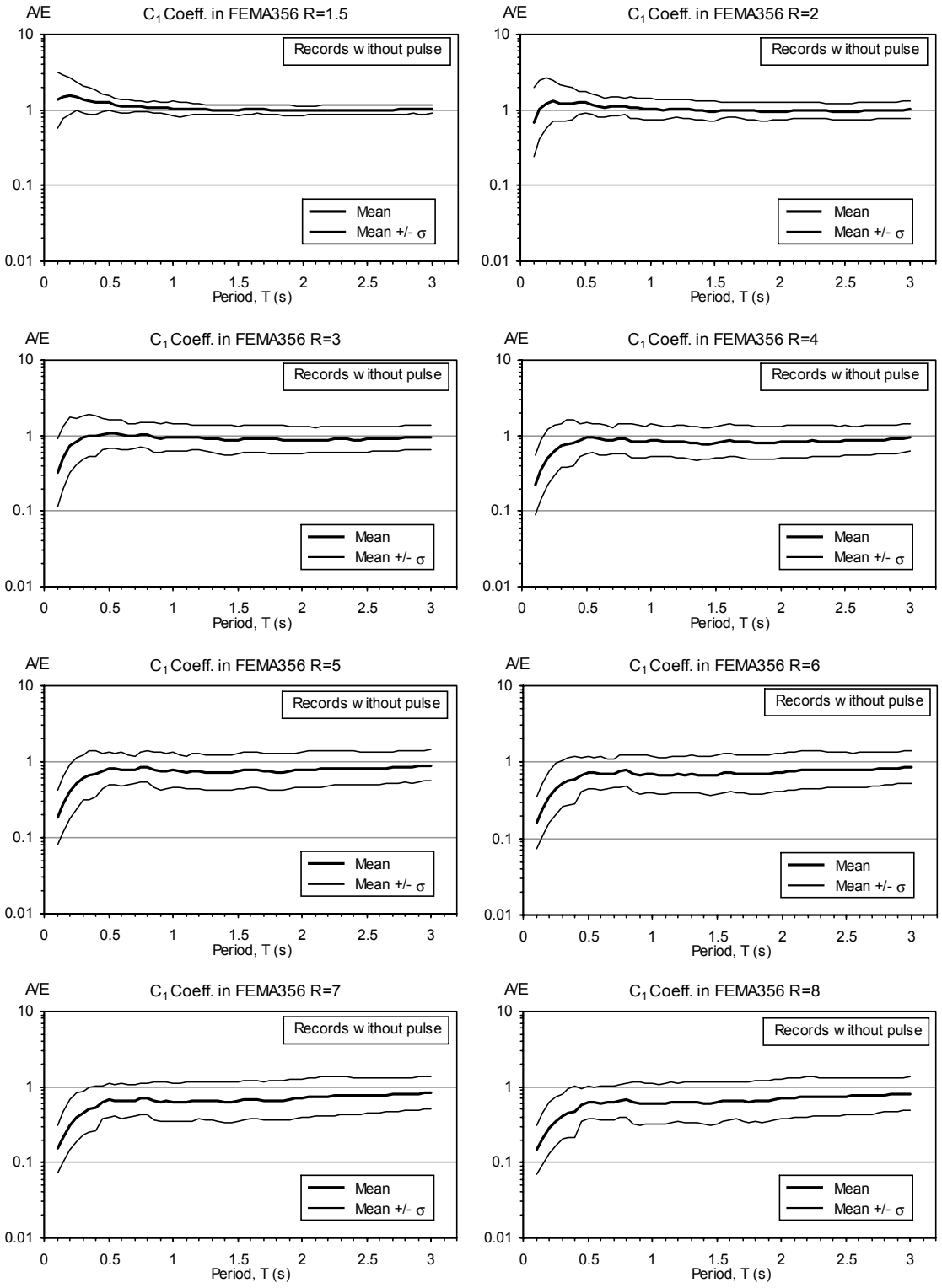

Figure 4.10(a) A/E Statistics for C_1 Coefficient Equation for Records without Pulse

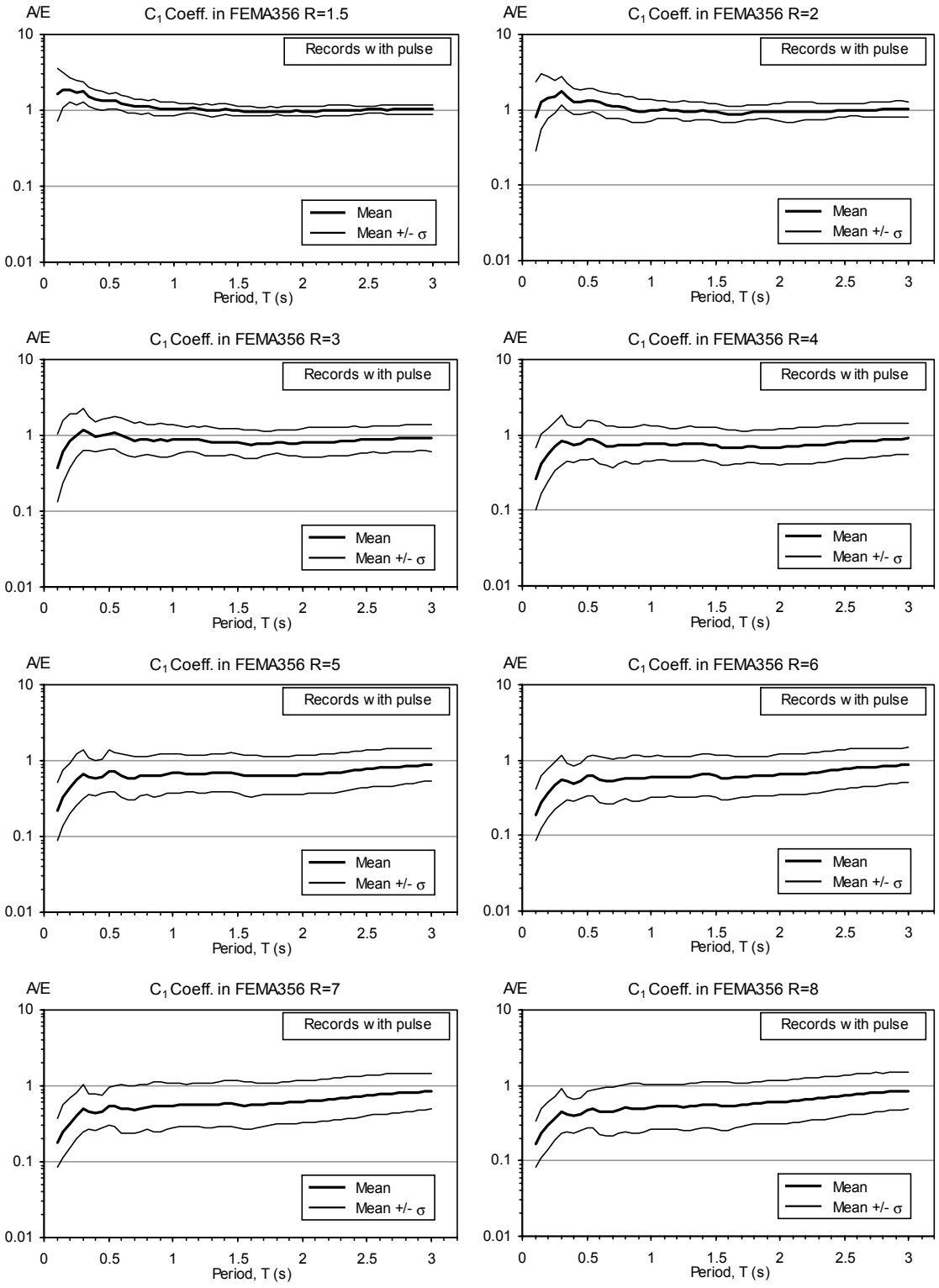

Figure 4.10(b) A/E Statistics for C_1 coefficient equation for records with pulse

Every approximate method inevitably results in estimates different than the "exact" response. The amount and the type (i.e. overestimation or underestimation) of the deviation from the exact response is the critical performance parameter for approximate methods. The A/E statistics presented in Figures 4.1, 4.2, 4.3 and 4.5 may provide the probable range of error associated with Equations 3.5, 3.12 and 3.16. Similarly the A/E statistics presented in Figures 4.7, 4.8 and 4.9 may be used to find the probable range of error associated with Equations 3.22 and 3.26. It should also be noted that, these errors may increase due to a number of other factors affecting the response of structure and not taken into consideration in this study. In conclusion, it may be stated that the equations proposed in this study may be used for obtaining quick and rough estimates of displacement demands imposed on regular frame type of structures subjected to near-fault ground motions. However, the assumptions made in the derivation of equations and the error ranges presented in Figures 4.1-4.5 and 4.7-4.9 should be considered carefully.

CHAPTER 5

SUMMARY, CONCLUSIONS AND RECOMMENDATIONS FOR FUTURE STUDIES

5.1 Summary

Excessive lateral displacements are the main cause of structural damage in structures subjected to earthquakes. Local displacement demands are particularly important for structures excited by near-fault ground motions. This study presents a methodology for developing a simple tool for estimating the ground story and maximum interstory displacement demands of moment resisting frames.

Important properties of near-fault ground motions have been summarized in Section 2.2. A total of 148 near-fault ground motion records were used in the analyses. The ground motion record set was sub-divided into two as "records with pulse" and "records without pulse". The relative success of various attenuation relationships, in estimating the peak ground acceleration and arias intensity, were evaluated using the near-fault ground motions from the record set. Peak ground acceleration to peak ground velocity ratio versus distance plot of near-fault records was examined. The correlation of pulse period with moment magnitude, distance and faulting mechanism were investigated. Pulse period versus moment magnitude relationships available in the

literature were plotted on the data obtained from near-fault records used in this study. Displacement spectra of the near-fault records with and without pulse were compared. Also, the spectral displacements in the maximum velocity direction of records with and without pulse were examined.

Elastic response of moment resisting frames and inelastic response of non-degrading SDOF systems subjected to near-fault ground motions were analyzed. Fundamental mode shapes and response characteristics of a set of 190 idealized moment resisting frames (corresponding to 10 different beam-to-column stiffness ratios and 19 different numbers of stories ranging between 2 and 20) were analyzed. Nonlinear regression analyses were performed on the results obtained from the modal analysis of idealized moment resisting frames. Two equations (Equations 3.12 and 3.16) for estimating the elastic ground story and maximum interstory drifts of moment resisting frames were established. The equations were established as modifying coefficients for the approximate ground story drift estimation equation proposed by Gülkan and Akkar (2002). A total of 28120 elastic MDOF response history analyses (corresponding to 190 idealized moment resisting frames and 148 ground motions) were performed. Using the results obtained from these response history analyses, important response characteristics of moment frames to near-fault ground motions were examined. Higher mode effects on the elastic ground story and maximum interstory drifts of moment resisting frames subjected to near-fault ground motions were investigated. Error statistics of the proposed approximate ground story and maximum interstory drift estimation equations (Equations 3.5, 3.12 and 3.16) were computed. Errors associated with elastic ground story and maximum interstory drift estimates were evaluated comparatively with the errors of similar studies (Miranda 1999, Miranda and Reyes 2002).

Fundamental response characteristics of inelastic non-degrading SDOF systems to near-fault ground motions were investigated. Elasto-plastic load deformation model was used for modeling the inelastic behavior of SDOF systems. A total of 96288 inelastic SDOF response history analyses were performed for better insight into the

statistics of the range of variation. Inelastic displacement ratios of SDOF systems having natural periods covering a range from 0.1 s to 3 s with the increments of 0.05 s and strength reduction factors varying between 1.5 and 8 were analyzed. Effects of the strength reduction factor and the natural period on the inelastic displacement ratio were examined. Inelastic displacement ratios for the SDOF systems subjected to strong ground motions with and without pulse were compared. Two equations, listed as Equation 3.23a and 3.23b for estimating the inelastic displacement ratios for SDOF systems subjected to near-fault ground motions with and without pulse were established. These equations have the capability of providing estimates of the inelastic displacement ratios for systems with specific strength reduction factors and natural periods. In order to examine the effect of natural period to pulse period ratio on the inelastic displacement ratio, a series of non-degrading SDOF systems having pulse period normalized natural periods ranging from 0.1 to 3 was analyzed. A third equation (Equation 3.26) was established for estimating the inelastic displacement ratios for systems with specific strength reduction factors and natural period to pulse period ratios. Errors associated with the approximate equations were compared with a similar equation employed in FEMA356 (2000).

5.2 Conclusions

The following conclusions were drawn based on the results obtained in this study:

- Equations, proposed by Somerville et al. (1999), Rodrigez-Marek (2000) and Alavi and Krawinkler (2001), for estimating the pulse period should be further studied. Correlation of pulse period with various parameters, such as faulting mechanism and orientation of station with respect to rupture surface, should be refined.

- Pulse period of a near-fault ground motion is strongly correlated with the predominant period in the pseudo-velocity spectrum of the ground motion.

- When the orientation of the rupture plane is unknown and the fault normal component of the ground motion record can not be established a priori, a relatively severe component may be practically found in the maximum velocity direction. This result confirms the claim of Akkar and Gülkan (2002) about the peak ground velocity direction components of near-fault ground motions.

- Ground story drifts and the maximum interstory drifts are noticeably higher for elastic structures having fundamental periods close to pulse period of the near-fault ground motion compared to structures with different fundamental periods than the pulse period.

- For the case of regular moment resisting frames (like the idealized frames used in this study) with fundamental periods between 0.2 and 1.2 seconds, errors of elastic ground story and maximum interstory drift estimation range between +20 to -10 percent. For frames with fundamental periods equal to 2 seconds underestimation reaches to -20 percent.

- Inelastic displacement ratios computed for the same strength reduction factor were found to be noticeably higher for the SDOF systems subjected to strong ground motions with pulse compared to those excited by ground motions without pulse (Figure 3.16).

- Inelastic displacements of non-degrading SDOF systems with natural periods longer than the pulse period, on the average, were found to be less than the maximum displacement of the elastic SDOF system with the same period and damping (Figure 3.18).

- Dispersion of the inelastic displacement ratios for specific strength reduction factors and natural period to pulse period ratios were found to be significantly less compared to the dispersion of the inelastic displacement ratios for the same strength reduction factors and natural periods. (Figures 3.17 and 3.19)

- The approximate equation (Equation 3.26), proposed for estimating the inelastic displacement ratios of non-degrading SDOF systems with specific strength reduction factors and natural period to pulse ratios were found to provide acceptably accurate estimates, particularly for systems with $T_n/T_v > 0.2$ (Figure 4.9).

- The use of C_1 coefficient in given FEMA356(2000) for estimating the inelastic displacement ratios of inelastic SDOF systems subjected to near-fault ground motions, may result in significantly unsafe estimates (Figures 4.10).

- Characteristic ground period, used for representing the smallest period at which equal displacement rule is applicable, results in inaccurate estimates of inelastic displacement ratios for the case of near-fault ground motions. On the other hand, considering the pulse period in the estimation of inelastic displacement ratios may significantly improve the accuracy of estimates for the case of near-fault ground motions.

5.3 Possible Future Extensions

This study can be extended in the future as stated below:

- Semi-empirical models for predicting the effects of forward directivity on the amplitude and frequency content of near-fault ground motions may be developed. Relationships for predicting the pulse period may be developed.

Such models may be utilized in the probabilistic seismic hazard analysis of structures close to active faults.

- Effects of different structural configurations on the modal properties of frames type of structures should be studied. A series of correction factors may be established for taking into account the effects of various structural configurations on ground story drifts and maximum interstory drifts.

- Modal properties associated with the higher modes of idealized moment resisting frames should be analyzed. An approximate equation for estimating the effects of higher modes on the local displacement demands of moment resisting frames may be established.

- Inelastic displacement computations may be repeated using different hysteretic models. A new correction factor, similar to C_1 in FEMA356(2000), may be introduced for considering the effects of various hysteretic properties on the inelastic displacement ratios of structures subjected to near-fault ground motions.

- Inelastic time history analyses of the idealized moment resisting frames excited by near-fault ground motions should be performed. The proposed approximate method for estimating the ground story drifts and maximum interstory drifts may be further developed for considering the inelasticity effects.

- This study is mainly based on the estimation of local displacement demands imposed on moment resisting frame structures by near-fault ground motions. In order to facilitate the use of this methodology in the design of new structures, design guidelines should be prepared for proportioning and

detailing structural components consistent with the estimated local displacement demands.

APPENDIX A

LIST OF THE NEAR-FAULT RECORDS

A.1 List of Basic Properties of the Near-Fault Ground Motions

Basic properties of the 148 near-fault ground motions used in this study are listed in Tables A.1 and A.2.

Table A.1 Records with Pulse

No	Record Name	Earthquake	M_w	Mech.	Station	Comp.	r_{rup} (km)	r_{jb} (km)	T_v (s)	T_{p-v} (s)	PGA (g)	PGV (cm/s)
1	CHY028N	Chi-Chi 1999	7.6	R	CHY028	N	7.31	7.31	0.81	0.85	0.82	67
2	CHY035W	Chi-Chi 1999	7.6	R	CHY035	W	18.12	18.12	1.29	1.40	0.25	45.6
3	chy080n	Chi-Chi 1999	7.6	R	CHY080	N	6.95	6.79	1.38	0.95	0.90	102
4	chy080w	Chi-Chi 1999	7.6	R	CHY080	W	6.95	6.79	0.92	0.85	0.97	108
5	CHY101N	Chi-Chi 1999	7.6	R	CHY101	N	11.14	11.14	4.69	4.80	0.44	115
6	CHY101W	Chi-Chi 1999	7.6	R	CHY101	W	11.14	11.14	3.38	3.20	0.35	70.6
7	nsye	Chi-Chi 1999	7.6	R	NSY	E	9.7	9.7	8.14	8.00	0.14	47.5
8	nsyn	Chi-Chi 1999	7.6	R	NSY	N	9.7	9.7	3.73	4.60	0.13	41.8
9	TCU036W	Chi-Chi 1999	7.6	R	TCU036	W	16.69	16.69	5.79	4.20	0.14	59.6
10	tcu053n	Chi-Chi 1999	7.6	R	TCU053	N	6.69	6.69	6.59	6.00	0.14	41.1
11	TCU057N	Chi-Chi 1999	7.6	R	TCU057	N	12.57	12.57	6.59	7.50	0.09	42.6
12	TCU059W	Chi-Chi 1999	7.6	R	TCU059	W	17.84	17.84	5.99	6.50	0.17	59.4
13	tcu060w	Chi-Chi 1999	7.6	R	TCU060	W	9.46	9.46	8.37	11.00	0.20	36.3
14	TCU063N	Chi-Chi 1999	7.6	R	TCU063	N	10.39	10.39	5.22	3.40	0.13	73.1
15	TCU064N	Chi-Chi 1999	7.6	R	TCU064	N	15.07	15.07	7.16	7.00	0.12	54
16	TCU068N	Chi-Chi 1999	7.6	R	TCU068	N	1.09	0.5	10.88	9.00	0.46	263
17	TCU087N	Chi-Chi 1999	7.6	R	TCU087	N	3.18	3.18	4.40	4.00	0.12	37.1
18	TCU087W	Chi-Chi 1999	7.6	R	TCU087	W	3.18	3.18	9.48	8.00	0.13	40.8
19	TCU101W	Chi-Chi 1999	7.6	R	TCU101	W	2.94	2.94	7.56	8.50	0.20	67.9
20	TCU102N	Chi-Chi 1999	7.6	R	TCU102	N	1.79	1.79	2.80	2.40	0.17	77.1
21	TCU103W	Chi-Chi 1999	7.6	R	TCU103	W	4.01	4.01	7.93	7.00	0.13	61.9
22	TCU104N	Chi-Chi 1999	7.6	R	TCU104	N	13.64	13.64	6.44	5.50	0.09	47.2
23	TCU128N	Chi-Chi 1999	7.6	R	TCU128	N	9.7	9.7	3.97	4.80	0.17	68.8
24	TCU128W	Chi-Chi 1999	7.6	R	TCU128	W	9.7	9.7	7.84	7.50	0.14	73
25	WGKE	Chi-Chi 1999	7.6	R	WGK	E	11.14	11.14	3.25	3.20	0.33	69
26	WGKN	Chi-Chi 1999	7.6	R	WGK	N	11.14	11.14	4.47	4.80	0.48	74.4
27	PET090	Cape Mendocino 1992	7.1	R	Petrolia	090	9.5	-	0.70	0.70	0.66	89.8
28	RIO270	Cape Mendocino 1992	7.1	R	Rio Del OVP FF	270	18.5	12.3	1.18	1.30	0.39	44
29	KJM000	Kobe 1995	6.9	SS	KJM	000	0.6	-	0.90	0.90	0.82	81.3
30	KJM090	Kobe 1995	6.9	SS	KJM	090	0.6	-	1.38	0.80	0.60	74.3

31	CLS090	Loma Prieta 1989	6.9	RO	Corralitos	090	5.1	-	0.70	0.80	0.48	45.2
32	G02090	Loma Prieta 1989	6.9	RO	Gilroy #2	090	12.7	12.1	1.41	1.50	0.32	39.1
33	G03090	Loma Prieta 1989	6.9	RO	Gilroy #3	090	14.4	14.9	2.06	2.00	0.37	44.7
34	STG090	Loma Prieta 1989	6.9	RO	Saratoga Aloha	090	13	11.7	3.10	3.80	0.32	42.6
35	LOS270	Northridge 1994	6.7	R	W. Lost Canyon	270	13	12.2	0.70	0.70	0.48	45.1
36	SCS052	Northridge 1994	6.7	R	Slymar Converter	052	6.2	0.2	2.51	2.60	0.61	117
37	SPV270	Northridge 1994	6.7	R	Sepulveda VA	270	8.9	0.4	0.77	0.80	0.75	84.8
38	SYL360	Northridge 1994	6.7	R	Slymar Hospital	360	6.4	3.6	1.91	1.60	0.84	130
39	WPI046	Northridge 1994	6.7	R	Newhall-W. Pico C.	046	7.1	7.1	3.20	2.00	0.45	92.8
40	WPI316	Northridge 1994	6.7	R	Newhall-W. Pico C.	316	7.1	7.1	1.89	1.80	0.33	67.4
41	PTS225	Superstition Hills 1987	6.6	SS	PTS	225	0.7	-	2.17	1.90	0.45	112
42	BRA225	Imperial Valley 1979	6.5	SS	Brawley Airport	225	8.5	8.5	3.39	3.00	0.16	35.9
43	E04230	Imperial Valley 1979	6.5	SS	El Centro #4	230	4.2	6.8	4.27	4.00	0.36	76.6
44	E05230	Imperial Valley 1979	6.5	SS	El Centro #5	230	1	4	3.87	3.40	0.38	90.5
45	E06140	Imperial Valley 1979	6.5	SS	El Centro #6	140	1	1.3	2.86	2.40	0.41	64.9
46	E06230	Imperial Valley 1979	6.5	SS	El Centro #6	230	1	1.3	3.87	3.40	0.44	110
47	E07230	Imperial Valley 1979	6.5	SS	El Centro #7	230	0.6	0.6	3.77	3.20	0.46	109
48	E08230	Imperial Valley 1979	6.5	SS	El Centro #8	230	3.8	3.8	4.01	4.00	0.45	49.1
49	E10050	Imperial Valley 1979	6.5	SS	El Centro #10	050	8.6	8.5	3.94	3.80	0.17	47.5
50	E10320	Imperial Valley 1979	6.5	SS	El Centro #10	320	8.6	8.5	1.97	1.50	0.22	41
51	ECC092	Imperial Valley 1979	6.5	SS	EC Center FF	092	7.6	7.6	3.27	3.20	0.23	68.8
52	EDA270	Imperial Valley 1979	6.5	SS	El Centro DA	270	5.3	5.1	4.50	2.60	0.35	71.2
53	EMO270	Imperial Valley 1979	6.5	SS	EC Overp FF	270	0.5	0.5	3.12	3.00	0.30	90.5
54	HVP225	Imperial Valley 1979	6.5	SS	Holtville PO	225	7.5	7.5	2.43	4.00	0.25	48.8
55	HVP315	Imperial Valley 1979	6.5	SS	Holtville PO	315	7.5	7.5	3.69	3.40	0.22	49.8
56	NPS210	N. Palm Springs 1986	6	RO	N. Palm Spr. PO	210	8.2	-	1.38	1.10	0.59	73.3

Mechanism: SS - Strike Slip / R- Reverse / RO - Reverse Oblique

r_{rup} : Closest distance to rupture surface (km) (Figure 2.8)

r_{jb} : Closest distance to surface projection of rupture surface (km) (Figure 2.8)

T_v : Pulse period (s)

T_{p-v} : Predominant period in the pseudo-velocity spectrum (s)

Table A.2 Records without Pulse

No	Record Name	Earthquake	M_w	Mech.	Station	Comp	r_{rup} (km)	r_{jb} (km)	T_{p-v} (s)	PGA (g)	PGV (cm/s)
1	CHY006E	Chi-Chi 1999	7.6	R	CHY006	E	14.93	14.93	1.90	0.36	55.4
2	CHY006N	Chi-Chi 1999	7.6	R	CHY006	N	14.93	14.93	1.00	0.35	42.8
3	CHY028W	Chi-Chi 1999	7.6	R	CHY028	W	7.31	7.31	0.65	0.65	72.8
4	CHY035N	Chi-Chi 1999	7.6	R	CHY035	N	18.12	18.12	0.85	0.25	37.6
5	CHY036N	Chi-Chi 1999	7.6	R	CHY036	N	20.38	20.38	6.50	0.21	41.4
6	CHY036W	Chi-Chi 1999	7.6	R	CHY036	W	20.38	20.38	3.40	0.29	38.9
7	TCUE	Chi-Chi 1999	7.6	R	TCU	E	5.73	5.73	4.80	0.18	40.5
8	TCUN	Chi-Chi 1999	7.6	R	TCU	N	5.73	5.73	3.60	0.19	34.4
9	TCU036N	Chi-Chi 1999	7.6	R	TCU036	N	16.69	16.69	5.50	0.13	50.2
10	TCU039N	Chi-Chi 1999	7.6	R	TCU039	N	16.7	16.7	5.50	0.14	54
11	TCU039W	Chi-Chi 1999	7.6	R	TCU039	W	16.7	16.7	7.50	0.21	50
12	TCU048N	Chi-Chi 1999	7.6	R	TCU048	N	14.38	14.38	4.80	0.18	48.3
13	TCU048W	Chi-Chi 1999	7.6	R	TCU048	W	14.38	14.38	3.80	0.12	32.6
14	TCU049N	Chi-Chi 1999	7.6	R	TCU049	N	4.48	4.48	6.00	0.25	61.2
15	TCU049W	Chi-Chi 1999	7.6	R	TCU049	W	4.48	4.48	9.00	0.29	47.9
16	TCU050N	Chi-Chi 1999	7.6	R	TCU050	N	10.33	10.33	5.50	0.13	42.3
17	TCU050W	Chi-Chi 1999	7.6	R	TCU050	W	10.33	10.33	11.00	0.15	36.9
18	TCU051N	Chi-Chi 1999	7.6	R	TCU051	N	8.27	8.27	7.00	0.23	38.4
19	TCU051W	Chi-Chi 1999	7.6	R	TCU051	W	8.27	8.27	7.50	0.19	49.3
20	TCU052N	Chi-Chi 1999	7.6	R	TCU052	N	0.24	0.06	8.50	0.42	118
21	TCU052W	Chi-Chi 1999	7.6	R	TCU052	W	0.24	0.06	5.00	0.35	159
22	TCU053W	Chi-Chi 1999	7.6	R	TCU053	W	6.69	6.69	9.50	0.22	41.3
23	TCU054N	Chi-Chi 1999	7.6	R	TCU054	N	5.92	5.92	9.50	0.19	38.5
24	TCU054W	Chi-Chi 1999	7.6	R	TCU054	W	5.92	5.92	6.50	0.15	59.4
25	TCU055N	Chi-Chi 1999	7.6	R	TCU055	N	6.88	6.88	4.00	0.20	51.5
26	TCU055W	Chi-Chi 1999	7.6	R	TCU055	W	6.88	6.88	2.20	0.24	26.2
27	TCU057W	Chi-Chi 1999	7.6	R	TCU057	W	12.57	12.57	4.80	0.12	35.2
28	TCU059N	Chi-Chi 1999	7.6	R	TCU059	N	17.84	17.84	5.50	0.17	56.2
29	TCU060N	Chi-Chi 1999	7.6	R	TCU060	N	9.46	9.46	5.50	0.11	45.3
30	TCU061N	Chi-Chi 1999	7.6	R	TCU061	N	17.75	17.75	3.60	0.14	43.6
31	TCU061W	Chi-Chi 1999	7.6	R	TCU061	W	17.75	17.75	5.50	0.14	40.3

32	TCU063W	Chi-Chi 1999	7.6	R	TCU063	W	10.39	10.39	5.50	0.17	59
33	TCU064W	Chi-Chi 1999	7.6	R	TCU064	W	15.07	15.07	7.00	0.11	39.2
34	TCU068W	Chi-Chi 1999	7.6	R	TCU068	W	1.09	0.5	9.50	0.57	177
35	TCU070N	Chi-Chi 1999	7.6	R	TCU070	N	19.1	19.1	5.00	0.17	62.3
36	TCU070W	Chi-Chi 1999	7.6	R	TCU070	W	19.1	19.1	5.00	0.25	52.1
37	TCU082N	Chi-Chi 1999	7.6	R	TCU082	N	5.73	5.73	3.60	0.19	40.5
38	TCU082W	Chi-Chi 1999	7.6	R	TCU082	W	5.73	5.73	6.50	0.22	58.4
39	TCU084N	Chi-Chi 1999	7.6	R	TCU084	N	10.39	0.01	0.95	0.42	45.6
40	TCU084W	Chi-Chi 1999	7.6	R	TCU084	W	10.39	0.01	0.90	1.15	115
41	TCU100N	Chi-Chi 1999	7.6	R	TCU100	N	12.74	12.74	5.50	0.12	46.5
42	TCU100W	Chi-Chi 1999	7.6	R	TCU100	W	12.74	12.74	4.80	0.12	34.6
43	TCU101N	Chi-Chi 1999	7.6	R	TCU101	N	2.94	2.94	5.50	0.25	49.4
44	TCU102W	Chi-Chi 1999	7.6	R	TCU102	W	1.79	1.79	2.60	0.30	112
45	TCU103N	Chi-Chi 1999	7.6	R	TCU103	N	4.01	4.01	6.50	0.16	26.8
46	TCU104W	Chi-Chi 1999	7.6	R	TCU104	W	13.64	13.64	5.50	0.11	36.6
47	TCU106N	Chi-Chi 1999	7.6	R	TCU106	N	15.22	15.22	5.00	0.13	43.7
48	TCU106W	Chi-Chi 1999	7.6	R	TCU106	W	15.22	15.22	6.50	0.16	46.6
49	TCU107N	Chi-Chi 1999	7.6	R	TCU107	N	20.35	20.35	2.40	0.16	47.4
50	TCU107W	Chi-Chi 1999	7.6	R	TCU107	W	20.35	20.35	5.00	0.12	36.8
51	TCU109N	Chi-Chi 1999	7.6	R	TCU109	N	13.09	13.09	3.40	0.15	53.1
52	TCU109W	Chi-Chi 1999	7.6	R	TCU109	W	13.09	13.09	2.60	0.16	50.8
53	TCU136E	Chi-Chi 1999	7.6	R	TCU136	E	8.97	8.97	9.00	0.17	55.8
54	TCU136N	Chi-Chi 1999	7.6	R	TCU136	N	8.97	8.97	7.00	0.18	47.5
55	WNTE	Chi-Chi 1999	7.6	R	WNT	E	2.21	1.94	0.50	0.96	68.8
56	WNTN	Chi-Chi 1999	7.6	R	WNT	N	2.21	1.94	0.95	0.63	42
57	TAB-LN	Tabas 1978	7.4	R	Tabas	LN	-	-	0.85	0.84	97.8
58	TAB-TR	Tabas 1978	7.4	R	Tabas	TR	-	-	4.80	0.85	121
59	PET000	Cape Mendocino 1992	7.1	R	Petrolia	000	9.5	-	0.75	0.59	48.4
60	RIO360	Cape Mendocino 1992	7.1	R	Rio Del OVP FF	360	18.5	12.3	0.44	0.55	42.1
61	CLS000	Loma Prieta 1989	6.9	RO	Corralitos	000	5.1	-	0.75	0.64	55.2
62	G02000	Loma Prieta 1989	6.9	RO	Gilroy #2	000	12.7	12.1	0.40	0.37	32.9
63	G03000	Loma Prieta 1989	6.9	RO	Gilroy #3	000	14.4	14.9	0.48	0.55	35.7
64	G04000	Loma Prieta 1989	6.9	RO	Gilroy #4	000	16.1	15.8	0.46	0.42	38.8
65	G04090	Loma Prieta 1989	6.9	RO	Gilroy #4	090	16.1	15.8	0.55	0.21	37.9

66	STG000	Loma Prieta 1989	6.9	RO	Saratoga Aloha	000	13	11.7	1.80	0.51	41.2
67	WVC000	Loma Prieta 1989	6.9	RO	Saratoga Valley	000	13.7	12	1.10	0.25	42.4
68	WVC270	Loma Prieta 1989	6.9	RO	Saratoga Valley	270	13.7	12	1.20	0.33	61.5
69	LOS000	Northridge 1994	6.7	R	Lost Canyon	000	13	12.2	0.60	0.41	43
70	NWH090	Northridge 1994	6.7	R	Newhall	090	7.1	4.5	1.30	0.58	75.5
71	NWH360	Northridge 1994	6.7	R	Newhall	360	7.1	4.5	0.70	0.59	97.3
72	PKC090	Northridge 1994	6.7	R	Pacomia Kagel C.	090	8.2	8.1	0.90	0.30	31.4
73	PKC360	Northridge 1994	6.7	R	Pacomia Kagel C.	360	8.2	8.1	0.70	0.43	51.5
74	SPV360	Northridge 1994	6.7	R	Sepulveda VA	360	8.9	0.4	0.85	0.94	76.6
75	SCS142	Northridge 1994	6.7	R	Slymar Converter	142	6.2	0.2	1.60	0.90	102
76	SYL090	Northridge 1994	6.7	R	Slymar Hospital	090	6.4	3.6	0.85	0.60	78.2
77	TAR090	Northridge 1994	6.7	R	Tarzana-Cedar Hill	090	17.5	4.1	0.34	1.78	114
78	TAR360	Northridge 1994	6.7	R	Tarzana-Cedar Hill	360	17.5	4.1	0.75	0.99	77.6
79	PCD164	San Fernando 1971	6.6	R	Pacoima Dam	164	2.8	2.8	1.20	1.22	113
80	PCD254	San Fernando 1971	6.6	R	Pacoima Dam	254	2.8	2.8	0.50	1.16	54.3
81	PTS315	Superstition Hills 1987	6.6	SS	PTS	315	0.7	-	1.20	0.38	43.9
82	BCR140	Imperial Valley 1979	6.5	SS	Bonds Corner	140	2.5	2.6	0.85	0.59	45.2
83	BCR230	Imperial Valley 1979	6.5	SS	Bonds Corner	230	2.5	2.6	0.60	0.77	45.9
84	BRA315	Imperial Valley 1979	6.5	SS	Brawley Airport	315	8.5	8.5	1.60	0.22	38.9
85	ECC002	Imperial Valley 1979	6.5	SS	EC Center FF	002	7.6	7.6	1.30	0.21	37.5
86	EMO000	Imperial Valley 1979	6.5	SS	EC Overp FF	000	0.5	0.5	2.60	0.31	71.8
87	E04140	Imperial Valley 1979	6.5	SS	El Centro #4	140	4.2	6.8	0.90	0.49	37.4
88	E05140	Imperial Valley 1979	6.5	SS	El Centro #5	140	1	4	2.60	0.52	46.9
89	E07140	Imperial Valley 1979	6.5	SS	El Centro #7	140	0.6	0.6	1.10	0.34	47.6
90	E08140	Imperial Valley 1979	6.5	SS	El Centro #8	140	3.8	3.8	1.40	0.60	54.3
91	EDA360	Imperial Valley 1979	6.5	SS	El Centro DA	360	5.3	5.1	1.40	0.48	40.8
92	NPS300	N. Palm Springs 1986	6	RO	N. Palm Spr. PO	300	8.2	-	0.30	0.69	33.8

Mechanism: SS - Strike Slip / R- Reverse / RO - Reverse Oblique

r_{rup} : Closest distance to rupture surface (km) (Figure 2.8)

r_{jb} : Closest distance to surface projection of rupture surface (km) (Figure 2.8)

T_{p-v} : Predominant period in the pseudo-velocity spectrum (s)

APPENDIX B

ATTENUATION FUNCTIONS

B.1 Attenuation Function Proposed by Boore et al. (1997)

Coefficients of Equation 2.2 are given by Boore et al. (1997) for the estimation of peak ground acceleration as follows:

b_1= -0.313 – for stike slip earthquakes

-0.117 – for reverse slip earthquakes

-0.242 – if mechanism is not specified

b_2= 0.527

b_3= 0

b_5= -0.778

b_V= -0.371

h= 5.57

V_A= 1396 (m/s)

σ_{lnY}= 0.52

B.2 Attenuation Function Proposed by Sadigh et al. (1997)

The attenuation function for estimating the peak ground acceleration proposed by Sadigh et al. (1997) is:

$$\ln(Y) = C_1 + C_2 M - C_3 \ln\left(r_{rup} + C_4 e^{C_5 M}\right) + C_6 + C_7 \left(8.5 - M\right)^{2.5} \tag{B.1}$$

where Y is the peak ground or spectral acceleration in g, M is the moment magnitude of earthquake, r_{rup} is the closest distance to rupture surface.

C_1= -2.17 – for stike slip earthquakes

-1.92 – for reverse and thrust earthquakes

C_2= 1.0

C_3= 1.7

C_4=2.1863, C_5=0.32 for $M \leq 6.5$

C_4=0.3825, C_5=0.5882 for $M > 6.5$

C_6= 0

C_7= 0

σ_{lnY}= min⟨ 1.52-0.16M , 4⟩

B.2 Attenuation Function Proposed by Travasarou et al. (1997)

The attenuation function for estimating the arias intensity proposed by Travasarou et al. is:

$$\ln\left(I_a\right) = c_1 + c_2\left(M-6\right) - c_3 \ln\left(M/6\right) + c_4 \ln\left(\sqrt{r_{rup}{}^2 + h^2}\right) + \left(s_{11} + s_{12}\left(M-6\right)\right) S_C + \left(s_{21} + s_{22}\left(M-6\right)\right) S_D + f_1 F_N + f_2 F_R \tag{B.2}$$

where I_a is the Arias Intensity in m/s, M is the moment magnitude, R is the closest distance to the rupture surface in km, h is a fictitious hypocentral depth in km determined by the regression, S_C and S_D are indicator variables for the soil types (both 0

for site category B (BRM Site Classification), 1 and 0 for site category C, and 0 and 1 for site category D), and FN and FR are indicator variables for the fault types (both 0 for strike slip faults, 1 and 0 fornormal faults and 0 and 1 for reverse or reverse-oblique faults). The values of regression coefficients are given below:

$c_1 = 2.8$, $c_2 = -1.981$, $c_3 = 20.72$, $c_4 = -1.703$, $h = 8.78$,
$s_{11} = 0.454$, $s_{12} = 0.101$, $s_{21} = 0.479$, $s_{22} = 0.334$,
$f_1 = -0.166$, $f_2 = 0.512$

The standard error of this estimate is computed as follows:

$$\sigma_{tot}\left(M, I_a, site\right) = \sqrt{\sigma\left(I_a, site\right)^2 + \tau\left(M\right)^2} \tag{B.3}$$

$$\sigma\left(I_a, site\right) = \begin{cases} \sigma_1 & for\ I_a \le 0.013 m/s \\ \sigma_1 - 0.106\left(\ln\left(I_a\right) - \ln\left(0.0132\right)\right) & for\ 0.013 < I_a \le 0.125 m/s \\ \sigma_2 & for\ I_a \ge 0.125 m/s \end{cases}$$

$$\tau\left(M\right) = 0.611 - 0.047\left(M - 4.7\right) \quad for\ 4.7 \le M \le 7.6$$

where M is the moment magnitude, Ia is the estimated Arias Intensity,
$\sigma_1 = 1.18$, $\sigma_2 = 0.94$ for B Class Sites,
$\sigma_1 = 1.17$, $\sigma_2 = 0.93$ for C Class Sites,
$\sigma_1 = 0.96$, $\sigma_2 = 0.73$ for D Class Sites.

REFERENCES

Akkar, S. and P. Gülkan, 2002, "A critical examination of near-field accelerograms from the Sea of Marmara region earthquakes", Bulletin of the Seismological Society of America, 92(1), 428-447.

Alavi B. and H. Krawinkler, 2001, "Effects of Near-Fault Ground Motions on Frame Structures", The John A. Blume Earthquake Engineering Research Center, Report No. 138, Stanford University, California.

Anderson J.C. and V.V. Bertero, 1986, "Uncertainties in establishing design earthquakes", Journal of Structural Engineering, ASCE, Vol. 113(8), 1709-1724.

Ang, A.H.S. and W.H. Tang, 1975, Probability Concepts in Engineering Planning and Design, Vol.1-Basic Principles, John Wiley and Sons, Canada

ATC-40 (Applied Technology Council), 1996, "Seismic Evaluation and Retrofit of Concrete Buildings", Report No. ATC 40, Vol. 1, Redwood City, California.

Arias A., 1970, "A Measure of Earthquake Intensity", Design of Nuclear Power Plants, Hansen J.(ed.), MIT Press, Cambridge, MA, 1970, 438-483.

Aydınoğlu M.N. and Ü. Kaçmaz, 2002, "Strength-based Displacement Amplification Spectra for Inelastic Seismic Performance Evaluation", Kandilli Observatory and Earthquake Research Institute (KOERI), Report No. 2002/02

Ayre, R.S., 1956, "Methods for calculating the earthquake response of "shear" buildings", Proceedings of the World Conference on Earthquake Engineering, Berkeley, California.

Baez, J.I, and E. Miranda, 2000, "Amplification factors to estimate inelastic displacement demands for the design of structures in the near-field", Proc. 12th World Conference on Earthquake Engineering, New Zealand

Blume J.A., 1968, "Dynamic characteristics of multistory buildings", Journal of the Structural Division, ASCE, Vol. 94(ST2), 377-402

Boore D.M., W.B. Joyner, and Fumal. T.E., 1997, "Equations for estimating the horizontal response spectra and peak accelerations from Western North American Earthquakes: A summary of recent work", Seismological Research Letters, Vol.68(1), 128-153.

Boore D.M., 2001, "Comparisons of ground motions from the 1999 Chi-Chi Earthquake with empirical predictions largely based on data from California", Bulletin of the Seismological Society of America, Vol.91(5), 1212-1217.

Chopra A.K., 1996, "Modal analysis of linear dynamic systems physical interpretation", Journal of Structural Engineering, Vol.122(5), 517-527

Chopra A.K., 2000, Dynamics of Structures: Theory and Application to Earthquake Engineering, Prentice Hall, Upper Saddle River, New Jersey.

Chopra, A.K. and C. Chinatanpakdee, 2001a, "Drift spectrum vs. modal analysis of structural response to near-fault ground motions", Earthquake Spectra, Vol. 17(2), 221-234.

Chopra, A.K. and C. Chinatanpakdee, 2001b, "Comparing the response of SDF systems to near-fault and far-fault earthquake motions in the context of spectral regions", Vol. 30, 1769-1789.

Chopra, A.K. and E.F. Cruz, 1986a, "Elastic earthquake response of building frames", Journal of Structural Engineering, ASCE, Vol. 112(3), 443-459.

Chopra, A.K. and E.F. Cruz, 1986b, "Simplified procedures for earthquake analysis of buildings", Journal of Structural Engineering, ASCE, Vol. 112(3), 461-480.

Chopra, A.K. and E.F. Cruz, 1986c, "Evaluation of building code formulas for earthquake forces", Journal of Structural Engineering, ASCE, Vol. 112(8), 1881-1899.

Diaz O., E. Mendoza and L. Esteva, 1994, "Seismic ductility demands predicted by alternate models of building frames", Earthquake Spectra, Vol.10(3), 465-487

Douglas, J., 2001, "A Comprehensive Worldwide Summary of Strong-Motion Attenuation Relationships for Peak Ground Acceleration and Spectral Ordinates (1969 to 2000)", ESEE Report No. 01-1, Department of Civil and Environmental Engineering, Imperial, College, London.

FEMA356, 2000, "NEHRP Guidelines for the Seismic Rehabilitation of Buildings", Federal Emergency Management Agency (FEMA), Report FEMA 356(Guidelines).

Freeman, S.A., J.P. Nicoletti and J.V. Tyrell, 1975, "Evaluation of Existing Buildings for Seismic Risk – A Case Study of Puget Sound Naval Shipyard, Brementon, Washington", Proceedings of the First U.S. National Conference on Earthquake Engineering, Seattle Washington.

Gülkan, P. and M.A. Sözen M., 1974, "Inelastic response of reinforced concrete structures to earthquake motions", Journal of the American Concrete Institute, Vol. 71, 601-609.

Gülkan P. and Akkar S., 2002, "A simple replacement for the drift spectrum", Engineering Structures, Vol. 24, 1477-1484.

Hiedebrecth A.C. and B. Stafford Smith, 1973, "Approximate analysis of tall wall frame structures", Journal of Structural Division, ASCE, 99(2), 199-221.

Heidebrecht A.C. and N.D. Naumoski, 1997, "Development and application of a displacement-based design approach for moment-resisting frame structures", Seismic Design Methodologies for the Next Generation of Codes, Fajfar P. and Krawinkler H. eds., pp. 33-42. Balkema: Roterdam.

Heidebrecht A.C. and A. Rutenberg, 2000, "Applications of drift spectra in seismic desgin", Proceedings of the 12th World Conference on Earthquake Engineering, Paper No. 0209, Auckland, New Zeland.

Iwan W.D., 1980, "Estimating inelastic response spectra from elastic spectra", Earthquake Engineering and Structural Dynamics, Vol. 8, pp. 375-388.

Iwan W.D., 1997, "Drift spectrum: measure of demand for earthquake ground motions", Journal of Structural Engineering, Vol. 123(4), 397-404.

Iwan W.D, C.T. Huang and A.C. Guyader, 2000, "Important features of the response of inelastic structures to near-field ground motion" , Proceedings of the 12th World Conference on Earthquake Engineering, Paper No. 1740, Auckland, New Zeland.

Kayen R. E. and J.K. Mithchell, 1997, "Assessment of liquefaction potential during earthquakes by arias intensity", Journal of Geotechnical and Geoenvironmental Engineering, Vol. 123(12), 1162-1174.

Malhotra, P.K., 1999, "Response of buildings to near-field pulse-like ground motions", Earthquake Engineering and Structural Dynamics, 28(11), 1309-1326.

McGuire, R.K., 1978, "Seismic ground motion parameter relations", Journal of the Geotechnical Engineering Division, ASCE, Vol.104, No. GT4, 481-490.

Miranda, E., 1999, "Approximate seismic lateral deformation demands in multistory buildings", Journal of Structural Engineering, ASCE, Vol. 125(4), 417-425.

Miranda, E., 2001, "Estimation of Inelastic Deformation Demands of SDOF Systems", Journal of Structural Engineering, Vol 127(9), 1005-1012.

Miranda E. and C.J. Reyes, 2002, "Approximate lateral drift demands in multistory buildings with nonuniform stiffness", Journal of Structural Engineering, ASCE, Vol. 128(7), 840-849.

Nassar A.A. and H. Krawinkler, 1991, "Seismic Demands for SDOF and MDOF Systems", The John A. Blume Earthquake Engineering Research Center, Report No. 95, Stanford University, California.

NEHRP, 2000, "NEHRP Recommended Provisions for Seismic Regulations for New Buildings and Other Structures, Part 1: Provisions (FEMA 368)", Building Seismic Safety Council for the Federal Emergency Management Agency, Washington, D.C.

Newmark, N.M., 1959, "A method of computation for structural dynamics", Journal of the Engineering Mechanics Division, ASCE, Vol.85, 67-94.

Newmark, N.M. and W.J. Hall, 1982, "Earthquake spectra and design", Earthquake Engineering Research Institute, Berkeley, California.

Osteraas, J.D. and H. Krawinkler, 1990, "Strength and Ductility Considerations in Seismic Design", The John A. Blume Earthquake Engineering Research Center, Report No. 90, Stanford University, California

Paz, M., 1985, Structural Dynamics, Theory and Computation, 2nd Edition, Von Nostrand Reinhold New York.

Richter, C.F., 1968, Elementary Seismology, W.H. Freeman and Co., San Francisco

Rodrigez-Marek, A., 2000, "Near-fault seismic site response", Ph.D. Dissertation, Department of Civil Engineering, University of California Berkeley.

Rodrigez-Marek, A., J.D. Bray and N.A Abrahamson, 2001, "An empirical geotechnical seismic site response procedure", Earthquake Spectra, Vol.17, 65-87.

Rosenblueth, E. and Herera, 1964, "On a kind of hysteretic damping", Journal of Engineering Mechanics Division, ASCE, Vol.90, 37-48.

Sadigh, K., C.-Y Chang, J.A Egan, F. Makdisi and R.R. Youngs, 1997, "Attenuation relationships for shallow crustal earthquakes based on California strong motion data", Seismological Research Letters, Vol.68(1), 180-198.

Somerville, P.G., N.F. Smith, R.W. Graves and N.A. Abrahamson, 1997, "Modification of empirical strong ground motion attenuation relations to include the amplitude and duration effects of rupture directivity", Seismological Research Letters, Vol.68(1), 199-222.

Sommerville, P.G., K. Irikura, R. Graves, S. Swada, D. Wald, N.A. Abrahamson, Y. Iwasaki, T. Kagawa, N. Smith and A. Kowada, 1999, "Characterizing crustal

earthquakes slip models for prediction of strong ground motion", Seismological Research Letters, Vol.70(1), 59-80.

Stewart J.P., S. Chiou, J.D. Bray, R.W. Graves, P.G. Sommerville and N.A. Abrahamson, 2001, "Ground Motion Evaluation Procedures for Performance-Based Design", Report No PEER 2001/09, Pacific Earthquake Engineering Research Center, University of California, Berkeley.

SYSTAT, 2002, "TableCurve 2D v5.01 for Windows ", SYSTAT Software Inc.

Travasarou T., J.D. Bray and N.A. Abrahamson, 2003, "Empirical attenuation relationship for arias intensity", Earthquake Engineering and Structural Dynamics, Vol. 32, 1133-1155.

Vidic, T., P. Fajfar and M. Fischinger, 1994, "Consistent inelastic design spectra: strength and displacement", Earthquake Engineering and Structural Dynamics, Vol. 23, 507-521.

Veletsos, A.S. and N.M. Newmark, 1960,. "Effect of inelastic behavior on the response of simple systems to earthquake motions", . Proceedings of the 2nd World Conference on Earthquake Engineering, Japan, vol. II., 895–912.

Wald, D.J., V. Quitoriano, T.H. Heaton and H. Kanamori, 1999, "Relationships between peak ground acceleration, peak ground velocity, and modified mercalli intensity in California", Earthquake Spectra, EERI, Vol. 15(3), 557-564

Zhu T.J., W.K. Tso, and A.C. Heidebrecth, 1988, "Effect of peak ground a/v ratio on structural damage", Journal of Structural Engineering, Vol. 114(5), 1019-1037.